UNIVERSITY OF CALIFORNIA,
IRVINE

Numerical simulation model of single and multiple reservoir operations: Concepts, Numerical modeling, operational rules, and operation optimization

THESIS

submitted in partial satisfaction of the requirements
for the degree of

MASTER OF SCIENCE

in Civil Engineering

by

Mustafa Onur Onen

Thesis Committee:
Associate Professor Jasper A. Vrugt, Chair
Associate Professor Amir AghaKouchak
Professor Efi Foufoula-Georgiou

2018

DEDICATION

For the memory of my main motivation source, the Head Teacher, Mustafa Kemal Atatürk and his fellows who contributed to the enaction of Revolutionary Educational Law of Turkish Republic No. 1416. We were sparks, now became flames as you had foreseen.

TABLE OF CONTENTS

LIST OF FIGURES

LIST OF TABLES

ACKNOWLEDGMENTS

To my parents who have been supporting me with a tireless devotion and boundless sacrifices from their life: because I owe it all to you. Many Thanks!

Foremost, to my advisor, Jasper A. Vrugt, I wholeheartedly appreciate everything you have done for me. You have been taking the leading role in the development of my academical skills and gaining positive and multi-perspective thinking. Your advisory has crowned the world-class-education that I had at UC Irvine. On top of that, you genuinely care about all of your students and firmly believe that we can succeed. I would also like to express my gratitude to you for being not only an academic advisor to me but a close friend who is ready to listen and help at every turn.

Besides my advisor, I would like to acknowledge the rest of my thesis committee: Amir AghaKouchak and Efi Foufoula-Georgiou, for generously offering their time, support and guidance throughout the preparation and evaluation of this thesis.

My sincere thanks also goes to The General Directorate of State Hydraulic Works (DSI-TURKEY), for offering me this opportunity and continuous support of my MS study and research.

In addition, I feel deep appreciation to my friends Matthew Brand, Sara Michelle Newsome, Rasul Torun, Enver Adas and Milad Abbasi who have assisted me on this work continuously and gratuitously. In addition, I am very thankful to all of my friends with whom I enjoyed the wonderful experiences together in US but also my other beloved ones whose eyes were always seeking me while I was far away.

My venture in the USA would not have been that unforgettable without my precious friends: Matthew Brand, Sara Michelle Newsome, Aditya Bajaj, Roohi Fakhartousi, Sam Reifsnyder, Francesca Cecconi, Mustafa Mert Bayer, Enver Adas, Milad Abbasi, Natalia Antonova, Emily Parker and Samantha Ruthledge.

Last but not least, thanks to my lovely sister, her irreplaceable love and support always motivated me to overcome the challenges being away from home.

ABSTRACT OF THE THESIS

Numerical simulation model of single and multiple reservoir operations: Concepts, Numerical modeling, operational rules, and operation optimization

By

Mustafa Onur Onen

Master of Science in Civil Engineering

University of California, Irvine, 2018

Associate Professor Jasper A. Vrugt, Chair

Reservoirs store a large proportion of the Earth's limited fresh water resources. This water sustains life and makes regional developments possible. The construction of reservoirs does not reveal the overall system success since it is assessed only by operating and measuring whether their proposed benefits are achieved for that single reservoir. Managers of the reservoir systems often face the challenges of fulfilling various conflicting operational objectives while complying with the contractual agreements, institutional limitations, water rights privileges, environmental concerns, and hydrological and demand uncertainties. Obtaining optimum reservoir operation strategies by honoring these restrictions necessitates computer modeling. In this thesis, we introduce the Elaborate Reservoir Operation Management model, EROM, which simulates the storage and power generation of a single reservoir or a system of reservoirs that have one or multiple purposes in response to the record of inflow values and site characteristics under a predetermined operation strategy. As the name suggests, the model differs from the other long term reservoir operation analysis models with its sophisticated tools that provide more thorough representation of the real systems to be modeled. We perform three case studies to test the model with the data of a real-world project which balances water supply, power generation and flood protection. Within these case studies, rule curve based operation optimization analysis of the system are successfully

performed by integrating EROM with the evolutionary multiobjective optimization algorithm, AMALGAM, and considering two objective functions as the maximization of average annual generated energy and the minimization of shortage index. The results of the case studies are presented and discussed.

Chapter 1

Introduction

Reservoirs, above or below-ground, store a large proportion of the Earth's fresh water resources. This water sustains life and makes regional developments possible. Indeed, reservoirs may serve many practical purposes, including (among others) water supply, electricity generation, flood control, drought mitigation, groundwater recharge, environmental management, navigation, fishery, recreational activities, and border security.

The planning, design and construction of a reservoir requires extensive, multidisciplinary, team work. The planning stage typically involves detailed hydrological analysis, coupled with geotechnical investigation, demand projections, environmental impact assessments and benefit-cost analysis to determine operational, economic, and ecosystem feasibility of a reservoir. The design and construction phases then aim to engineer and build the reservoir in such a way that it can achieve the various objectives anticipated during the planning stage. Construction of the system does not show the overall system success since it can be only assessed by operating and measuring the ultimate performance of the system and whether proposed benefits of the investment are achieved. Whether or not these objectives are achieved in practice is somewhat difficult to assess and dependent in part on reservoir operation. In ad-

dition, decision makers must consider restrictions from contractual agreements, institutional limitations, water rights privileges, environmental concerns and hydrological and demand uncertainties. To honor these restrictions reservoir managers/operators and/or decision makers must sacrifice, at least temporally, on reservoir benefits. This necessitates the use of trade-off analysis to help select the most appealing modus operandi.

Labadie [2004] reviews storage projects which failed to fulfill the level of benefits that were anticipated during the planning stage. The two most important causes for the apparent reservoir failures include unforeseen hydrological events and/or the use of inadequate future water demand projections. Labadie [2004] also points out that insufficient importance is given to operation which may lead to a dramatic loss of benefits. In addition, the authors claim that the operational efficiency and effectiveness of individual reservoirs can be further enhanced by adoption of a multi-reservoir - systems - viewpoint. Yet, the coordinated use of multiple different reservoirs increases manifold operational complexity. Indeed, since the number of reservoirs and accordingly the total area of impounded land increases, the number of variables and constraints related to various local conditions also increases. This demands use of advanced state-of-the-art optimization methods to explore rapidly and exhaustively the space of optimal solutions in pursuit of the best overall system (= multi-reservoir) performance. Furthermore, an expansion to multiple reservoirs enhances system nonlinearity, which, together with the uncertain nature of hydrologic conditions and future demand projections make the multiple reservoir optimization problem even more challenging [Nalbantis and Koutsoyiannis, 1997].

Reservoir operation has received considerable interest in the literature. For example, Yeh [1985], Wurbs [1993] and Labadie [2004] presented an excellent review of theories and applications of systems analysis methods to reservoir management problems. These papers summarized as well the most important reservoir computer models and addressed the remaining gaps between theoretical approaches and real-word applications. Yeh [1985] re-

viewed optimization techniques which are used in reservoir operation. This includes the use of linear, dynamic and nonlinear programming. Evolutionary algorithms have also been used popularly in reservoir systems management. Rani and Moreira [2010] provides a survey of simulation and optimization modeling methods in reservoir systems operation. They conclude that the evolutionary algorithms are very efficient in coping with the non-linearity and very applicable to simulation models. Labadie [2004] focused primarily on operation optimization of model systems having multiple reservoirs. According to Yeh [1985] no general algorithm exists for the optimization of reservoir operation because of each reservoir's unique physical and operational characteristics.

Optimization of reservoir operations involves the allocation of water resources, generation of streamflow regulation strategies and operating rules which help decision makers determine when and how much water to be stored and/or released to meet the objectives of the system of consideration [Wurbs, 1993]. These operation rules guide managers of the system while they are making the release decisions in ways that meet various demands in the most reliable and efficient manner. These rules may include one or more of the following definitions [Yeh, 1985]. 1. Target water levels or volumes: Reservoir managers are expected to honor these levels as much as possible while they try to fulfill the demands. 2. Multiple zoning: These rules are used to allocate the reservoir into different vertical zones to meet different objectives. General allocated zones are named as inactive zone (dead pool), conservation zone, flood control zone, buffer zone and surcharge zone. 3. Flow range: These types of operating rules are used to associate the rates of releases to be made with the zone which the reservoir level is presently in. 4. Conditional rule curves: These type of rules are used to describe the releases as functions of time of year, storage volume and natural inflow of reservoir expected to occur in a specified time period in the future.

For the derivation of predefined set of rules designed for single reservoir operation or so-called rule curves simulation models are widely used. Simulation models are the computer

algorithms developed to mimic the actual system behavior by extensively considering all physical characteristics of the system. Unlike the other mathematical programming methods simulation models are more flexible and useful in approximating the real response of the system [Yeh, 1985]. While Yeh [1985] listed the earlier applications of simulation models, Oliveira and Loucks [1997] summarized the widely adopted operation rules of multi-reservoir systems and they used Genetic Algorithm to evaluate the performance of operation rules for multi-reservoir systems by concluding that it is a suitable method to specify effective operation rules.

In this thesis, first, it is desired to build a Matlab program which is capable of approaching the nearest optimum coordinated operation policy of single or multiple reservoirs having either single or multiple objectives. Second, several case studies are performed by testing the algorithm with a real-world project data and their results are presented and discussed.

Chapter 2

Reservoir System Operations

The basic operation of reservoirs concerns when and how much water should be stored or released from a reservoir or multiple reservoir system. There are several factors that impact operational decisions. First, water is a valuable substance and its allocation between reservoir owners and water customers as well as between states and nations and its use are regulated by institutional considerations such as agreements, programs, political processes, legislation in the context of state water rights systems [Wurbs, 1996]. Second, funding and financial arrangements are also key factors for the construction of reservoir projects and their investment costs can generally be paid off through efficient operation.. Third, their massive size might endanger their surrounding ecosystems or a structural failure which generally results in dreadful consequences such as large scale deaths, wide destruction and environmental disasters in case of operational miscalculations.

An operating plan, policy, rule or schedule is the set of guidelines for the determination of water amounts to be released from and stored in a reservoir or a system of multiple reservoirs as a function of time. It may also involve the allocation of storage between the reservoirs in a system, beneficiaries, between various project purposes and between different time periods.

It also provides guidelines to reservoir operators and/or water managers.

In this chapter, first, the basic concepts of reservoir operation and methods are described. Second, theoretical optimization of reservoir systems explained and finally, the methodology of simulation-optimization approaches are applied to multiple case studies in the context of this thesis.

2.1 Reservoir Description: In Words

A reservoir is constituted by the construction of a dam and its compound outlet structures such as pipelines, canals and hydroelectric power plants. All streamflow which used to flow at the axis of the dam and diversions from upstream projects then becomes collected at its upstream side once it starts to retain water. The amount of water storage increases with the height of the dam because of the topography of the river valley. Therefore, the readily available storage can be diverted to different uses from outlet structures.

Releases from a reservoir to the river below the dam are directed through its spillway and/or outlet works. Spillway are a compulsory component of a reservoir to allow high flow rates during flood events to safely overflow downstream of the dam when the storage capacity is not enough to accommodate the excessive volume. There are various types of spillway structures however all of them can be first classified as uncontrolled or controlled. A controlled spillway is operated with one or multiple sluice gates when the reservoir needs to be emptied in case of floods. An uncontrolled spillway is an outlet structure with an uncontrolled upstream weir located in the forebay. The amount of excess water above the weir crest will overflow to downstream of the dam. The crest elevation of the weir is generally determined by considering the worst case scenario which involves the situation of receiving the design flood hydrograph when the reservoir is completely full. In case of a controlled spillway designers

establish spillway rating curves, plan a safe flood operation of sluice gates and specify the maximum flood level as well. In any case, the designer must also make sure to leave a clear height between the crest elevation of the dam and the maximum flood level to prevent wave action on the surface of the reservoir from overtopping the dam.

The dam outlet works are the systems where controlled releases are routed under, around or through the dam. Outlet works typically have one or multiple intake structures located in the reservoir, a conveyance system such as penstock and/or channel and a terminal structure which has valves or other release control structures. The terminal structure might be a hydroelectric power plant, a valve chamber, or a pump station which controls the municipal, irrigation and industrial water supply purposes. In addition, outlet works generally involve another terminal structure which discharges the stored water directly to the river below the dam in order to lower the reservoir levels down to the minimum operational level of the reservoir in case of necessity or to maintain the ecological water flow along the river below the dam.

2.1.1 Vertical Zoning and Operational Limits of a Reservoir

Reservoir operating rules generally involve dividing the total storage into vertical zones due to operational limits and purposes of the reservoirs. The designation of capacity between zones might be permanent or variable with time or other factors. The storage of a typical reservoir might be allocated into the vertical zones shown in the Figure 2.1 and described below.

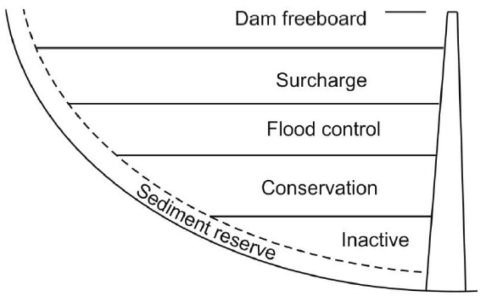

Figure 2.1: An example of the vertical zoning of a reservoir storage [Wurbs, 1996]

Inactive Zone: This zone is also known as dead storage which is always located at the bottom of a reservoir andis designed to capture sediment before it reaches the water intakes of the the outlet works. Therefore, withdrawal of clean water through outlet works is maintained for various objectives throughout the lifetime of the reservoir which is generally assumed as 50 to 100 years. However, designer of the dam must be very careful while specifying the top elevation of this zone and the sill of water intake structures. Undersized inactive zones can lead to premature dam siltation and result in excessive excavation and dam maintenance costs. In addition, it also leads to serious loss of benefits during the maintenance works by making the reservoir nonoperative. Similarly, overestimation of this storage and correspondingly raising the elevation of intakes to satisfy the necessary regulation volume for achieving main purposes of the reservoir might necessitate the increase of dam height and cause excessive construction costs. Since the top elevation of inactive zone is usually lower than the water intakes, the storage in this zone can not be used for water supply or hydropower purposes. Therefore, the only outflows of the reservoir become evaporation and seepage losses as long as the reservoir water level is within the inactive zone.

Conservation Zone: This zone is generally located just above the inactive zone and allocated to meet the purposes of the reservoir such as water supply and power generation. The main role of this zone to assure the delivery of constant rate of flow to downstream at any time throughout the entire lifetime of the reservoir. This highly reliable constant rate of

release is called as safe yield (firm yield) and its calculation is essential for the estimation at planning stage as well as for the operation management. Since the amount of water deficit occurring in dry periods is met by conserving the excessive flows of wet periods, the more volume allocation to conservation zone, the higher safe yield that consequently increases the net benefits of the reservoir is obtained. Recreational activities are also possible while the reservoir level is within this zone. The general operational approach is to keep water level as close as possible to the top of this zone to maintain supply demands during dry periods.

Flood Control Zone: If the reservoir is proposed to protect the downstream lands from floods, a sufficient part of total reservoir capacity is designated above the conservation zone to capture flood volume and attenuate the spillway outflow. It remains empty except during the expected period of floods and shortly after the floods. If the spillway of the reservoir has an uncontrolled weir, crest elevation of its upstream weir is set to the top elevation of this zone. However, if the spillway is controlled with gates, elevation of the top of this zone can be higher than the spillway weir. Once the flood control zone is filled during a flood, the excess volume is spilled down to the river with a nondestructive discharge for downstream areas. Hence, the volume of designated flood control zone is crucial for flood protection.

Surcharge Zone: This zone is an uncontrolled storage which takes place above the flood control zone. If the flood control zone is not designated in the reservoir, it is formed on the conservation zone. Reservoir water levels which exceed the flood control zone is spilled to the river. Its upper limit is theoretically defined as the maximum flood level which is mentioned earlier in this chapter.

Freeboard: Since an overtopping of a dam is a dangerous situation to be avoided especially for the structures with earth fill type of embankments, a clear height called as freeboard is left between the crest elevation of the dam and the maximum flood level. The height of the freeboard must be larger than the highest wave run up on the upstream slope of the dam which is driven by wind forces occurring on the reservoir surface.

Definitions of other reservoir terms related to the subject of this thesis are also provided below.

Maximum Operational Level: This is the maximum reservoir water level which is observed below the surcharge zone. It is usually assigned as the crest elevation of the upstream weir of the spillway if the spillway of the reservoir is uncontrolled type. This level is determined during the planning studies and its value is considered in all hydraulic calculations and design of outlet structures and water supply systems by assuming the highest long term water level. Hence, it is also named as normal operation level especially for reservoirs that does not have a flood control zone.

Minimum Operational Level: This is the minimum reservoir water level at which the outlet works can safely convey water. The operation of outlet works when the reservoir storage is below this level might cause air to enter the system and that might damage the components of water supply or hydropower facilities .

Active Storage Capacity: This is the total usable storage via outlet works which is estimated by the subtraction of storage at minimum operational level from the storage at maximum operational level.

2.1.2 Operational Rule Curves

Most of reservoir operations are based on operational rules which provide guidance to operators. These rules involve the water releases or target reservoir storage or elevation with respect to time of the year. As a result, a two dimensional graph which is called rule curve or guide curve is widely adopted for the determination of volume of water to be released and/or stored by comparing the current state with the target state of the system which is prescribed by rule curve. Plotting of top of conservation storage is a popular use of rule curve. Figure

2.2 shows a typical rule curve which designates conservation and flood protection zones in a reservoir. In this rule curve, one can easily understand the period which starts in September and ends in April is wetter period with higher probability of floods than the rest of the year. The operator is to release water as necessary to keep the actual reservoir water level as close as possible to the rule curve elevations which maintains empty space to mitigate the outcomes of probable floods. If minimum and maximum release constraints are also known, one can easily estimate how fast the target storage levels can be achieved. The rule curve shown in Figure 2.2 is a yearly rule curve that defines a policy which does not change from one year to another. The operator may change the releases regarding to inflows which lead to changes in reservoir storage. The rule curve can be also plotted as a function of time and other variations such as snow thickness, soil moisture, inflow forecasts and storage in the other reservoirs within the system under consideration [Loucks et al., 2005].

Reservoir rule curves are derived from simulation models that calculates reservoir storage and specified objective function(s) which may represent the net benefits or losses by using water balance equation, inflow series and reservoir operation policy as inputs. The detailed information about reservoir simulation model is given in Section 2.2 and 2.3.

2.1.3 Rule Curves Combined with Hedging Rules

Meeting reservoir operational targets and storage is not an issue during normal periods. However, during the periods with scarce inflow, it might be impossible to reach both storage and release targets. Bower et al. [1962] suggests the implementation of hedging rules during the periods of inflow shortage if the marginal value of water is decreasing with the amount of water supplied. He claims that it is beneficial to accept a small deficit so as to decrease the probability of having a more severe water shortage in the future. The studies explained below are examples of the application of rule curves associated with hedging rules.

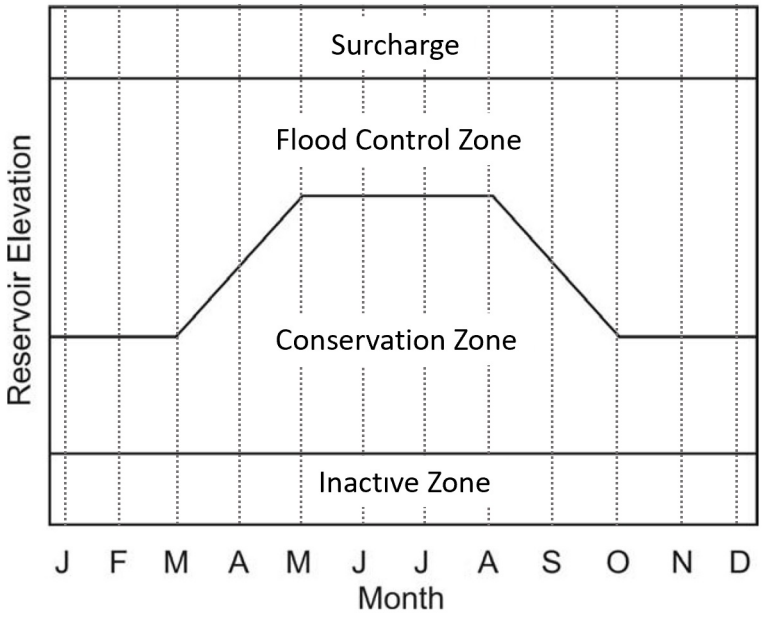

Figure 2.2: An example of the boundary rule curve varying with time of the year [Wurbs, 1996]

Tung et al. [2003] implemented traditional rule curves combined with hedging rules to optimize the operation of a single reservoir meant as water supply in Taiwan. In their case study, firstly, they predefined the shape of the rule curves to be optimized by routing the reservoir by considering known inflows and demands to be supplied. After that they parameterized the breakpoint coordinates of two rule curves which divide the active volume of the reservoir into three operational zones according to the predefined shape. Having different fixed percentages of water supply discounts specified for each of the zones in which the actual reservoir water level follows, they determined the optimum annual operational zones of the reservoir which minimizes the shortage severity in water supply.

Tu et al. [2003] developed an optimization model that associates rule curves with hedging rules to manage and operate a system having multiple reservoirs and multiple purposes. They built a numerical representation of network of the system considering local diversion constraints and optimized the operational zones of each reservoir by using Mixed Integer Linear Programming with the objective function involving maximization of water supply and storage within the system.

2.2 Reservoir Description: Numerical Model

In this section, numerical model which is developed to accurately simulate the operational behavior of a real reservoir system for given time series of inflow, site characteristics and operational rule descriptions is introduced. The computational procedures of the model are described and discussed in detail how the resulting objective functions (including cost functions or benefits) are computed. The model, henceforward referred to as Elaborated Reservoir Operation Management or EROM, is developed in MATLAB software. The first main advantage of using EROM for the derivation of optimum operational rules for a single reservoir or system of multiple reservoirs is its flexibility that allows user to compute the system response by using any of two different solver types which execute the water balance calculation of the system. Second, the model which is designed for operation analysis of reservoirs having hydropower energy purposes more in particular provides thorough representation of the elements of the hydropower system. It can perform the unit based energy generation calculations by considering almost full assembly of power generating units, enabling user to select the method of hydraulic loss calculations, sophisticated turbine efficiency specifications and dynamic or stable tailwater level assumptions. Third, its simple call function allows the user to integrate the model to the most of the heuristic optimization algorithms. Fourth, the option of selecting any of wide range of time step size from 1 hour up to 1 month helps define the level of desired computational accuracy and speed regarding to the purpose of the study especially in case the model is to be integrated with the optimization algorithms. Finally, its elaborative but simple design aims to converge the response of the real system to be simulated without exhausting the user while detecting the input or conceptual errors. The following sections discuss the main equations of the system.

2.2.1 Water Balance Calculation

The main state variable of the model is water storage in the reservoir and all releases to be made are the function of the current state of the system and the proposed rule curve. The rate of change in storage level $\frac{dS}{dt}$ where S (m^3) and t (s) denote storage and time, respectively, at any time of interest can be calculated by mass balance equation given in Equation (2.1) which is simply defined by subtracting total outflow O (m^3/s) from total inflow I (m^3/s) of the reservoir.

$$\frac{dS}{dt} = I(t) - O(t) \tag{2.1}$$

If the initial storage level is known and inflow and outflow are constant throughout the current time interval, ΔT (s), the equation can be rewritten in the form of Euler's forward (explicit) method with a fixed time step as follows

$$S_{t+\Delta T} = S_t + (I_t - O_t)\Delta T, \tag{2.2}$$

where S_t, $S_{t+\Delta T}$, I_t and O_t denote the initial and final storage levels, rates of inflow and total outflow, respectively. Here, selection of ΔT is particularly important in the model because the larger it is specified, the higher integration error may be resulted in depending on how extent the other terms in the equation change by time. Equation (2.2) is promptly calculated by the explicit solver of EROM that takes user defined initial storage and time step as an input.

As an alternative to the explicit solver, EROM also provides its user to perform water balance calculations by using its ODE solver. This solver utilizes MATLAB's "ode45" function that is designed to solve ordinary differential equations. ode45 implements a Runge-Kutta method with a variable time step for efficient computation to minimize the integration errors. It handles solving the Equation (2.1) by taking the initial storage of the reservoir S_0 as initial condition and the start and end of the calculation period as integration limits. Even though its capable of solving various equation(s) accurately by using default options, ode45 also

gives opportunity to the user to specify the maximum allowed time step size and change the integration error thresholds. However, using highly efficient ODE solver may result in a longer computation time during the simulation process. It may even take more considerable amount of time to complete the runs once EROM is integrated to optimization algorithms. However, the presence of a highly efficient alternative solver to the explicit solver used in EROM paves the way of measuring the integration errors as a result of using explicit solver to decide what time step size is sufficient for the analysis.

Inflow of the reservoir is the sum of all flows which feed reservoir storage. Generally, inflow comes from the runoff driven from whole catchment that belongs to the dam axis of the reservoir. Besides, there can be also other upstream reservoirs whose downstream releases and spills as well as diversions from other catchments contribute to the total inflow of the reservoir of interest. Therefore, for the water balance calculations of a reservoir, the inflow must be derived by considering the releases of all upstream structures as well. Inflows can be estimated by historical stream gauge records assuming that the same record will repeat in the future. The user needs to enter the time series of inflows to EROM.

Total outflow from the reservoir in a specified period might consist of one or multiple of rates of evaporation Q_{evap} (m^3/s), seepage Q_{seep} (m^3/s), spillway or spillage Q_{spill} (m^3/s) and sum of releases Q_{r} (m^3/s). Therefore the sum of outflows can be written as follows

$$O = Q_{\text{evap}} + Q_{\text{seep}} + Q_{\text{spill}} + Q_{\text{r}} \tag{2.3}$$

The evaporation rate of a reservoir can be obtained by relying on the evaporation pan measurements in the vicinity of the reservoir under the condition that a pan coefficient to be additionally considered in the calculation in order to convert the evaporation in the pan to the real water body evaporation rate [Finch and Calver, 2008]. The equation that calculates Q_{evap} in (m^3/month) is given as follows

$$Q_{\text{evap}} = E_{\text{pan}}\{t\}\, K_{\text{pan}}\, A\{S\}, \tag{2.4}$$

where E_{pan} (m/month) denotes overall monthly pan measurement, K_{pan} (-) signifies evaporation pan coefficient and A (m^2) characterizes the surface area of the reservoir. Braces indicate the dependency of E_{pan} and A on time and storage in the reservoir, respectively. Apart from changes in its exact value depending on location, surface area and depth of reservoir as well as the weather conditions throughout the year and pan type, various papers about reservoir evaporation suggests that mean annual K_{pan} can be taken as around 0.7 [Alvarez et al., 2008, Elba, 2017, Finch and Calver, 2008, Linacre, 2004, Wurbs, 1996].

Q_{seep} is related to the pressure head of the reservoir. Therefore, EROM is designed as the user needs to enter a piecewise linear relationship of reservoir water level (m) and seepage rate (m^3/s) as an input.

As it is mentioned earlier, spillway flow rate is a factor when storage exceeds the reservoir capacity, S_{max} (m^3). If that is the situation the volume of spillage, V_{spill} (m^3) can be equaled to excessive water volume beyond the reservoir capacity at the end of current time interval after calculating Equation (2.2) by the initial assumption of $Q_{\text{spill}} = 0$. Then, the final storage of that time interval, $S_{t+\Delta T}$ (m^3) will be equaled to S_{max}. Otherwise, V_{spill} is equal to zero. The procedure described above can be mathematically expressed in Equation (2.5). Assuming stable spillway discharge throughout the current time interval, one can easily calculate Q_{spill} by using Equation (2.6).

$$V_{\text{spil}} = \begin{cases} S_{t+\Delta T} - S_{\text{max}}, & \text{if } S_{t+\Delta T} > S_{\text{max}} \\ 0, & \text{otherwise} \end{cases} \tag{2.5}$$

$$Q_{\text{spill}} = \frac{V_{\text{spill}}}{\Delta T} \tag{2.6}$$

Depending on its design purpose, total release of a reservoir Q_{r} might consist of one or multiple of the following constituents. These are potable, irrigation, industrial and ecological water supply releases as well as hydropower release and they are withdrawn from the reservoir depending on demands which usually change with years or time of the year. In EROM, while

these releases can be attributed to the amount of demand directly to simulate the reservoir response and/or calculate desired operational performance measures, at least one of them can be defined as decision variable to optimize the releases once it is integrated to an optimization algorithm.

2.2.2 Energy Calculation

A hydropower plant consists of one or several energy generating units. Each of these units is the combination of an intake structure, a penstock assembly that conveys water from reservoir to the turbine, a turbine which is connected to a generator and a terminal structure from upstream to downstream. Here, the term "unit" is attributed to one complete energy generating unit. Figure 2.3 illustrates the plan view of a dam with a hydropower plant and a longitudinal profile of one of its units.

The penstock is formed by the assembly of pipes which might be made from steel, polyethylene or glass fiber reinforced pipes. If there are multiple units in a powerplant, each of the units might have their separate penstocks from water intake to the turbines or there might be a main penstock that conveys water from intake to the branch member after which the conveyed water is distributed and diverted to each of the units such as in Figure 2.3. Since, the characteristics (diameters, lengths and the roughness) of each member in the penstock are important to specify the amount of potential energy lost during energy generation correctly, the hydraulic (frictional) losses occurring along the penstock network must be accurately analyzed. For this, EROM allows user to enter the detailed information of any tree-branch-shaped penstock network easily and analyze its hydraulic losses conveniently. The calculation of hydraulic losses within the penstock network will be explained later in this section. The amount of energy generated from a hydropower plant involving n units during a period between $t = 0$ to $t = \Delta T$ can be calculated by Equation (2.7) assuming

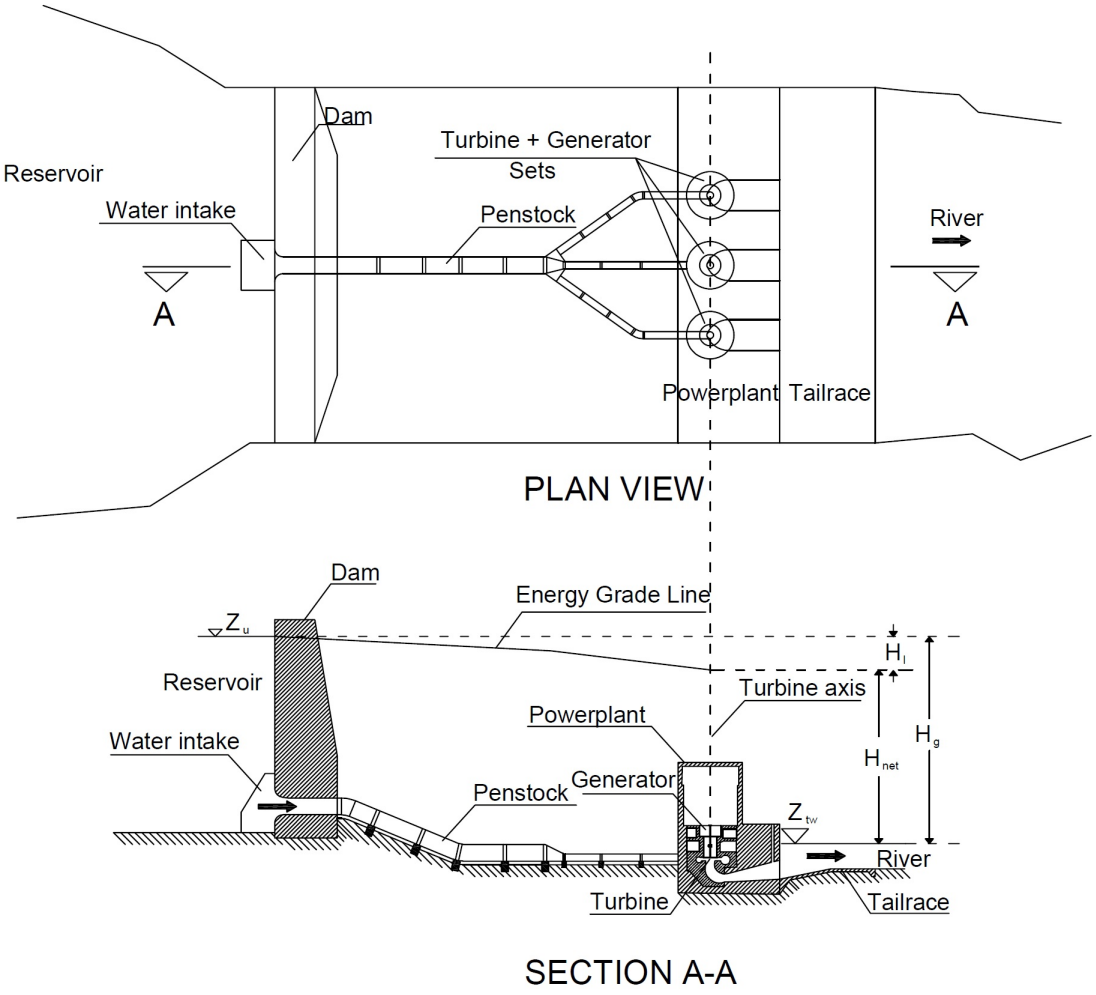

Figure 2.3: Plan and longitudinal profile of a dam with a hydropower plant

that the penstock assembly of each of the units comprising K number of elements. This equation is calculated by the model by selecting either explicit solver or ODE solver as they are implemented to the solution of Equation (2.2).

$$E = \int_0^{\Delta T} \rho\, g \sum_{j=1}^{n} \Big[H_{\mathrm{net},j}\{S(t), q_j(t), D_{j,k}, L_{j,k}, \mu_{j,k}, \nu, \gamma_j\}\; q_j(t)\, \eta_{\mathrm{t}j}\{q_j(t), q_{\mathrm{d}j}\}\, \eta_{\mathrm{g}j} \Big] \qquad (2.7)$$

In this equation, ρ (kg/m^3) signifies the density of water, g (m/s^2) indicates gravitational acceleration, $H_{\mathrm{net},j}$ (m) characterizes the net head occurring on the jth unit and $q_j(t)$ (m^3/s) unit discharge at time t and $\eta_{\mathrm{t}j}$ (-) and η_g (-) specify the efficiencies of turbine and generator located in the jth unit, respectively. The braces in this equation denote the dependency of the related term to the terms inside the brace. The other terms inside the braces are

described as follows. $D_{j,k}$ (m), $L_{j,k}$ (m) and $\mu_{j,k}$ (m) represents the diameter, length and roughness of kth penstock part of the jth unit, respectively. ν signifies the kinematic viscosity of water and γ_j is the ratio of total minor hydraulic loss to total major hydraulic loss along the penstock assembly of jth unit.

The net head in a unit can be calculated by subtracting total hydraulic loss H_{f} (m) from the gross hydraulic head H_{g} (m) (Equation 2.8). H_{g} is the elevation difference between the water level in the reservoir and the total potential energy level at the terminal structure exit. The exit can be designed in two possible ways corresponding to the type of the turbine installed to the unit. If the turbine is reaction type as shown in Figure 2.3, it is to be located and operated under downstream water level which is also known as tailwater level Z_{twl} (m) that occupies during the operation. This is due to the fact that reaction turbine has to have a pressure difference between the inlet and the outlet of its runner which necessitates the turbine runner to be submerged into water. For the impulse type of turbines, the flow is discharged from a nozzle directly into the atmosphere by forming a jet which turns the turbine runner. In this case, the potential energy at downstream will be equal to the elevation of nozzle jet which also means that there is no pressure difference between the inlet and outlet of the runner. Equation (2.9) shown below summarizes the abovementioned calculation.

$$H_{\mathrm{net}} = H_{\mathrm{g}} - H_{\mathrm{f}} \tag{2.8}$$

$$H_{\mathrm{g}} = \begin{cases} Z_{\mathrm{up}} - Z_{\mathrm{twl}}, & \text{for reaction turbines} \\ Z_{\mathrm{up}} - Z_{\mathrm{jet}}, & \text{for impulse turbines} \end{cases} \tag{2.9}$$

In case of having reaction type turbine in the unit whose H_{net} to be computed, Z_{twl} should be taken account as a function of total downstream discharge if the discharge fluctuations causing considerable differences in Z_{twl}. For this, EROM provides two different options to assume Z_{twl} as stable level or a dynamic level that changes with the total release that is passing in the river section intersecting with the tailrace. Selection of dynamic tailwater

assumption needs stage discharge relationship of the related cross section of the river. EROM expects user to enter the discharge and corresponding water level values to describe that relationship as a piecewise linear function. If the total downstream discharge does not affect Z_{twl}, the user can select stable tailwater assumption and enter Z_{twl} as a constant value.

The total hydraulic loss is the summation of hydraulic losses occurring along each pipe member of penstock assembly. Generally, vast majority of H_{f} come from the frictional energy dissipation caused by the roughness of the pipe material along its internal walls, the rest arises from the local energy losses at several members of the penstock system such as contraction, expansion, trashrack, valve, elbow, bend etc. While the first component of H_{f} is called as major hydraulic loss, H_{f}^{+} (m), the latter is named as minor headloss H_{f}^{-}(m) headloss. H_{f}^{+} can be calculated by using either Darcy-Weisbach or Manning's equation which are given in Equation (2.10) and Equation (2.11), respectively. In these equations, $q_{j,k}$ (m^3/s) is the discharge passing through the kth member located on the penstock assembly which is connected to the jth unit and K_j (-) is the total number of members which constitute the penstock of the jth unit. EROM allows user to specify one of these equations to be accounted during the calculations. However, it should be noted that the parameters inside the braces of the term H_{net} given in Equation (2.7) belong to Darcy-Weisbach equation.

$$H_{\text{f}j}^{+}(t) = \sum_{k=1}^{K_j} \frac{8\, f\, L_{j,k}\, q_{j,k}^2(t)}{D_{j,k}^5\, \pi^2\, g} \tag{2.10}$$

$$H_{\text{f}j}^{+}(t) = \sum_{k=1}^{K_j} \frac{n_{\text{man}}^2 L_{j,k} q_{j,k}^2(t) \pi^2 D_{j,k}^{8/3}}{2.52} \tag{2.11}$$

In Equation (2.10), f (-) represents the friction factor which is the function of average water velocity in the pipe and pipe roughness, ε (m) and it can be calculated by the equations given in Appendix. However, in Equation (2.11), friction of the pipe is attributed to Manning's roughness coefficient, n_{man} ($\text{s}/\text{m}^{1/3}$) and it is only a function of pipe material.

Minor head loss, H_{f}^{-}, is calculated by multiplying the minor loss coefficients of every related

member in the assembly by the kinetic energy of the flow passing by that member. However, calculation of minor losses requires a significant amount of user input. Therefore, for simplicity, EROM expects user to enter only the ratio of minor losses to major losses, γ (-). Both H_{f}^{+} and H_{f}^{-} are function of Q^2 and the contribution of H_{f}^{-} may not exceed 10 percent of H_{f} in real penstock systems. Hence, H_{f} can be expressed as follows.

$$H_{\mathrm{f}} = H_{\mathrm{f}}^{+} + H_{\mathrm{f}}^{-} \tag{2.12}$$

$$\gamma = \frac{H_{\mathrm{f}}^{-}}{H_{\mathrm{f}}^{+}} \tag{2.13}$$

Other terms in Equation (2.7) which impacts the generated energy is the turbine η_{t} (-) and generator efficiency η_{g} (-) because the energy generation at the output of powerplant will be smaller than the available stored energy of water in the reservoir due to losses in turbine and generator excluding frictional losses along the penstock system. Here, we introduce unit efficiency, η_{u}(-) in case of representation of turbine and generator performance together. Since designers pursue to reach maximum power output harnessed from every cubic meter of flow to use the water resource efficiently, any currently installed unit has its own design characteristics depending its location. The peak turbine efficiency can be governed for a turbine operating at constant speed under one head and one power output. The unit will operate at reduced efficiency at any other head or power output. The net head at which the peak efficiency value is achieved is the design head (rated head) of the turbine [Krueger et al., 1976]. Rated discharge, q_{d} (m^3/s), is the turbine discharge when the turbine is operated with the full gate opening at design head [Krueger et al., 1976]. Turbine manufacturers provide efficiency curves of their installed products as a function of turbine discharge, head or power output on which they guarantee minimum performance during operations for the owner of the powerplant [Jarry-Bolduc and Cote, 2014]. Figure 2.4 shows the efficiency curves of 4 different type of turbines with respect to the ratio between discharge and design discharge. In order to establish these curves, the manufacturers test the installed turbine

and generator sets within allowable ranges of discharge, head and power, and they establish relationships between unit efficiency and related parameters periodically. However, it might be also expensive and time consuming to perform these tests which may cause loss of benefits during the test period. Therefore, researchers derived equations which represent the peak value of efficiency curve and its shape as a function of discharge [Brandt et al., Gordon, 2001]. In any case, there has to be an efficiency relationship to be considered in energy calculations which represents near actual system performance. Thus, EROM allows users to simulate the reservoir operation by considering either stable or variable turbine or unit efficiency for each of the units. In case of selecting variable efficiency for any unit, a relationship between its turbine or unit efficiency and either discharge, head or power is to be supplied as an input. The relationship can be given as piecewise linear or mathematical expression. Minimum and maximum operational discharge limits of the unit $q_{\min}$ (m^3/s) and $q_{\max}$ (m^3/s), respectively, are also needed. Hence, the efficiency of the unit can be specified for any known unit discharge decision.

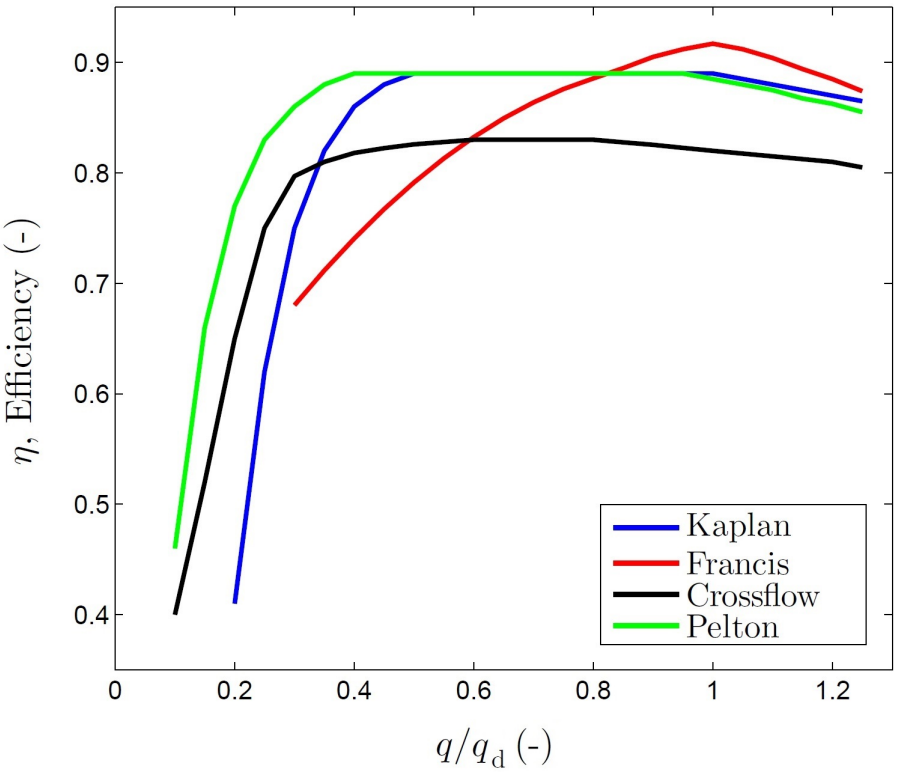

Figure 2.4: Efficiency curves of Kaplan (blue), Francis (red), crossflow(black), and Pelton (green) type turbines with respect to the ratio between discharge and design discharge [Yildiz, 2015].

If the powerplant consists of multiple units having different characteristics and specific discharge limits, there are infinite number of combinations which satisfy given plant discharge decision and unit discharge limits but only the selection of one or a limited number of those make it possible to reach the optimum overall efficiency of the plant. Here, finding the global maximum of overall efficiency analytically usually becomes very challenging work especially if the number of units in the plant increases and every unit in the plant has a different efficiency curve. This problem is recognized in the literature as hydro unit dispatch or hydro unit commitment problem on which numerous research have been performed especially for the short term reservoir operation [Ohishi et al., 2005, Ponrajah and Galiana, 1997, Santos and Ohishi, 2004, Séguin et al., 2016, Sousa et al., 2007]. In EROM, the complexity of this problem is circumvented with a simpler procedure performed by the Unit Dispatch Optimizer (UDO) of EROM which consequently establishes a new relationship between the

near optimum overall turbine or unit efficiency and corresponding plant discharge by using the discharge limits and efficiency curves of each unit with Monte Carlo Sampling. As a result of this, the new relationship will be the ultimate efficiency curve of the plant and it is performed once at the initialization stage of EROM prior to simulation. Then, during the reservoir simulation at every time step, EROM will use this curve to decide which units to switch on and at what load percentage they will generate power to fulfill the proposed operational rules. However, in this method, convergence to the global maximum overall efficiency may be sacrificed slightly as a result of limited number of samples and inadequate discretization of the interval between minimum and maximum discharge of the plant Q_{Pmin} (m^3/s) and Q_{Pmax} (m^3/s). However, since the aim of this thesis to perform long term reservoir operation analysis to specify storage, release or energetic targets which are to be complied with in further complementary unit based short term operation analysis, the level of approximation to the global maximum overall efficiency is found adequate. Nevertheless, the followed procedure as it stands is far beyond the limits of complexity considered in most of the research conducted on long term reservoir operation. Detailed information about the calculations of UDO module is given in Appendix.

2.2.3 Numerical Solution of EROM

EROM consists of several sections that perform specific tasks. Every section is embedded with the building blocks (equations, routines and procedures) which help sections achieve their tasks. While it performs the simulation of a reservoir operation model under given inputs, EROM calls the sections which it is composed of in an appropriately organized sequence to obtain the requested outputs. The organization of the sections within EROM is illustrated in Figure 2.5 and described as follows.

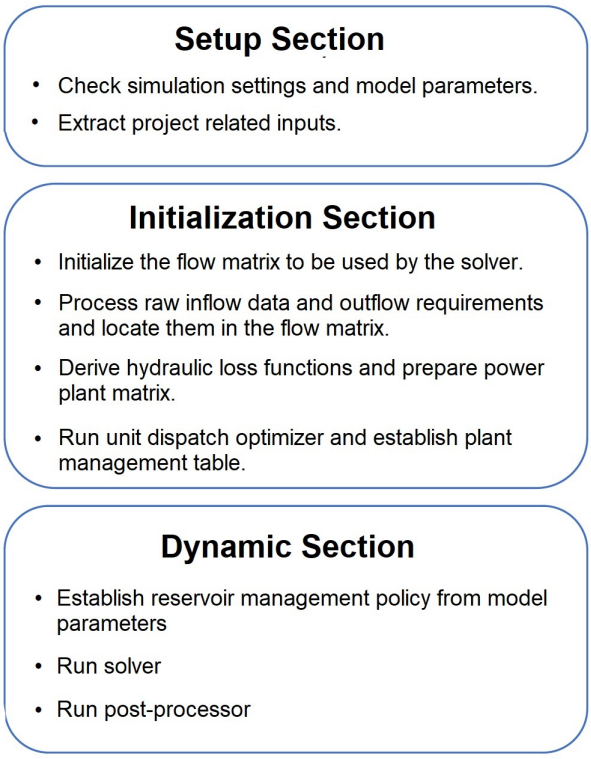

Figure 2.5: Organization of sections in EROM

First, EROM takes the model parameters and simulation settings defined by the user which involves the period, time step size and solver preferences of the simulation to be performed. Second, it runs the "Setup Section" to read all inputs related to project area to be modeled including initial and boundary conditions of reservoir storage and checks if the input data contains any error and it is consistent with the simulation parameters and settings. Third, the "Initialization Section" is performed to process the raw input data and arranges them into vectors and matrices that are used by the next section by considering the time step size and simulation period. In this section, user-defined penstock assembly information is processed to derive the total hydraulic loss occurring on each of the power generation units as a function of its turbine discharge. Then, the inputs related to hydropower plant are put in order so as to make it ready for the energy calculations at dynamic section. Unit dispatch optimizer (UDO) is also performed in the initialization section to derive a power

plant management table that gives the optimum discharge allocation over the units and lists overall efficiency of the power plant corresponding to the power plant discharge values between minimum and maximum operative plant discharge, Q_{Pmin} and Q_{Pmax}.

The dynamic section is the part where simulation parameters are incorporated into the data matrices and the preferred solver type is run. In this section, inflows and outflows except power plant discharge are defined for each time t. Then, the power plant discharge, Q_{P}, is specified with respect to the actual state at t which is storage in the reservoir and rule curve parameters. After that, the total power plant discharge is allocated into units by using power plant management table. Next, given turbine discharge values, hydraulic losses occurring on each of the units are evaluated (see Equations 2.10, 2.11, 2.12 and 2.13). And then, at each time t, the gross hydraulic head of each of the units are estimated and the net hydraulic head, H_{net}, is calculated by subtracting the total hydraulic loss, H_{f}, for each of the penstock assembly from the gross head of the related unit (see Equations 2.8 and 2.9). Finally, the reservoir storage and cumulative energy generated at time $t+1$ are calculated by using Equation 2.2 and 2.7, respectively. In addition, apart from the calculated storage and energy values, outflows that are used in these calculations are also stored in result matrix as a function of time. At the end of the dynamic section, a post processor which uses the result matrix is performed to obtain the objective function values and illustrations are also plotted if the user desires.

2.2.4 Operational Rules for Multireservoir Systems

Several rules have been introduced for the multireservoir system operations. Bower et al. [1962] proposed two rules: named as pack rule and hedging rule that help determine the releases during the periods of excessive inflows and droughts, respectively, for water supply and hydropower purposes. Pack rule attempts to increase the empty space in a reservoir

when the available water is excessive and releases over the targets still have benefits. Making empty space available in a reservoir might also decrease the probability of future spills in the system. Hedging rule specifies that during the periods of scarce inflow and demands are impossible to be fully met by the system a small deficit in downstream releases might be helpful to decrease the likelihood of more severe droughts in water supply and/or energy shortages in the future [Oliveira and Loucks, 1997].

Lund and Guzman [1999] introduced several widely used operational rules of single purpose multireservoir systems in order to understand their working mechanism. They classified the rules in accordance with the configuration of the reservoirs within the system as the rules for the reservoirs in series and parallel and described them as given below. In a water supply system, maximization of water amount delivered to the clients must be a reasonable objective which is the same as minimization of spills from the system. The shortages can most likely be prevented by fully utilizing the total runoff of the watershed. In a system where reservoirs are in series configuration, this objective can be achieved by simply filling the upstream reservoirs first and the ones located at downstream last. During the drawdown period, releases must be made by starting from the lowermost to uppermost reservoir in order to avoid an uncontrolled spillage from the system in case of early onset of refill season or continuous side flows unless keeping the storage upstream reservoirs causes a considerable loss by evaporation or seepage. If the latter is the case, the allocation of total storage of the system should be decided by weighting the evaporation and seepage losses against the spillage from the system due to maintaining the storage in lower reservoirs. The same rule can be applied for the systems having purpose of flood protection for a flood-prone zone at the downstream of the entire system as well since emptying lower most reservoir gives higher controllability of spills from the system which cause floods. In the same study, hydropower rules are classified as energy storage rules and hydropower generation rules which are valid for refill and drawdown seasons, respectively, for reservoirs in series formation. Energy storage rules suggest the same refilling order as of water supply and flood protection since

storage in higher reservoirs provides higher energy per unit volume of water stored and any spillage can then be captured in lower reservoirs. However, unlike the energy storage rules, hydropower production rules which are applied in drawdown season are different. Because upper reservoirs generate hydropower which eventually provide head and storage to downstream reservoirs to be used in power generation. This rule attempts to increase the generated energy from one unit volume of water by considering head, discharge and efficiency which are the products of energy equation. For this, water storage of the system is favored to be concentrated in reservoirs where rise in head is relatively higher with unit volume of water stored. In order to increase the efficiency of power generation, power must be generated from the power plants which have higher efficiency with regards to the current state of their storage levels. If the efficiency is not changing with head, the reservoirs that have power plants with higher efficiency should be used to store water. If the objective is to maximize the generated energy in a specified period in the system, this can be achieved by increasing the water release rates for power generation assuming rest of the variables of energy equation are the same. This time the storage of the system can be concentrated at the most downstream reservoir to obtain a high head for generation with an increased risk of spills since the all lateral inflows and releases of other reservoirs are more likely to fill the most downstream reservoir first. In some situations when the reductions or increase of total system storage might be obligatory, these reductions or increases must be made in the reservoirs which have least or highest ability of generating power, respectively.

For water supply reservoirs in parallel configuration with joint demands, that is, demands that can be met by either one or more of the multiple reservoirs in the system, space rule and NYC rule are applied. The space rule tries to equalize the ratios of empty space in reservoirs in parallel configuration at the end of a specified period to their forecasted inflow volume during the rest of the refill period. Unlike the space rule, the NYC rule aims to level the probability of filling of each reservoir however both rules are inclined to prevent the situation of spilling of one reservoir while the others have available storage space. It can be

also noted that a parallel configured reservoir system might consist of reservoirs with side demands, that is to say, each demand can be supplied by only one reservoir. In that case, the space rule can be modified to distribute the total available space in the system proportionally to the expected cumulative net inflow (inflow out of side demand) into each reservoir from the beginning of the period till the end of the refill season. During the drawdown season, total available water in the system should be allocated proportionally to the cumulative demand of each reservoir along the rest of the drawdown season [Oliveira and Loucks, 1997]. In some systems involving reservoirs with the purposes where operational benefits increase proportionally with surface level of the stored water, the reservoir in which unit volume of inflow reservation results in maximum water level change should be primarily used for storage. This operational strategy would be suitable for purposes such as hydropower and recreation as well as water supply where supplied water quality and pressure minimizes the cost of water to be supplied.

2.2.5 Performance Measures of Reservoir System Operations

Obtaining optimum reservoir operation strategy is an elaborate decision making process which necessitates computer modeling. In these models, due to the various purposes which are peculiar to the river/reservoir system under consideration, decision variables and decision criteria must be formulated appropriately in order to fit these purposes substantially. Therefore, the determination of how close given design solution converges the optimum operation strategy is an essential factor to be evaluated in order to measure the performance of the model at achieving the set objectives. In this thesis, the measure which helps analyze the performance of a set of decision variables is named as objective function and the events considered in its formulation as well as its calculation are described in Section 2.3.2.

The objective function can be selected as a penalty or a mathematical formulation which

reflects the operational benefits or costs of a reservoir system of interest. If the benefits of the system is in consideration and their measure can be represented with values in the analysis, the objective function is to be maximized. However, if the objective function is a penalty or a cost of failure which stands for the extent of meeting an objective, it is to be minimized. For instance, for a reservoir system with water supply purposes objective function can be expressed in terms of water supply revenues which are to be maximized or losses due to water supply shortages to be minimized. In addition, the benefits and the costs which can be represented in units such as dollars can be also formulated in the same objective function. However, different purposes of reservoirs usually make it difficult to quantify the objectives in a single function. Therefore, multiple decision criteria analysis can be performed by prioritizing the objectives as constraints

2.3 Nonlinear Optimization and Objective Functions

2.3.1 The Optimization Algorithm

The case studies of our interest within this thesis involve reservoir projects having both water supply and hydropower purposes that are discussed in Section 2.4 in detail. Since our aim is to increase the energy generation without causing serious shortage in water supply, the extent of fulfillment of these objectives can not be directly measured in terms of one conjoint unit. Therefore, we integrate the EROM with the evolutionary multiobjective optimization algorithm, AMALGAM, to judge the value of given set of decision variables with regard to the separately evaluated objective values in their actual units. The AMALGAM is a novel design which enables its user to achieve computationally fast and efficient as well as highly reliable results by implementing adaptive multimethod search concept [Vrugt, 2016].

Considering d number of decision variables arranged in a vector $\mathbf{x} = \{x_1, x_2, ..., x_{\mathrm{d}}\}$ and m

$(m > 1)$ objectives in the problem $\mathbf{F} = \{f_1(\mathbf{x}), f_2(\mathbf{x}), ..., f_{\mathrm{m}}(\mathbf{x})\}$ where $\mathbf{F}$ and $f(.)$ stand for objective space and the function or numerical model that computes the objective values of given $\mathbf{x}$, respectively. The mathematical expression of the problem where the objective values are to be minimized is given in Equation 2.14. Here, χ represents the feasible space of the decision variables to be selected from.

$$\arg\min_{\mathbf{x}\in\chi} \mathbf{F}(\mathbf{x}) = \{f_1(\mathbf{x}), f_2(\mathbf{x}), ..., f_{\mathrm{m}}(\mathbf{x})\} \tag{2.14}$$

Since the problem has multiple objectives, the solution will be a set of Pareto-optimal solutions, $\mathbf{P}(\mathbf{x})$, depending on the trade-offs among the m objectives [Vrugt, 2016]. Providing the set of optimal Pareto solutions, AMALGAM enables user to make the final decision to specify the most desirable variables regarding to the various possible points of perspectives.

2.3.2 Objective Functions

In the case studies we performed in this thesis, we specify 2 objective functions ($m = 2$ in Equation 2.14). These are average annual energy generated from the system ($f_1(\mathbf{x})$: E_{av}) in GWh/year and shortage index ($f_2(\mathbf{x})$: SI) that are arranged in the optimization equation given below (Equation 2.15). Here, the first objective function E_{av} accounts for the i th powerplant in the system of w powerplants unlike Equation 2.7 which is derived for only one power plant. Other terms T and T_{RC} represent the length of calculation period in terms of selected time step size and the number of time steps within the period that the adopted operation strategy repeats. In our simulations, we consider the time step size as one day, $T = 19724$ days and $T_{RC} = 365$ days that indicates we are seeking an optimum yearly operation strategy. The minus sign in $f_1(\mathbf{x})$ helps us convert the optimization process from minimization to maximization.

In order to effectively analyze the performance of the parameters in terms of water supply we opt for SI since it measures the magnitude of shortage in every time step unitless and

quantifies them quadratically along the calculation period. The terms V_{Shortage} and V_{Demand} in SI equation are the volume of water shortage and demand, respectively.

$$\arg\min_{\mathbf{x}\in\chi} \mathbf{F}(\mathbf{x}) = \begin{cases} E_{\text{av}} : f_1(\mathbf{x}) = & \dfrac{-\int_0^T \rho\, g\, \sum_{i=1}^{w} \sum_{j=1}^{n} \left[H_{\text{net } i,j}\; q_{i,j}(t)\, \eta_{\text{u } i,j}\right]}{T} T_{RC} \\ SI : f_2(\mathbf{x}) = & \dfrac{100}{T} \sum_{t=1}^{T} \left(\dfrac{V_{\text{Shortage}}}{V_{\text{Demand}}}\right)^2 \end{cases} \tag{2.15}$$

Chapter 3

Case Studies and Results

In this section, we illustrate three case studies performed on real-world projects for the purpose of testing EROM. The case studies involve the application of operation management analysis and optimization to two consecutive reservoirs which are named as Trinity and Lewiston Reservoirs located in the northern part of California Central Valley Project (CVP) by using EROM. Related reservoirs as well as their components (dams, powerplants and conveyance structures) form the Trinity River Division (TRD) of CVP. In the first part of this section, the aim is to describe the overview of TRD and the interaction of its facilities by elucidating the operational concerns of the process of water diversion to Sacramento River basin. The second part involves detailed information of numerical modeling procedure from the viewpoint of how project area is applied to EROM. The third part elaborates the assumptions, calculations and/or parameterization methods considered in each of the case studies by presenting the results and their interpretations.

3.1 Trinity River Division (TRD)

The Trinity River which is the main tributary of the Klamath River has a total drainage area of 7770 km^2 in northern California. Until the completion of the TRD facilities located on the river in the early 1960s, the basin provided approximately one third of the Klamath River average annual runoff volume which was consequently discharged into the Pacific Ocean. Figure 3.1 illustrates the TRD facilities and their interaction within the project area. Completion of the dams and starting operations in 1963 paved the way of supplying the CVP needs by storing and diverting up to 90 percent of the Trinity River's annual yield at Lewiston, California into Sacramento River basin. However, riverine habitats below Lewiston Dam degraded the fishery of the river declined significantly as a result of massive diversion. In order to determine the amount of water to release annually through the river to help fisheries recover and habitats improve, The Trinity River Flow Evaluation study was directed by Secretary of the Interior in 1981 [Fish et al., 1999].

Trinity Lake (formerly known as Clair Engle Lake) was constituted by the construction of Trinity Dam on the elevation of 588.26 m of the Trinity River. It can store up to 3019.50 hm^3 when it is operating on its maximum operation level of 722.38 m. By regulating its flows and reserving storage, Trinity Dam serves for multiple purposes. These include providing a storage source for the trans-basin diversion of Trinity River water to CVP with an average annual supply of 868.37 hm^3 by considering the needs of the Trinity River Basin, hydropower generation, flood protection and offering recreational activities on Trinity Lake.

On the immediate downstream side of the Trinity Dam is Lewiston Reservoir, whose water storage is held by Lewiston Dam, located about 11 km downstream from Trinity Dam, can impound up to 18.08 hm^3 of water between the elevations of 557.48 m and 579.73 m of Trinity River. The dam forms an afterbay to the outlet structures of Trinity Dam and regulates the needs of Trinity River Basin. In addition, it also provides a forebay to the 17.2-km-long

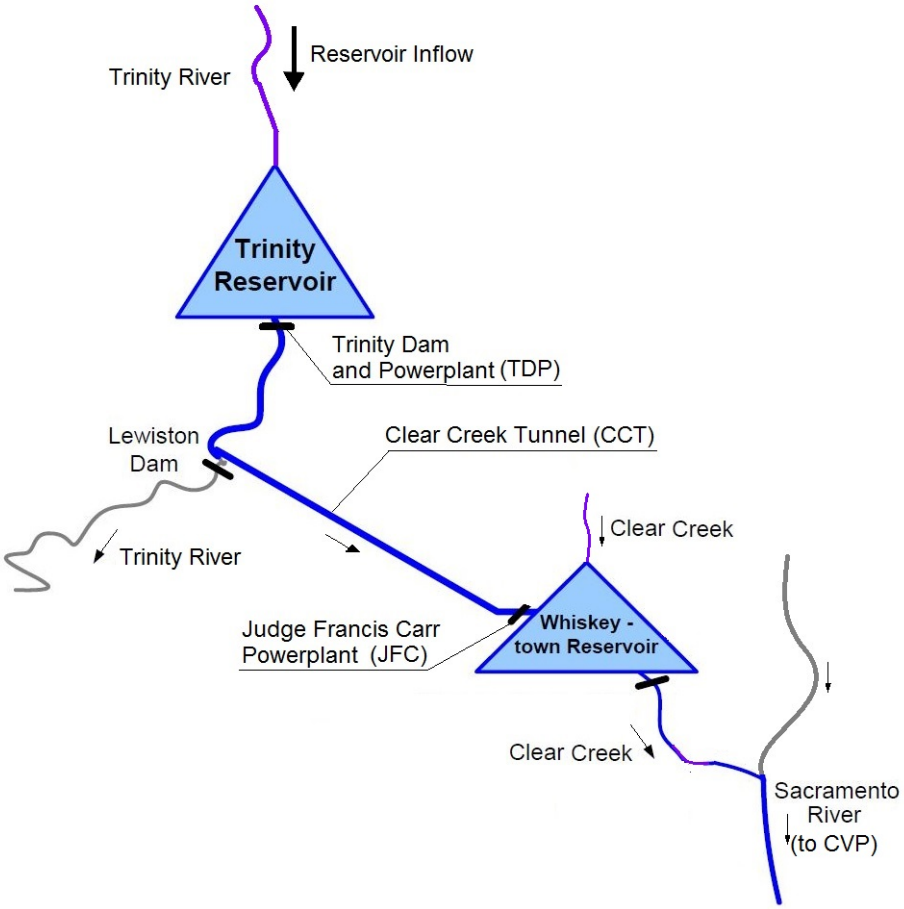

Figure 3.1: Schematic representation of Trinity River Division

Clear Creek Tunnel which conveys water from Trinity River to Whiskeytown Lake for the purpose of supplying CVP demands. Judge Francis Carr Powerhouse (JFC) located on the Clear Creek at the downstream end of the tunnel utilizes the potential energy of conveyed water with a total installed capacity of 154 MW before spilling down to Whiskeytown Lake.

3.2 TRD Numerical Model: Forcing Variables and Constraints

This section focuses on numerical modeling of Trinity Dam and Reservoir operations combined with Lewiston Dam, Clear Creek Tunnel and Judge Francis Carr Powerhouse by using EROM and integrating it with AMALGAM, the evolutionary multi-objective optimization algorithm, to obtain single reservoir optimum operations management strategy. The optimum strategy can be achieved by making the most appropriate release decisions from the Trinity Reservoir by taking several forcing variables (model inputs) and constraints into consideration. The following paragraphs describe the specifications of these forcing variables and constraints in detail.

One of the forcing variables of the Trinity Dam and Reservoir operations model is the daily inflow record of Trinity Reservoir which is obtained from The California Data Exchange Center (CDEC). Considering the time of construction completion for the project and data availability as well as complying with the first and the last day of a USBR water year, the period of inflow record and model simulations is taken as between October 1, 1963 and September 30, 2017. There are 35 missing, 901 negative values observed in 19724-day-long daily record. Missing values are completed by averaging the nearest 20 values to the each of the missing values. However, it is considered that the negative values of the inflow data could anticipate the influence of the water balance terms with high uncertainty such as evaporation, seepage and/or measurement errors of available gages and their presence in the water balance calculations is obligatory since it ensures the matching of calculated storage values with the storage records of the reservoir. Apparently, positive values might have been calculated by the same balancing procedure in order to match the calculated storage values with observations as well. Yet, one of the negative inflow values that was calculated as -1875 m^3/s on January 6, 1995, is detected as the only negative value which differs extremely from

the other negative values whose mean value is -3.90 m^3/s. Therefore, it is replaced with zero. Other than these, the inflow record used in the model evaluations is taken as it is published and respected as if it is fully representing the hydrological features of the basin. The resulting inflow record and average inflow volumes based on months are given in Figure 3.2 and 3.3.

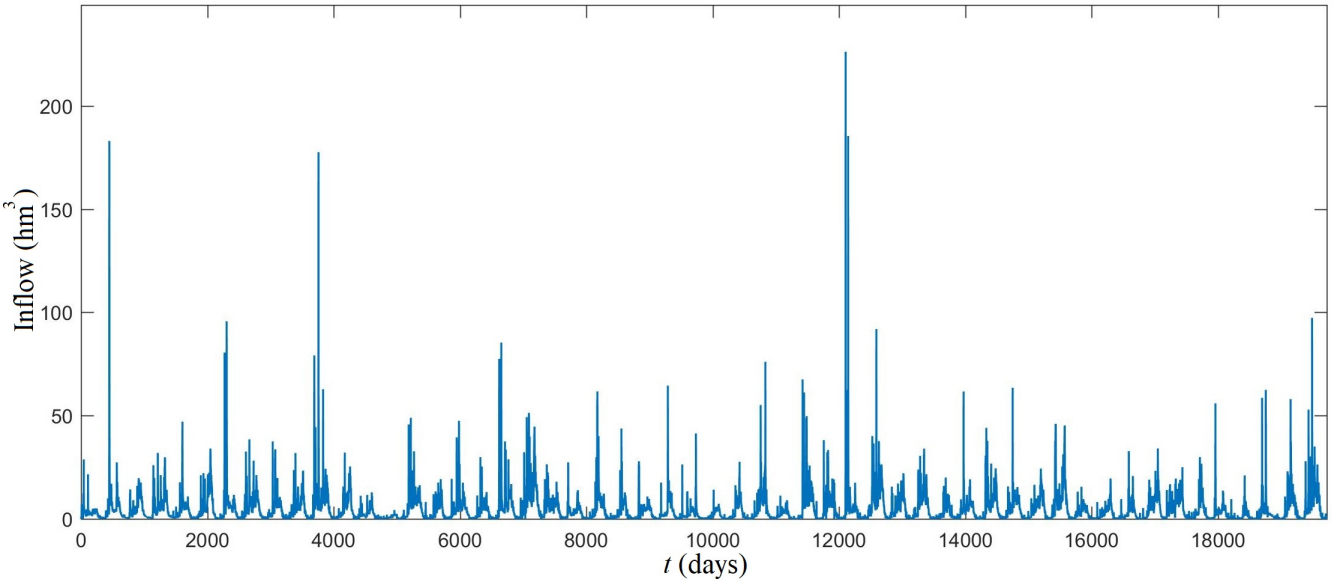

Figure 3.2: Daily Inflow Volume Record of Trinity Reservoir (Water Years 1964-2017)

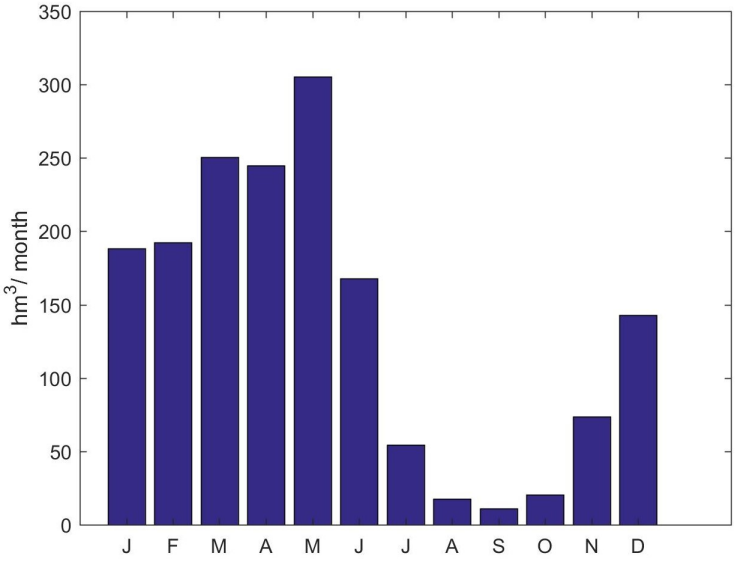

Figure 3.3: Monthly Average of Inflow Volumes of Trinity Reservoir (Water Years 1964-2017)

The second set of forcing variables of the model are the important water levels of the Trinity Reservoir. These are maximum and minimum operational water levels, $El_{\max}$ and $El_{\min}$ which define the upper and lower bounds of active storage, $S_{\max}$ and $S_{\min}$. While $El_{\max}$ is selected as the crest elevation of uncontrolled spillway weir of the dam, 722.38 m, $El_{\min}$ is considered as the minimum reservoir level needed for power generation, 653.80 m [Wahl and Cohen, 1999]. Corresponding values of $S_{\max}$ and $S_{\min}$ are 3019.50 and 386.22 hm^3, respectively.

The third forcing variable of the model is the elevation-area-volume relationship of the reservoir which is used as dataset while converting the water surface elevation to storage or vice versa and water surface elevation to water surface area. The elevation-storage relationship is obtained by plotting monthly water surface elevation versus monthly storage records of Trinity Reservoir found on CDEC website. Since, the resulting curve covers $S_{\max}$ and $S_{\min}$ sufficiently, it paves the way for using this relationship directly in EROM. However, the calculation of elevation-area relationship from the available elevation-storage record was not a convenient method for of approximating the known surface area values at specific reservoir levels. For this, we apply Equation (3.1) in order to add area function to the dataset [Marino and Loaiciga, 1983]. Figure 3.4 illustrates the established elevation-area-volume relationship of Trinity Reservoir.

$$A = 2.559S \tag{3.1}$$

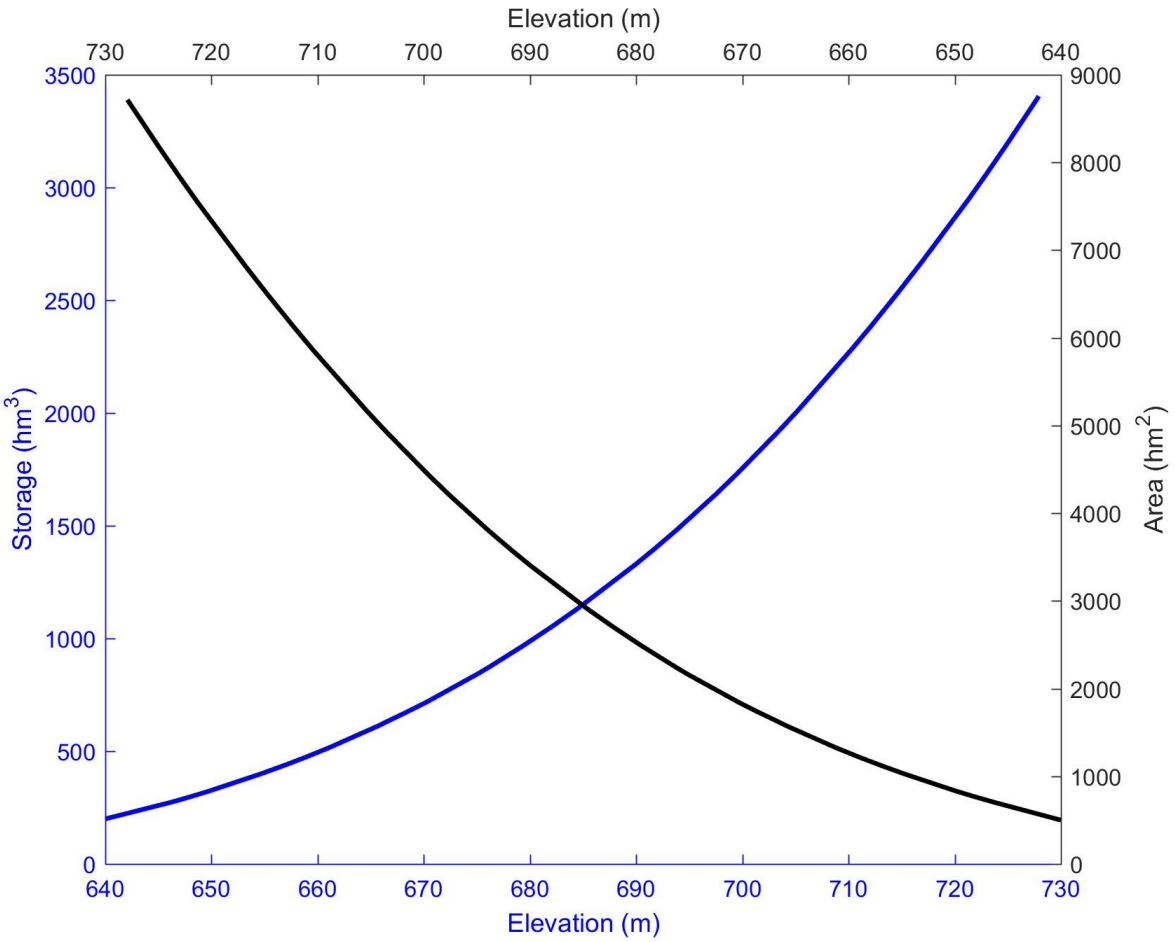

Figure 3.4: Elevation-Area-Storage Relationship of Trinity Reservoir

Another forcing variable is evaporation information which is first obtained as monthly volumetric values from CDEC. In order to better mimic the actual reservoir evaporation during the simulations, monthly evaporation depth of the reservoir is evaluated by dividing volumetric reservoir evaporation record by reservoir surface area corresponding to the recorded water level of that particular month. Then, monthly average evaporation depth is tabulated with respect to the months of the year (Table 3.1). Therefore, EROM can calculate the rate of evaporation, Q_{evap} (m^3/s), by considering the change in surface area of the reservoir and the month of any time within the simulation period by using Equation (2.4).

Table 3.1: Monthly Evaporation Depth of Trinity Reservoir in milimeters

J	F	M	A	M	J	J	A	S	O	N	D	Total
11	18	42	73	109	138	172	165	121	65	21	10	945

Trinity Dam can discharge water to downstream through power generation, river outlet works and an uncontrolled spillway. The water to be released from power plant and outlet works is conveyed by a penstock network. two of total four outlets of the network are connected to Trinity Dam Powerplant (TDP) with a total installed capacity of 140 MW that houses two identical energy generating units (turbine and generator set). Each of the units has one Francis turbine that can be operated up to a flow rate of 65.13 m^3/s. The flow rate of TDP and its maximum are symbolized as Q_{TDP} and Q_{TDPmax}, respectively. The latter two outlets of the penstock network are called as outlet works of the dam and they can discharge water to the river up to the total design flow rate of $Q_{\mathrm{TOWmax}} = 198.22\ m^3/s$ [Wahl and Cohen, 1999]. Thus, the total controlled release of the dam can be calculated as $Q_{\mathrm{rel,TDmax}} = 328.48\ m^3/s$ by summing the related capacity of these components. When the dam releases water through multiple outlets of the network at the same time, hydraulic losses occurring on penstock members located before the bifurcations increase quadratically with the flow rate passing through them (Equation 2.10 and 2.11). Consequently, these losses result in a considerable decline of generated energy depending on the frequency of multiple outlet releases made during the simulations. On the other hand, omitting this factor in the calculation of annual average energy which is the first objective function of the numerical model would derail the optimization results from their way to find the optimum operation strategy. As a result, it should not be underestimated and EROM takes this factor into consideration as well. It is also worth mentioning that in this study, we assume that the efficiencies of energy generating units (η_{u} in Equation 2.15) of two power plants (TDP and JFC) are constant. In fact, the actual efficiency of the units are dependent on the turbine discharge and the

hydraulic head. However, we anticipate that the public access to the efficiency- discharge - hydraulic head relationships to the units of both powerplants is restricted. Nevertheless, we desired to approximate the actual energy generation by assigning values that achieve the installed capacity of the units at maximum turbine discharge and the maximum hydraulic net head. The spillway of the Trinity Dam is a separate tunnel structure that discharges the excessive inflows of the reservoir safely to the river when the reservoir water level exceeds the crest elevation of its uncontrolled weir located in the reservoir. The flow capacity of the spillway is $Q_{\text{spill,TDmax}} = 835$ m^3/s [Rhone, 1960].

Releases from Trinity Dam constitute the inflow of Lewiston Dam. The contribution of run-off driven only from 66.3-km2-watershed of Lewiston Dam to its total inflow is neglected, because its drainage area corresponds to only 3.7 percent of that of Trinity Reservoir. The maximum and minimum observed operational water levels of Lewiston Reservoir are recorded as 580.61 and 580.06 m, respectively that bound 1.69 hm^3 of active storage. In other words, the dam has been used only as a small forebay for controlling the releases rather than utilizing its storage for future uses. Even though the active storage capacity of its reservoir is negligible compared to Trinity Reservoir, it ensures the fulfillment of Trinity River release objectives by using its controlled spillway with a flow rate capacity of 850 m^3/s. On the other hand, it also provides inter-basin transfer of its inflow via Clear Creek Tunnel with a flow rate of up to $Q_{\text{JFCmax}} = 102$ m^3/s. Hence, the presence of Lewiston Dam and its function has to be considered in this study.

Annual volume of water release from Lewiston Dam required for the restoration of fishery and riverine habitats of Trinity River which is determined by Trinity River Flow Evaluation study report are classified in 5 different water year classes with respect to the forecasted inflow of Trinity Reservoir given in Table 3.2. In that report, diverse flow-related geomorphic objectives and desired habitat conditions (microhabitat and temperature objectives) are aimed for each water-year class [Fish et al., 1999]. Figure 3.5 illustrates 5 different

hydrographs recommended by the report, each of them representing Lewiston Dam release schedule during the corresponding water year. In this thesis, the recommended release from the Lewiston Dam is denoted as Q_{Tr} and given in hm^3/day. The purpose of variable release flow rates which sum up to the corresponding annual release volumes given in Table 3.2 is to mimic the original within year flow regimes observed before the completion of TRD.

Table 3.2: Recommended annual release volumes in hm^3 from Lewiston Dam classified into water years with respect to the Trinity Reservoir annual inflow in hm^3 and their occurrence probability [Fish et al., 1999]

Water-Year Class	Release Volume	Trinity Reservoir Inflow	Occurrence Probability
Extremely Wet	1005.5	> 2467.0	0.12
Wet	864.7	1665.2 to 2467.0	0.28
Normal	797.9	1264.3 to 1665.2	0.20
Dry	558.3	801.8 to 1264.3	0.28
Critically Dry	454.7	< 801.8	0.12

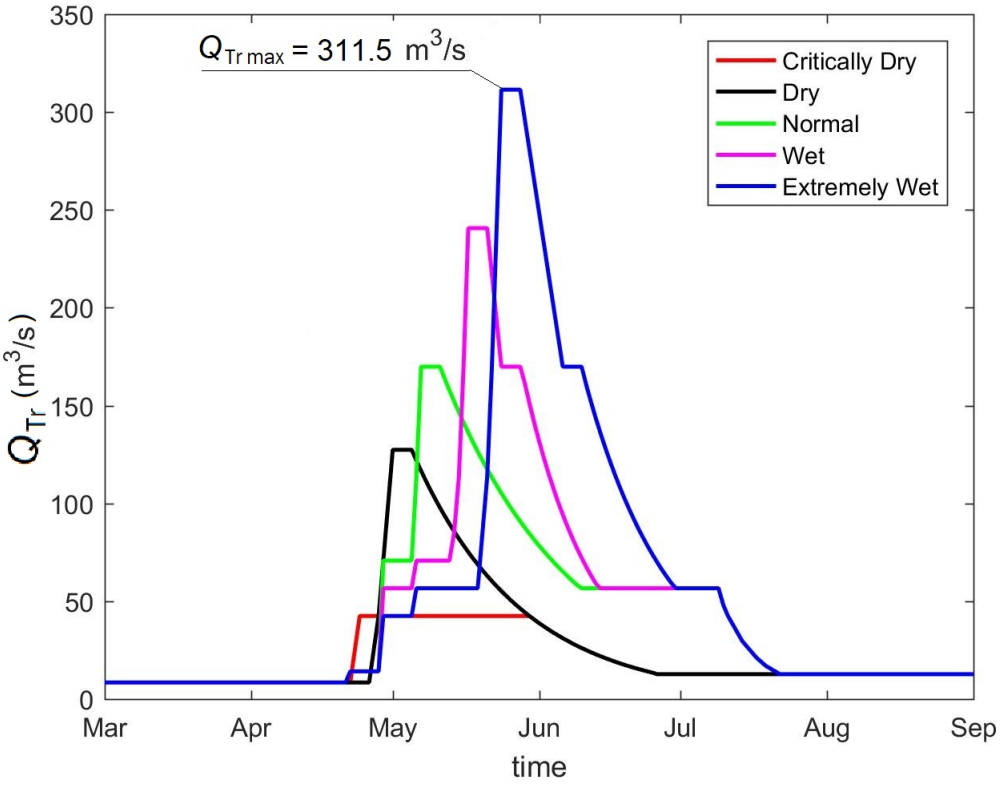

Figure 3.5: Annual recommended hydrographs of releases from Lewiston Dam (Q_{Tr}) for each water year class recommended by Trinity River Flow Evaluation study (For all hydrographs, Q_{Tr} = 12.74 m^3/s from July 22 to October 15 and Q_{Tr} = 8.50 m^3/s from October 16 to April 21)

Constraints:

The constraints of the Trinity Reservoir and Lewiston Dam operation study are listed below:

1. During the simulation of water storage at Trinity Reservoir at anytime if the reservoir water level exceeds the maximum operation level ($El_{\mathrm{max,\ TD}}$) of 722.38 m, spillway will release water at a constant rate of $Q_{\mathrm{spill,\ TD}}$ so as to lower the level back to $El_{\mathrm{max,\ TD}}$ at the end of the next day (Equations 2.5 and 2.6). If reservoir water level drops below the minimum operation level ($El_{\mathrm{min,\ TD}}$) of 653.80 m, the flow rates of other outlets that are TDP and outlet works (Q_{TDP} and Q_{TOW}, respectively) will be zero.

2. Total outflow rate of Trinity Reservoir out of evaporation rate which is also called as

tailwater flow rate of Trinity Dam and represented as $Q_{\text{tail, TD}}$ is the summation of Q_{TDP}, Q_{TOW} and $Q_{\text{spill, TD}}$. $Q_{\text{tail, TD}}$ that also forms the inflow rate of Lewiston Dam will be first used to supply Q_{Tr} to Trinity River from Lewiston Dam. If $Q_{\text{tail, TD}}$ is not adequate to satisfy Q_{Tr}, the difference is regarded as deficit and denoted by $Q_{\text{Tr, def}}$

3. If $Q_{\text{tail, TD}}$ larger than Q_{Tr}, the remainder flow after meeting Q_{Tr} will be diverted to CVP via Clear Creek Tunnel (CCT) and used in energy generation at Judge Francis Carr Power Plant (JFC) located at the end of the tunnel with a flow rate capacity of up to 102 m^3/s of CCT and JFC. The flow rate diverted to JFC through CCT and their capacity are represented with Q_{CVP} and Q_{JFCmax}

4. After all, if the inflow rate of Lewiston Dam still remains, it will be regarded as excess flow spilled from Lewiston Dam to Trinity River.

5. Flow rate of spillways must not exceed their flow capacity at any time for those belong to the Trinity Dam and Lewiston Dam.

The abovementioned procedure can be expressed in Equation 3.2 and 3.3 given below and used for the determination of Q_{CVP} and $Q_{\text{tail, LW}}$.

$$Q_{\text{CVP}} = \min(\max(Q_{\text{tail,TD}} - Q_{\text{Tr}}, 0), Q_{\text{JFCmax}}) \tag{3.2}$$

$$Q_{\text{tail, LW}} = Q_{\text{tail,TD}} - Q_{\text{CVP}} \tag{3.3}$$

3.2.1 Case Study I: Firm Yield Analysis

In this part, we aim to investigate the maximum constant flow rate that can be safely delivered to CVP from Trinity River along the inflow record length of 54 years of Trinity Reservoir and the applicability of this process without implementing any additional reservoir

management strategy. This constant flow rate is also called as "firm yield" in hydrology and it specifies the guaranteed benefits of the proposed water supply and hydropower projects. In the meantime, the desire is to evaluate the annual average firm energy generated from TDP and JFC, the annual average volume of water supplied to CVP as well as shortages of water delivery and excessive water release volumes on Trinity River from Lewiston Dam by complying with the constraints listed previously. For our upcoming case studies, we wish this investigation will provide a basis to compare and assess the performance of developed operation strategies with nonlinear multi-objective optimization by calculating how much additional energy (called as secondary energy) they can provide in addition to the firm energy.

In order to determine the firm yield that can be diverted to CVP, we perform several simulations with EROM by trialing a constant flow rate that will be diverted to CVP at each time. As a result, the firm yield supplied by the system to CVP is calculated as 22.7 m^3/s (1.96 hm^3/day). While the average total energy generation of the system is evaluated as 813.0 GWh/year, 46 % of the total generation is powered by TDP and the remaining 54 % is supplied from JFC. Apart from 52.8 hm^3/year evaporation loss, outflow of Trinity Dam which forms the inflow of Lewiston Reservoir is assessed as 1607.5 hm^3/year. While 1382.4 hm^3/year of this outflow takes source from energy generation at TDP, the remainder originates from the releases through outlet works and the overflows from the spillway with the rates of 89.3 and 135.8 hm^3/year, respectively. Related values are illustrated in Figures 3.6, 3.7 and 3.8. The results show that this operation strategy of Trinity Reservoir fails because of two reasons. First, discharge capacity of both Trinity Dam and Lewiston Dam spillways are exceeded once for 2 days with maximum average daily volumes of 175 hm^3 and 169 hm^3, respectively (Figure 3.6c). Second, 22.7 m^3/s of firm yield to CVP is not interrupted but it is decreased to 17 m^3/s 6 times (29 days in total) within the 54 years of calculation period (Figure 3.6b). The periods of shortage observed in the firm yield coincide with the days when at 311.5 m^3/s of peak rate of release to Trinity River from Lewiston Dam is demanded

in 6 of total 7 extremely wet years. In these periods, TDP and outlet works operates at their flow capacities are not sufficient to satisfy both Trinity River release and the firm yield. Therefore, in only one of the extremely wet years, the Trinity River peak demand can be compensated with the contribution of spilled flow rate observed in the same period to the total outflow. On the other hand, no shortage occurred in the supply of Trinity River recommended releases. However, the flow exceeds the recommended releases especially when the Trinity Dam spills. Average excess flow spilled from Lewiston Dam to Trinity River is calculated as 44 hm^3/year that occurs on 447 days out of total 19724 days of calculation period.

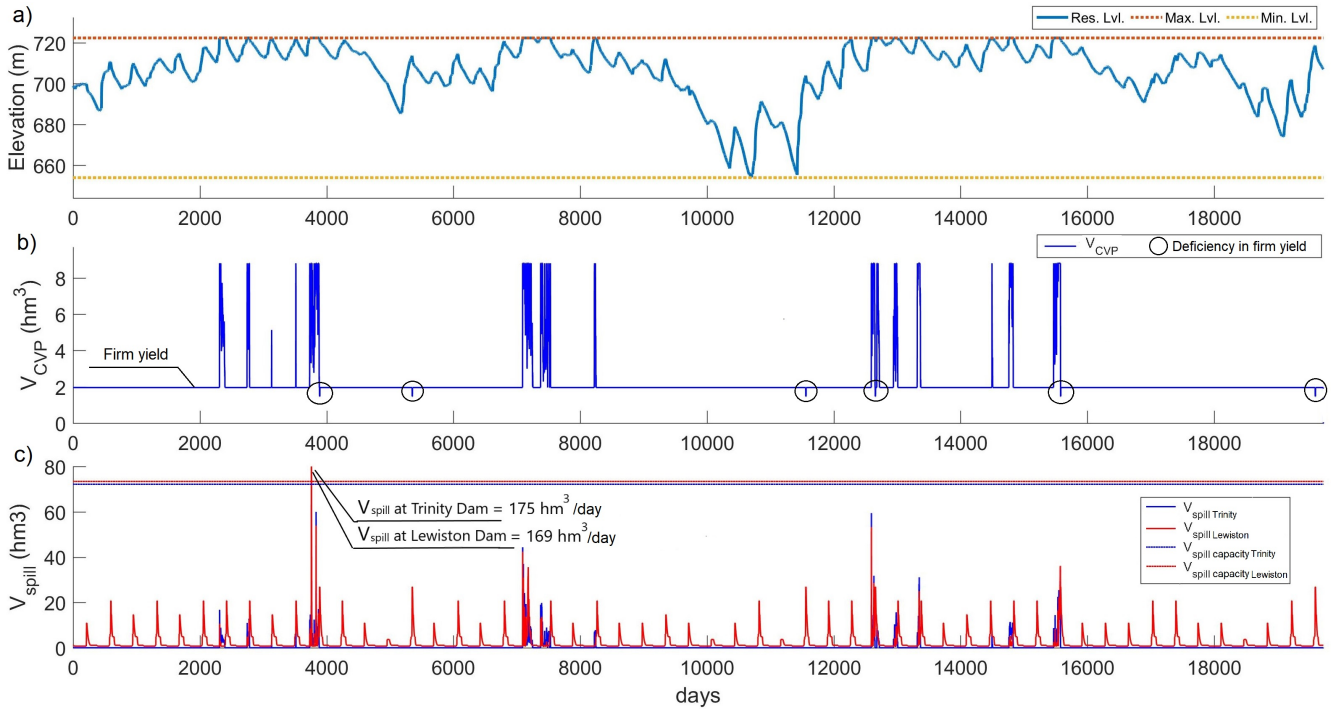

Figure 3.6: Reservoir elevation and flow related results of firm yield analysis in daily basis a) Reservoir water level b) Flow diverted to CVP c) Spilled flows from Trinity Dam (blue) and Lewiston Dam (red) and their spillway capacities (dashed horizontal blue and red lines, respectively)

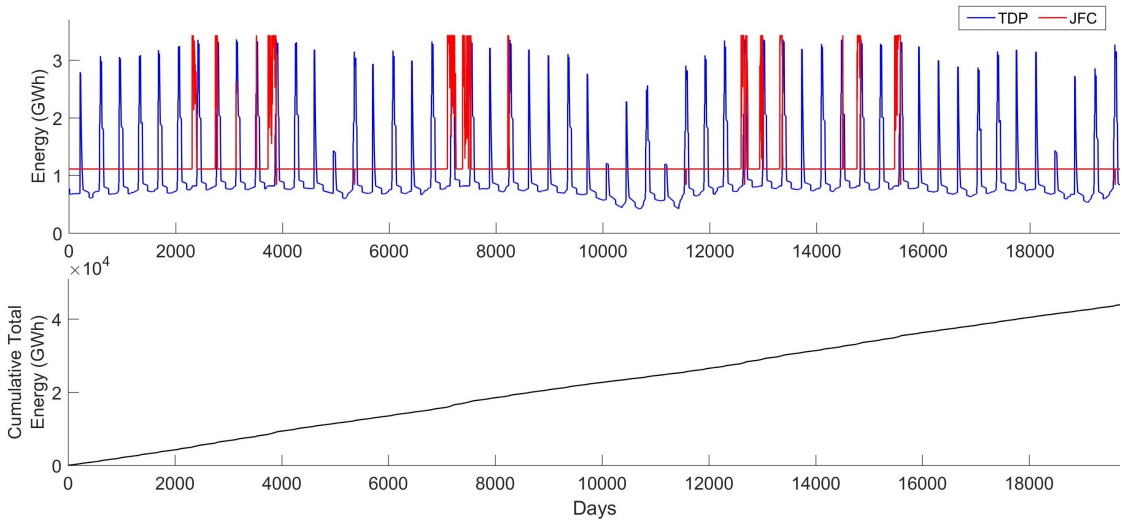

Figure 3.7: Generated energy related results of firm yield analysis in daily basis a) Daily energy generation at TDP (blue) and JFC (red) b) Cumulative plot of total generated energy

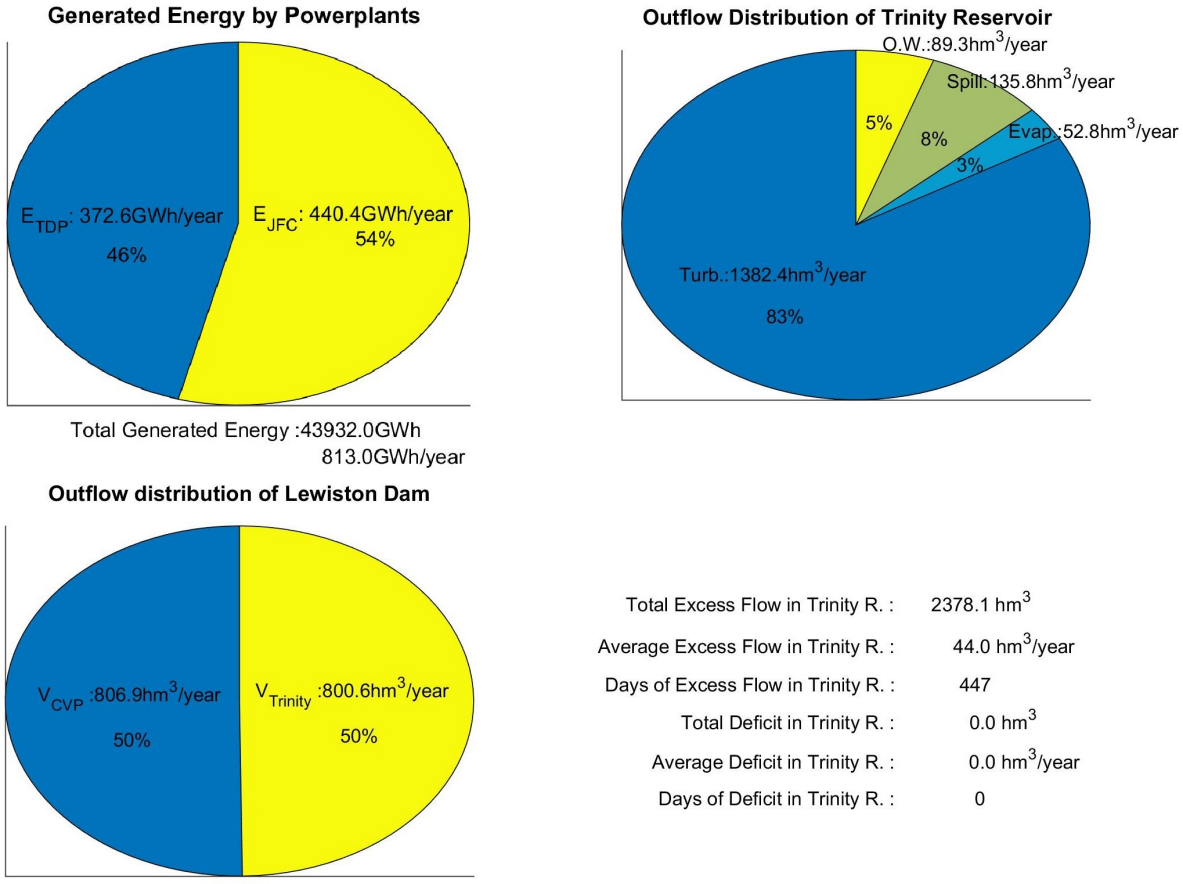

Figure 3.8: Pie charts of firm yield analysis showing a) allocation of energy generated by powerplants b) outflow distribution of Trinity Reservoir c) outflow distribution of Lewiston Dam

3.2.2 Case Study II: Optimization with RC 1

Apart from the failure caused by the surpass of spillway flow capacities for 2 days, it can be inferred from the results of the firm yield analysis that the 44.0 hm^3/year of excess flow of Trinity River, occurring on the days when the Trinity Reservoir spills, could be utilized by the energy generation at JFC as well as the CVP uses. This can be managed by designating a flood protection zone at the reservoir to mitigate the outflow rate of Trinity Dam (inflow rate of Lewiston Dam) by storing the severe part of the floods at the reservoir. However, reserving a constant empty space for this purpose along the entire water year could lead a considerable loss of hydraulic head unnecessarily. Instead, a boundary rule curve that separates a variable flood protection zone from the conservation storage by designating a higher empty space during the wet seasons such as in Figure 2.2 should be more useful not to sacrifice from the generated energy more than adequate.

In this case study, we intend to develop two 2-dimensional boundary rule curves which define the operational zones of Trinity Reservoir that yields more energy generation as well as more CVP water supply than those calculated in the firm yield operation strategy while complying with the same constraints. By considering the seasonal variability of Trinity Reservoir inflows, we predetermine the shape of these curves in terms of storage as a function of time as it is introduced by Tung et al. [2003] and here after we name this rule curve approach as RC1. As illustrated in Figure 3.9 where X and Y axis denote time, t, in days and storage, S, in hm^3, respectively, these 2 curves are identical in shape but the upper curve is formed by copying the lower rule curve entirely and shifting it on storage axis for a distance named as shift amount, $\Delta_{\text{U-L}}$, in hm^3. The shape of the curves consisting 3 plateaus and 2 inclined lines that connect two neighboring plateaus from the end of previous one to the beginning of the latter is assumed to be fixed for a water year and repeating along the calculation period of 54 years. Related shape can be expressed with 6 terms mathematically that indicate the coordinates of 4 break points of lower curve on time and storage axis. The

lower curve can be defined with four real time values (t_1, t_2, t_3 and t_4) in days between 0 and 365 and 2 storage values specified within the active storage range of the reservoir as the level of first plateau, $S_{\mathrm{L}(1,3)}$ and the level of second plateau, $S_{\mathrm{L}(2)}$ in hm^3 since the storage values of the first and the last plateau are equal. The mathematical expression of the curves are given in Equation 3.4 and 3.5 where the functions of upper and lower rule curves are symbolized with $S_{\mathrm{U}}(t)$ and $S_{\mathrm{L}}(t)$, respectively.

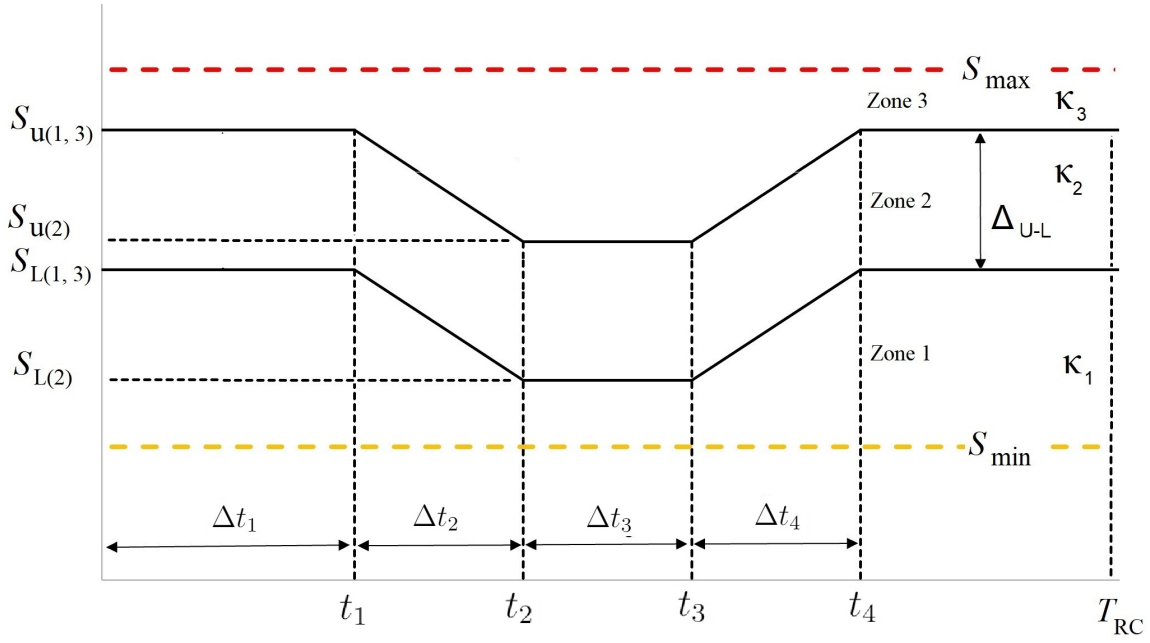

Figure 3.9: Schematic representation of upper and lower boundary rule curves (RC1 approach), $S_{\mathrm{U}}(t)$, $S_{\mathrm{L}}(t)$ respectively

$$S_{\mathrm{L}}(t) = \begin{cases} S_{\mathrm{L}(1,3)}, & \text{if} \quad 0 < t < t_1 \quad \text{or} \quad t_4 < t < T_{\mathrm{RC}} \\ S_{\mathrm{L}(1,3)} - \dfrac{S_{\mathrm{L}(1,3)} - S_{\mathrm{L}(2)}}{t_2 - t_1}(t - t_1), & \text{if} \quad t_1 < t < t_2 \\ S_{\mathrm{L}(2)}, & \text{if} \quad t_2 < t < t_3 \\ S_{\mathrm{L}(2)} + \dfrac{S_{\mathrm{L}(1,3)} - S_{\mathrm{L}(2)}}{t_4 - t_3}(t - t_3), & \text{if} \quad t_3 < t < t_4 \end{cases} \tag{3.4}$$

$$S_{\mathrm{U}}(t) = S_{\mathrm{L}}(t) + \Delta_{\mathrm{U\text{-}L}} \tag{3.5}$$

The role of the curves of RC1 approach for the operation of Trinity Reservoir can be described as follows: While the upper rule curve discerns the flood control zone (Zone 3 in Figure 3.9) from the conservation storage, the lower rule curve divides the conservation zone into two zones named as lower conservation zone and upper conservation zone (Zone 1 and Zone 2 in Figure 3.9, respectively). For each of the zones, we assign a fraction, κ, which corresponds to a specified constant rate of flow, $Q_{\mathrm{rel,TD}}$, to be released from the Trinity Dam. The idea here is to change $Q_{\mathrm{rel,TD}}$ from the dam in a water year corresponding to the storage deviations during a simulation. In other words, at any time the reservoir is to release water with the specified rate of release assigned to the zone into which current value of its storage falls. Equation 3.6 is designed to calculate $Q_{\mathrm{rel,TD}}$ according to which zone actual reservoir level is. One can easily observe from the equation that the dam will always release a mandatory flow rate at least to be able to meet Q_{Tr} unless the reservoir storage level drops below S_{min}. κ_1 and κ_2 decide how much flow to be released in addition to Q_{Tr} up to Q_{JFCmax} when the storage level is in conservation zone. Similarly, κ_3 of the flood protection zone specifies the rate of extra release but up to the total discharge capacity of the powerplant and outlet works. Now, the only question is how to decide whether the calculated value of $Q_{\mathrm{rel,TD}}$ is to be supplied from the turbined flow at TDP (Q_{TDP}) or the release from outlet works (Q_{TOW}) or using both. The allocation of $Q_{\mathrm{rel,TD}}$ over Q_{TDP} and Q_{TOW} is computed by using Equation 3.7. Here, the minimum flow required for the power generation from one unit at TDP (Q_{TDPmin}) is assumed as 7 m^3/s to make sure that the minimum value of Q_{Tr} (8.5 m^3/s) can be supplied by the flow released from power generation in case κ values are selected very low.

$$Q_{\mathrm{rel,TD}}(t) = \begin{cases} \kappa_3(Q_{\mathrm{TDPmax}} + Q_{\mathrm{TOWmax}} + \\ \quad - Q_{\mathrm{Tr}}(t)) + Q_{\mathrm{Tr}}(t), & \text{if} \quad S_{\mathrm{U}}(t) \leq S(t) \\ \kappa_2 Q_{\mathrm{JFCmax}} + Q_{\mathrm{Tr}}(t), & \text{if} \quad S_{\mathrm{L}}(t) \leq S(t) < S_{\mathrm{U}}(t) \\ \kappa_1 Q_{\mathrm{JFC}max} + Q_{\mathrm{Tr}}(t), & \text{if} \quad S_{\mathrm{min}} \leq S(t) < S_{\mathrm{L}}(t) \\ 0, & \text{if} \quad S(t) \leq S_{\mathrm{min}} \end{cases} \tag{3.6}$$

$$[Q_{\mathrm{TDP}}(t), Q_{\mathrm{TOW}}(t)] = \begin{cases} [Q_{\mathrm{TDPmax}}, \min(Q_{\mathrm{rel,TD}}(t)+ & \\ -Q_{\mathrm{TDPmax}}, Q_{\mathrm{TOWmax}})], & \text{if} \quad Q_{\mathrm{TDPmax}} \leq Q_{\mathrm{rel,TD}}(t) \\ [Q_{\mathrm{rel,TD}}(t), 0], & \text{if} \quad Q_{\mathrm{TDPmin}} \leq Q_{\mathrm{rel,TD}}(t) < Q_{\mathrm{TDPmax}} \\ [0, Q_{\mathrm{rel,TD}}(t)], & \text{if} \quad Q_{\mathrm{rel,TD}} < Q_{\mathrm{TDPmin}} \end{cases} \tag{3.7}$$

Decision Variables

In the present study, we consider 10 decision variables (parameters) whose best values are to be decided as a result of optimization procedure. Six parameters are used to represent the lower rule curve, four of which signify the periods between 0, t_1, t_2, t_3 and t_4, (Δt_1, Δt_2, Δt_3 and Δt_4 in days), and the last two parameters determine the height (measured in units of storage, hm^3) of the first and third plateau, $S_{\mathrm{L(1,3)}}$, and that of the second plateau, $S_{\mathrm{L(2)}}$, respectively. In addition to those, the shift amount, $\Delta_{\mathrm{U\text{-}L}}$ (in hm^3) that defines the upper rule curve and the release fractions of 3 zones (κ_1, κ_2 and κ_3) constitute the set of total 10 variables. The parameter set can be expressed in the decision vector, $\mathbf{x} = \{\Delta t_1, \Delta t_2, \Delta t_3, \Delta t_4, S_{\mathrm{L(1,3)}}, S_{\mathrm{L(2)}}, \Delta_{\mathrm{U\text{-}L}}, \kappa_1, \kappa_2, \kappa_3\}$. The flow diagram of the EROM model which illustrates the application of RC1 approach given in Figure 3.33 in Appendix section.

Feasible Ranges of Decision Variables

During the optimization process, each decision variable must be valued in a certain range in which they become technically feasible and/or meaningful. These ranges are defined with upper and lower limiting values of the variables. Each range forms 1 dimension of the solution space having a total number of dimensions equal to the total number of parameters considered. In order to not exceed the limits of the solution space, the optimization algorithm

suppresses the selection of the decision variables by using the values of limiting values defined for the each variable. The specified feasible ranges of designed parameters for this case study are tabulated below.

Table 3.3: Model parameters in Case Study 1 and their ranges

Decision Variable	Minimum	Maximum	Units
Δt_1	0	365	Days
Δt_2	0	365	Days
Δt_3	0	365	Days
Δt_4	0	365	Days
$S_{\mathrm{L}(1,3)}$	$S_{\min}$	$S_{\max}$	hm^3
$S_{\mathrm{L}(2)}$	$S_{\min}$	$S_{\max}$	hm^3
$\Delta_{\mathrm{U\text{-}L}}$	0	$S_{\min}$ - $S_{\max}$	hm^3
κ_1	0	1	-
κ_2	0	1	-
κ_3	0	1	-

Optimization Results

The multiobjective optimization is performed by using 100 population and 250 generations at AMALGAM. Figure 3.10 plots the objective function values of the final population after 250 generations that form the optimum Pareto front. The single-objective solutions are computed as follows. While the maximum average annual generated energy E_{av} is evaluated as 883.1 GWh, the shortage index (SI) becomes 13.55 % ($F_{1,\mathrm{opt}}$). When the minimum value of SI is achieved as 0 %, E_{av} is calculated as 871.9 GWh ($F_{2,\mathrm{opt}}$). The solutions out of $F_{1,\mathrm{opt}}$ and $F_{2,\mathrm{opt}}$ in the figure illustrate the tradeoff occurrence between E_{av} and SI.

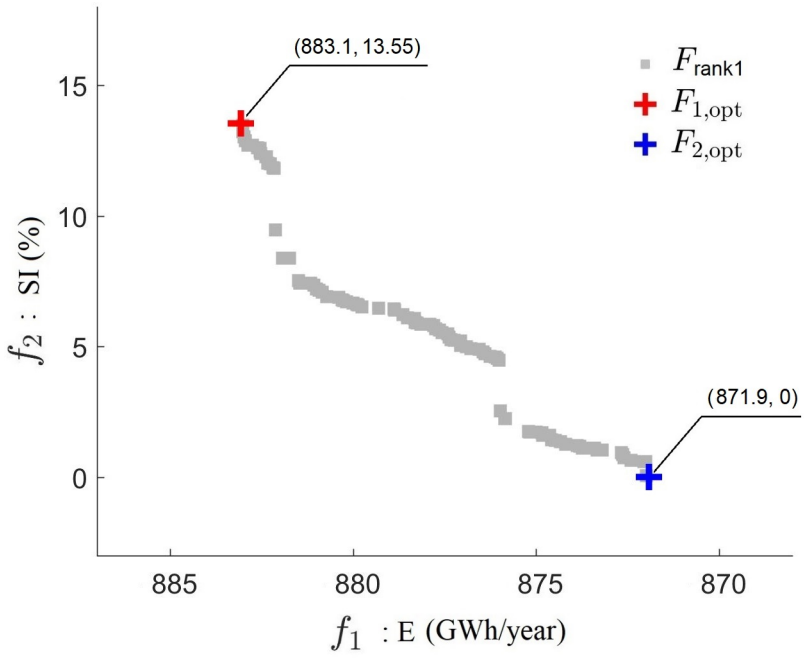

Figure 3.10: Illustration of objective function values of AMALGAM sampled rank1 Pareto front (RC1 assumption)

In Figure 3.11, Pareto uncertainty for each parameter of the model is elucidated. Individual parameters are located along the x-axis, while the y-axis specifies their normalized ranges. Each line of the graph represents one Pareto solution from the final population sampled with AMALGAM. The red and blue lines are plotted correspond to the parameter values of the single-objective solutions $F_{1,\text{opt}}$ and $F_{2,\text{opt}}$, respectively. It can be inferred from this plot that while the other parameters are valued in the regions within 0.15 to 0.25 of their feasible range, κ_3 has one specific value ($\kappa_3 = 0.12$) that satisfies the sampling of rank 1 Pareto front. Figure 3.12 maps the correlation coefficients of the parameters of final population. It shows that $\Delta_{\text{U-L}}$ is in a strong positive correlation with κ_2 while it has a negative correlation with $S_{\text{L}(1-3)}$. The physical meaning of this is that the more capacity is assigned to the upper conservation zone by procuring most of the volume for expansion from lower conservation zone, the more flow is to be released from the reservoir when the water level is within that zone. Figure 3.13 reveals the marginal distribution of the parameter values. One can easily

notice from this figure that while time parameters Δt_1, Δt_2, Δt_3 and Δt_4 of rank 1 solutions are relatively well-distributed over a wider span in their feasible ranges, other parameter values are clustered around one or more specific points.

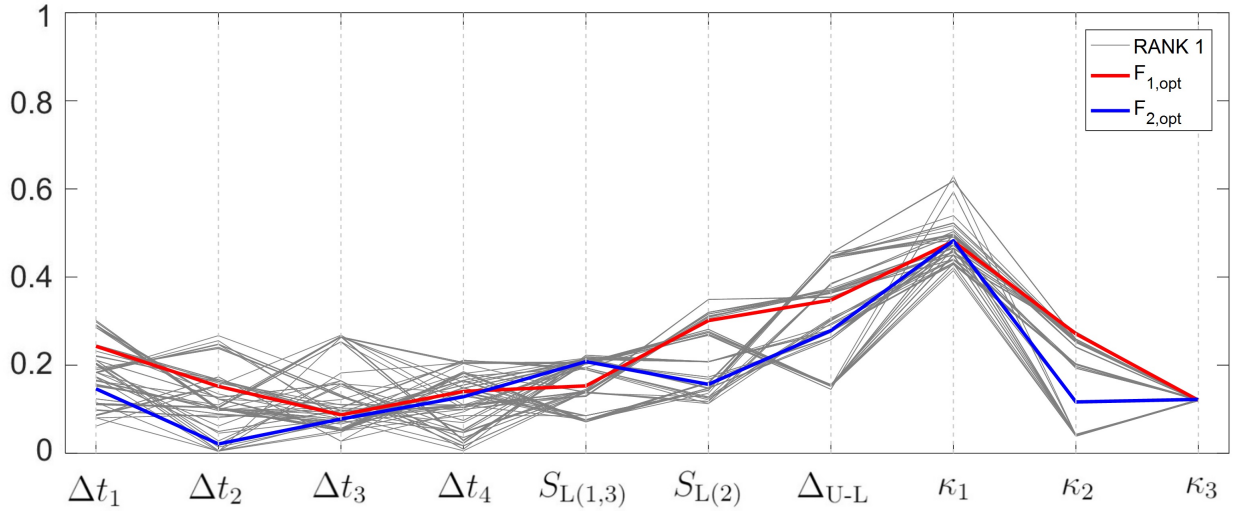

Figure 3.11: Normalized ranges of Pareto solution samples(RC1 assumption)

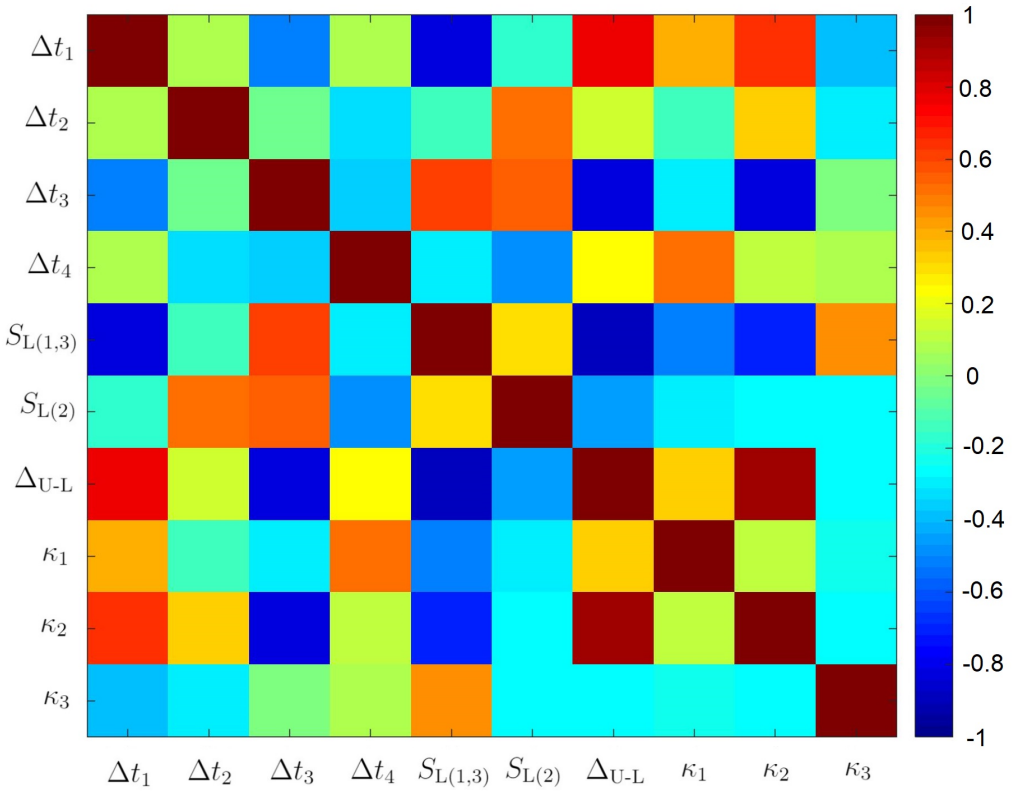

Figure 3.12: Map of correlation coefficients of Pareto parameter samples (RC1 approach)

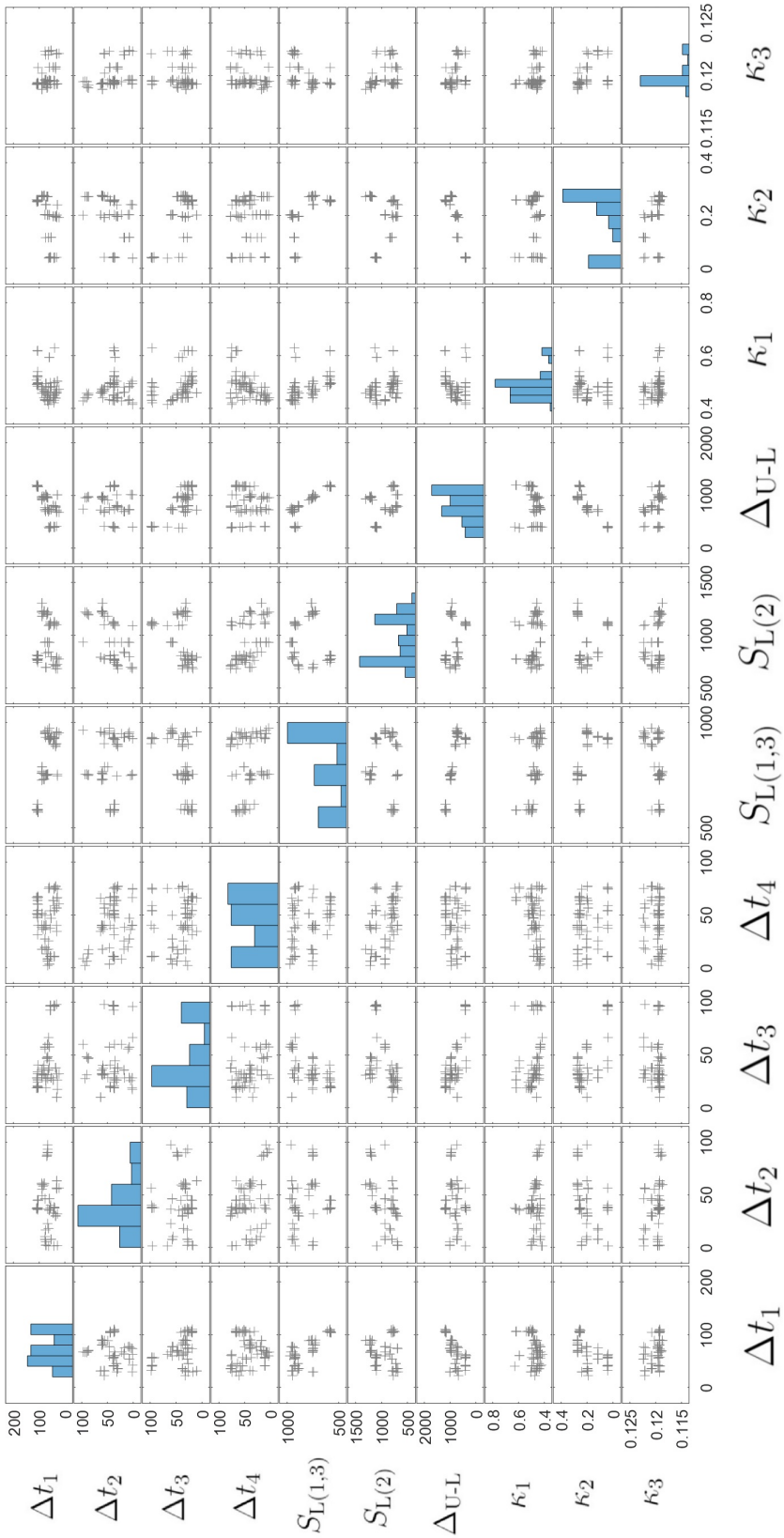

Figure 3.13: Marginal distributions and scatter plots of Pareto rank 1 solutions (RC1 approach)

Figure 3.14 aims to illustrate the boundary rule curves and the release fractions (release rule curves) established with the real values of the sampled parameters that form optimum Pareto front. Similarly, the previous graph the red and blue lines correspond to the parameter values of $F_{1,\text{opt}}$ and $F_{2,\text{opt}}$, respectively. The elevation differences between the plateaus of the resulting boundary rule curves are maximum 20 m and 15 m for those belong to lower and upper rule curves, respectively. The shape of the rule curve of $F_{1,\text{opt}}$ solution shows that the boundaries of the reservoir zones are shifted upwards starting from early January to late April by leading expansion of lower conservation zone and reduction of flood protection zone with a peak period during March. On the contrary, the zones belonging to $F_{1,\text{opt}}$ solution are shifted slightly downwards, resulting in a shrinkage at the lower conservation zone and expansion in flood protection zone during the period starting from early December till late February with a peak period occurring in throughout December. The grey curves drawn by the parameter values of other rank 1 samples deviate in time and elevation axes but they still conform with the shape of the curves belonging to the single-objective solutions.

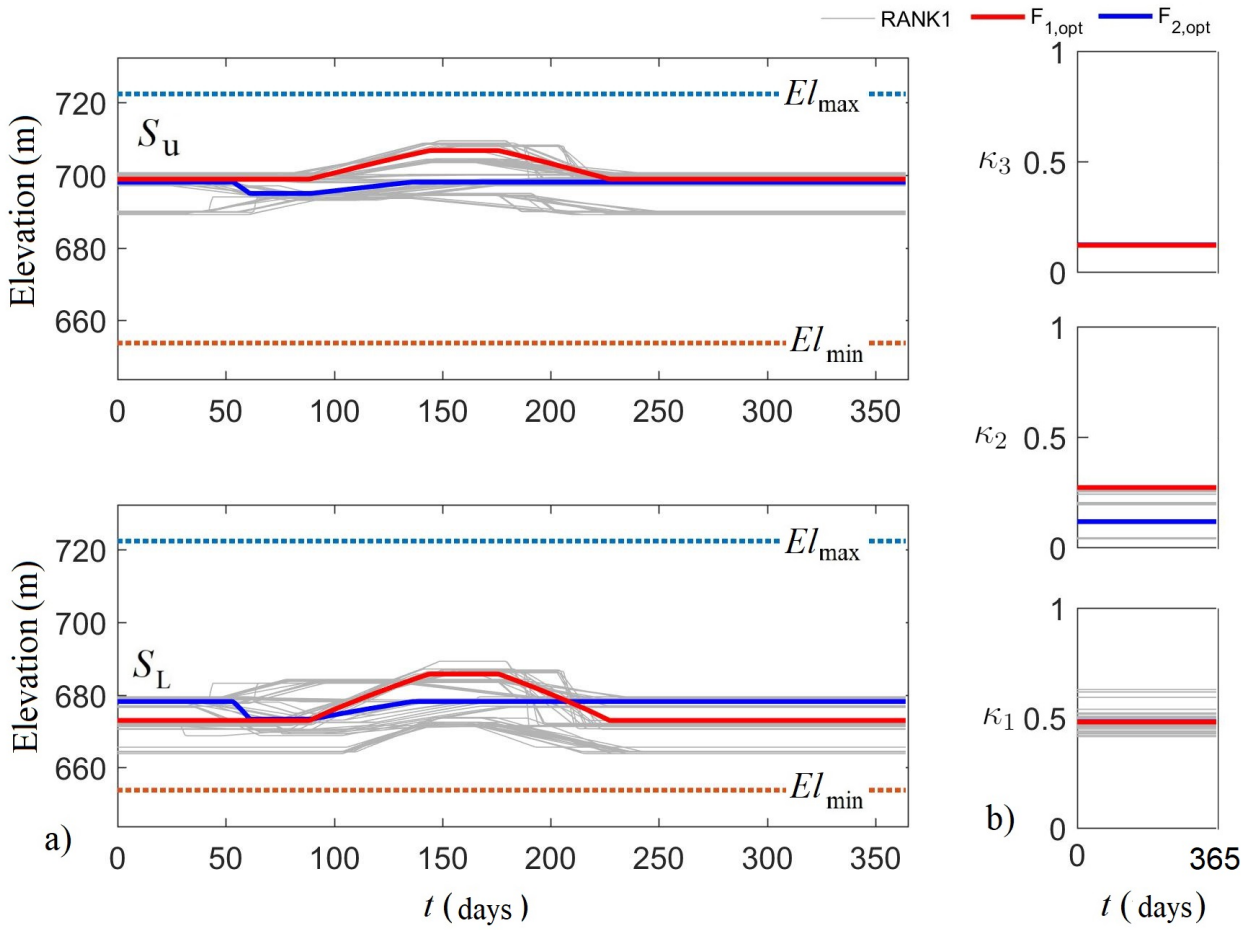

Figure 3.14: Boundary and release rule curves plotted from the values of associated rank 1 Pareto samples (RC1 approach) a) Lower and upper boundary rule curves (S_{L} and S_{U}) drawn with the values of rank 1 Δt_1, Δt_2, Δt_3, Δt_4, $S_{\mathrm{L}(1-3)}$, $S_{\mathrm{L}(2)}$ and $\Delta_{\mathrm{U\text{-}L}}$, respectively) on the active storage range (Lower graph illustrates the lower boundary rule curves that separate conservation zone into 2 zones, upper graph depicts upper boundary rule curves that discern flood control zone from conservation storage) b) Depiction of release rule curves plotted from the values of rank 1 κ_1, κ_2 and κ_3.

Simulation Results of $F_{\mathbf{1,opt}}$ solution

Parameter values that achieve $F_{1,\mathrm{opt}}$ are rerun to obtain the graphical outputs of that simulation. Figure 3.15a shows that the water level at Trinity Reservoir is mostly in the conservation zone and it drops below El_{min} frequently. However, it rises up and enters the flood protection zone, follows within that zone approximately 10 years in total and barely

reaches the maximum operation level 6 times in those periods. It is noted in Figure 3.17 that the number of days of deficit in Trinity River release is 2673 with an average magnitude of 57.6 hm^3/year that resulted in a shortage index of 13.55. In those days, the CVP water supply and energy generation at JFC ceased as well. Excessive releases to Trinity River is minimized to 0.3 hm^3/year since the Trinity Reservoir spills only 1.1 hm^3/year which corresponds to 0.7 % of it is annual average outflow and 98 % of its outflow flows through its controlled structures. Therefore, the designated flood protection zone works well for controlling the massive floods. Thus, the average annual turbined flow becomes 1552.9 hm^3/year and constitutes the 92 % of its annual outflow. Despite the increase of 170 hm^3/year water release through the turbines at TDP, the reduction of average water level in the reservoir reduces the hydraulic head on the units and results in a loss of approximately 9 GWh/year of generated energy at TDP compared to the one generated in the firm yield analysis. However, this energy loss is compensated by the increased energy generation at JFC owing to the minimized uncontrolled spills.Energy generation at JFC is increased approximately 78 GWh/year compared to the one generated in firm yield analysis. These results show that the designation of flood protection zone at Trinity Reservoir improves the energy efficiency of the system considerably.

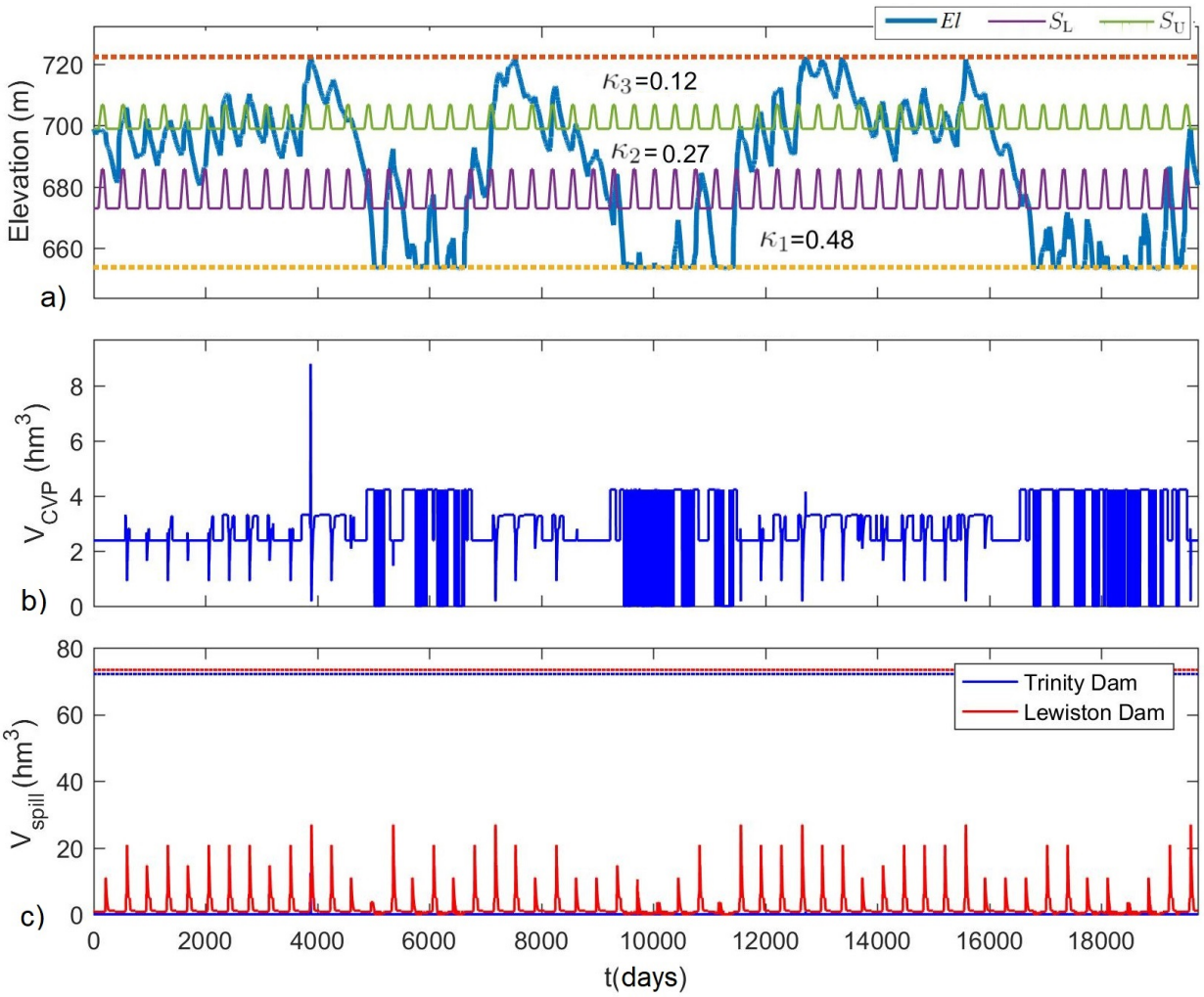

Figure 3.15: Simulation results of the run performed with the parameters of $F_{1,\text{opt}}$ solution in daily basis. a) Reservoir water level along with boundary rule curves (S_U and S_L) and release fractions of the operational zones (κ_1, κ_2 and κ_3) b) Flow diverted to CVP (V_{CVP}) c) Spilled flows (V_{spill}) from Trinity Dam (blue) and Lewiston Dam (red) and their spillway capacities (dashed horizontal blue and red lines, respectively)

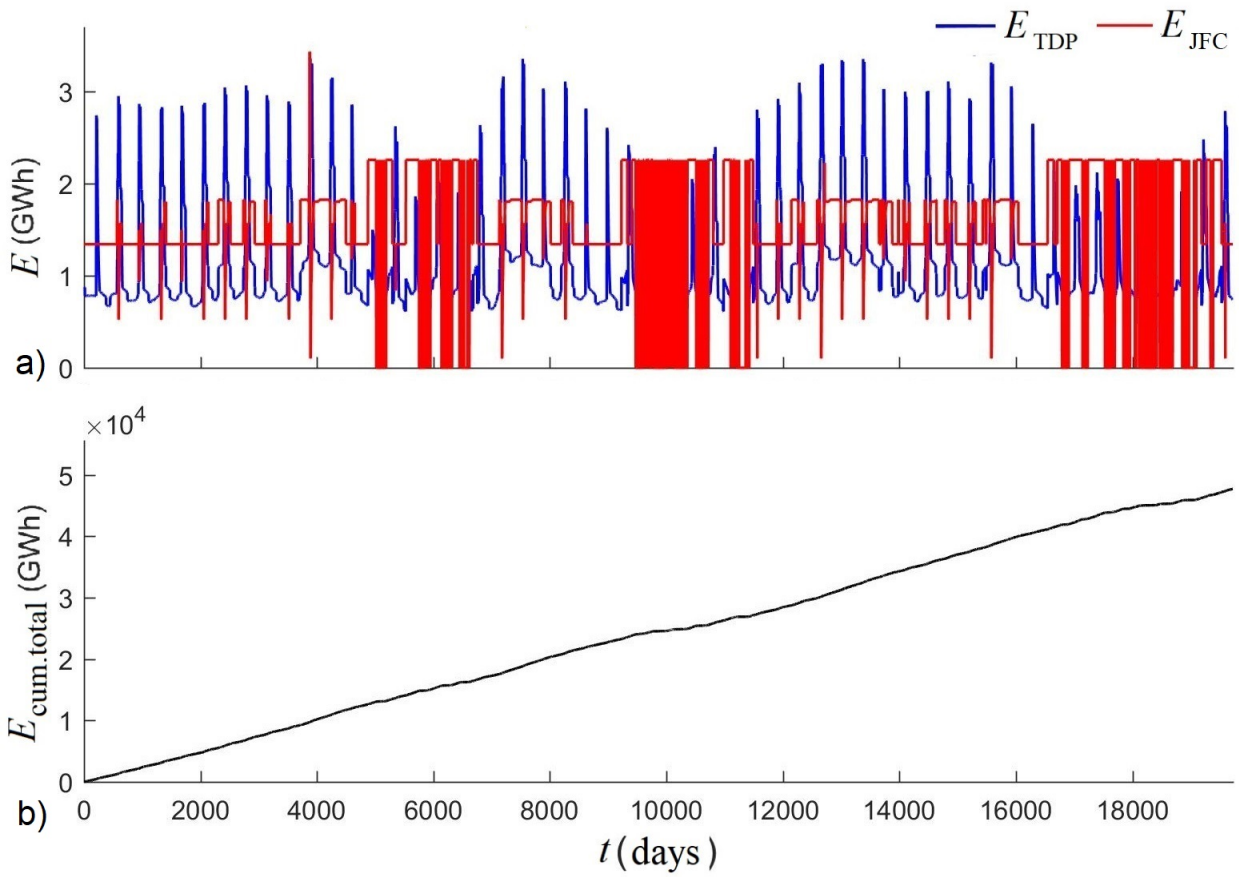

Figure 3.16: Energy related simulation results of the run performed with the parameters of $F_{1,\text{opt}}$ solution in daily basis. a) Daily energy generation at TDP (blue) and JFC (red) b) Cumulative plot of total generated energy

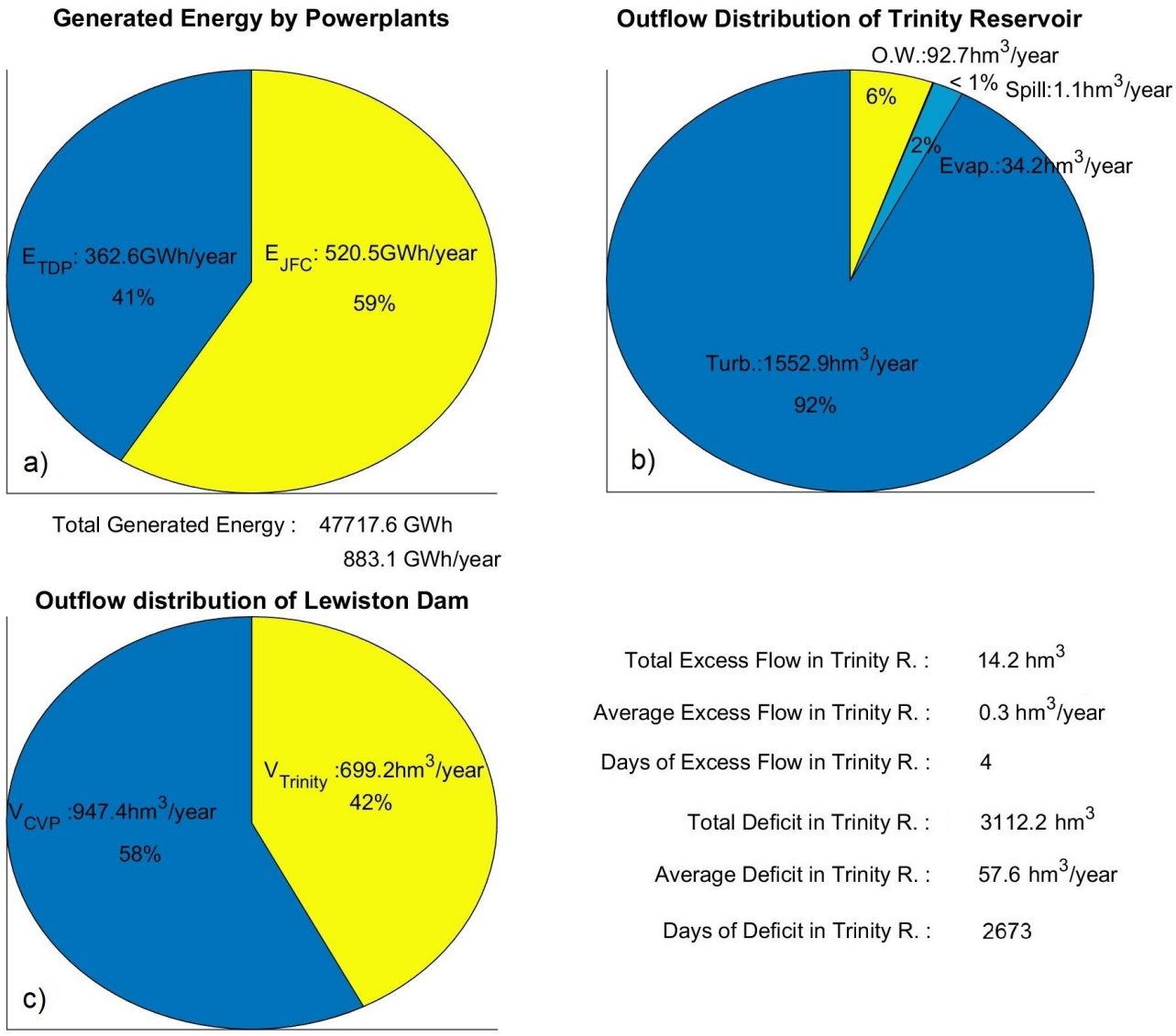

Figure 3.17: Pie chart simulation results of the run performed with the parameters of $F_{1,\text{opt}}$ solution a) allocation of energy generated by TDP (E_{TDP}) and JFC (E_{TDP}) b) Outflow distribution of Trinity Reservoir c) Outflow distribution of Lewiston Dam

Simulation Results of $F_{2,\text{opt}}$ solution

After running the simulation with the parameter values of $F_{2,\text{opt}}$ solution, this time reservoir level traces within the flood protection zone for most of the calculation period. Apart from the small reduction in the plateaus of boundary rule curves the only parameter which attempts to maintain the reservoir level far from the minimum water level is the reduced

value of $\kappa_2 = 0.12$ while κ_1 and κ_3 are selected the same as the ones belong to $F_{1,\text{opt}}$ solution. This attempt leads to a 20.7 hm^3/year rise in spill and 11.4 hm^3/year evaporation and 26 hm^3/year drop in turbined outflows at Trinity Dam. The spilled flow from Trinity Dam constitutes a massive inflow volume in a small period that its majority can not be diverted to CVP because of limited CCT capacity and turns into excessive releases to Trinity River from Lewiston Dam for 83 days in 54 years of calculation period with an average annual flow of 4.2 hm^3/year whereas $F_{1,\text{opt}}$ solution fails to meet 57.6 hm^3/year portion of Trinity River demands. These two contradicting occurrences between $F_{1,\text{opt}}$ and $F_{2,\text{opt}}$ result in the majority of 75.7 hm^3/year of reduction in CVP water supply as well as the generated energy at JFC. Even though the average water level at Trinity Reservoir increases the energy generation at TDP in $F_{2,\text{opt}}$, it can only compensate 33.9 of 44.1 GWh/year energy loss in JFC compared to the one obtained from $F_{1,\text{opt}}$. The Figures 3.18, 3.19 and 3.20 summarizes the values discussed above by illustrating them in the related graphs and charts.

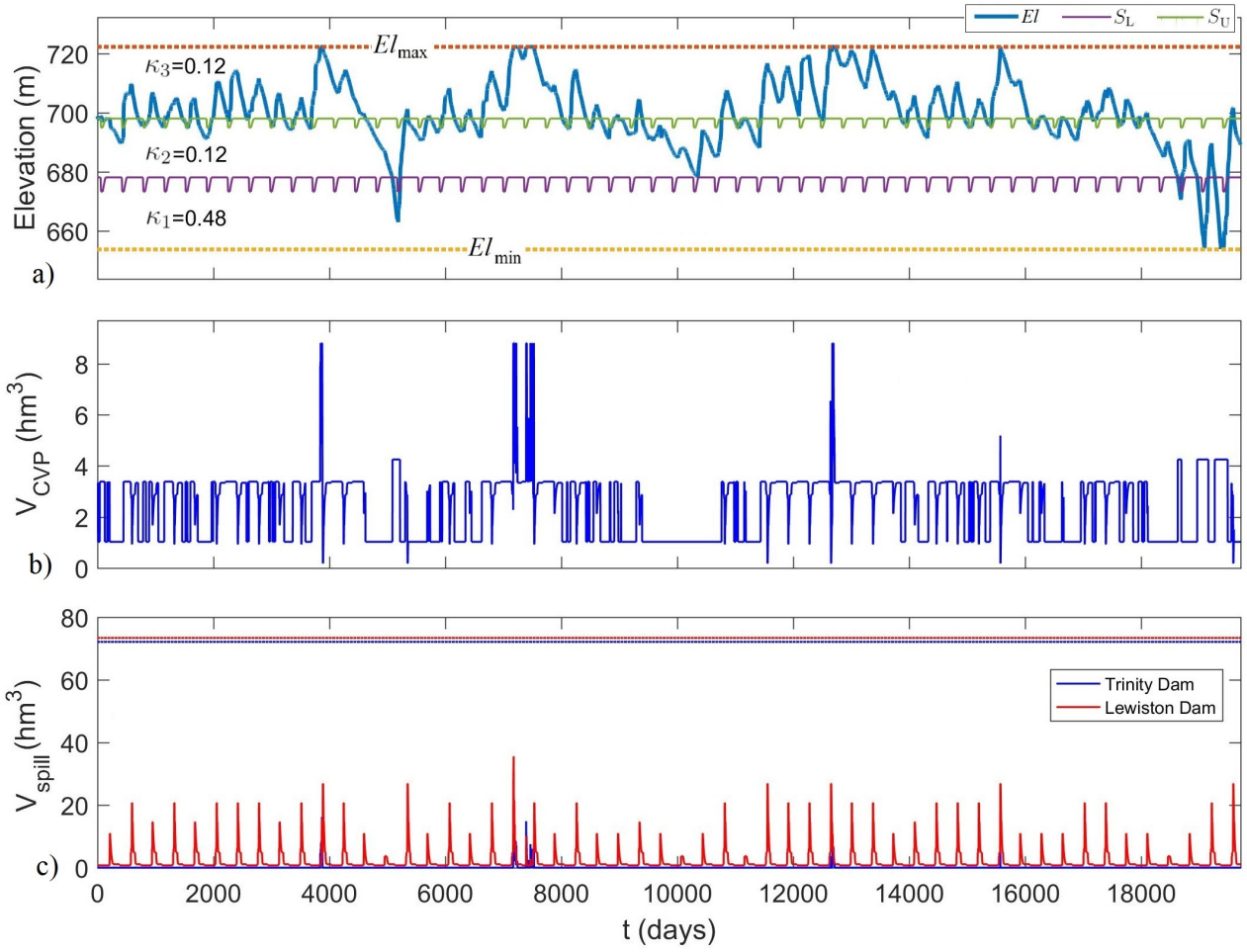

Figure 3.18: Simulation results of the run performed with the parameters of $F_{2,\text{opt}}$ solution in daily basis. a) Reservoir water level along with boundary rule curves (S_U and S_L) and release fractions of the operational zones (κ_1, κ_2 and κ_3) b) Flow diverted to CVP (V_CVP) c) Spilled flows (V_spill) from Trinity Dam (blue) and Lewiston Dam (red) and their spillway capacities (dashed horizontal blue and red lines, respectively)

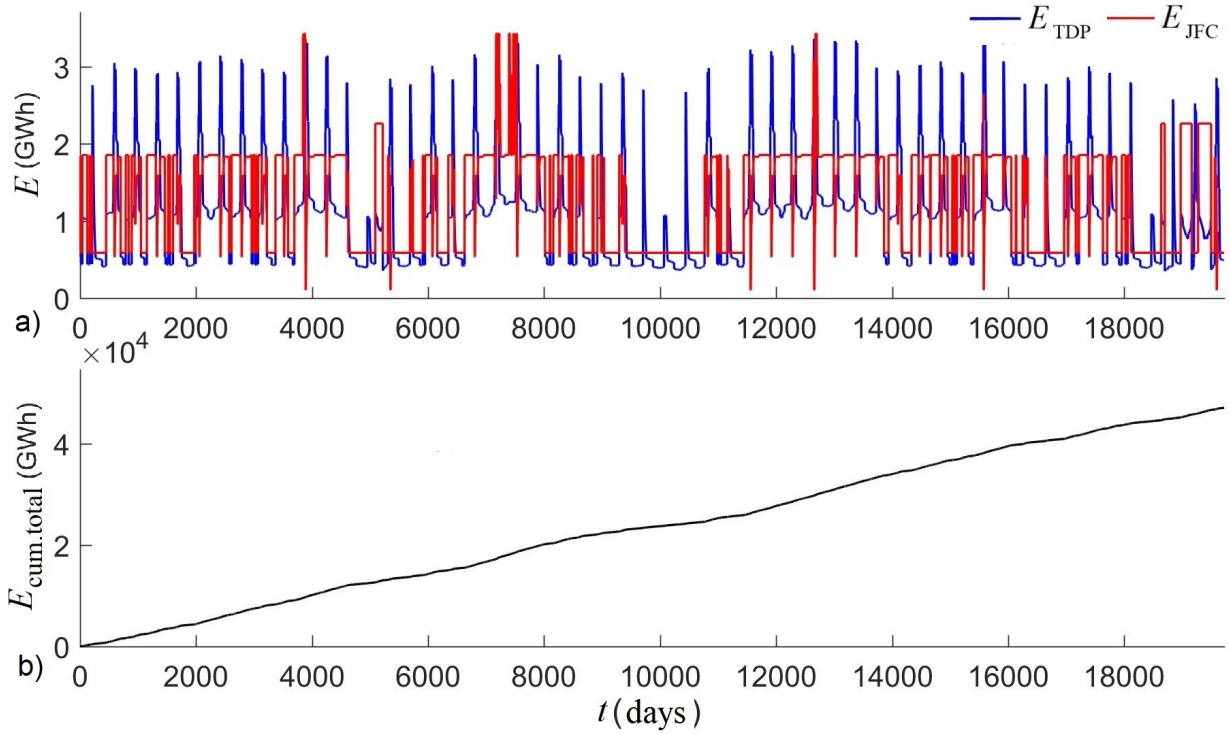

Figure 3.19: Energy related simulation results of the run performed with the parameters of $F_{2,\text{opt}}$ solution in daily basis. a) Daily energy generation at TDP (blue) and JFC (red) b) Cumulative plot of total generated energy

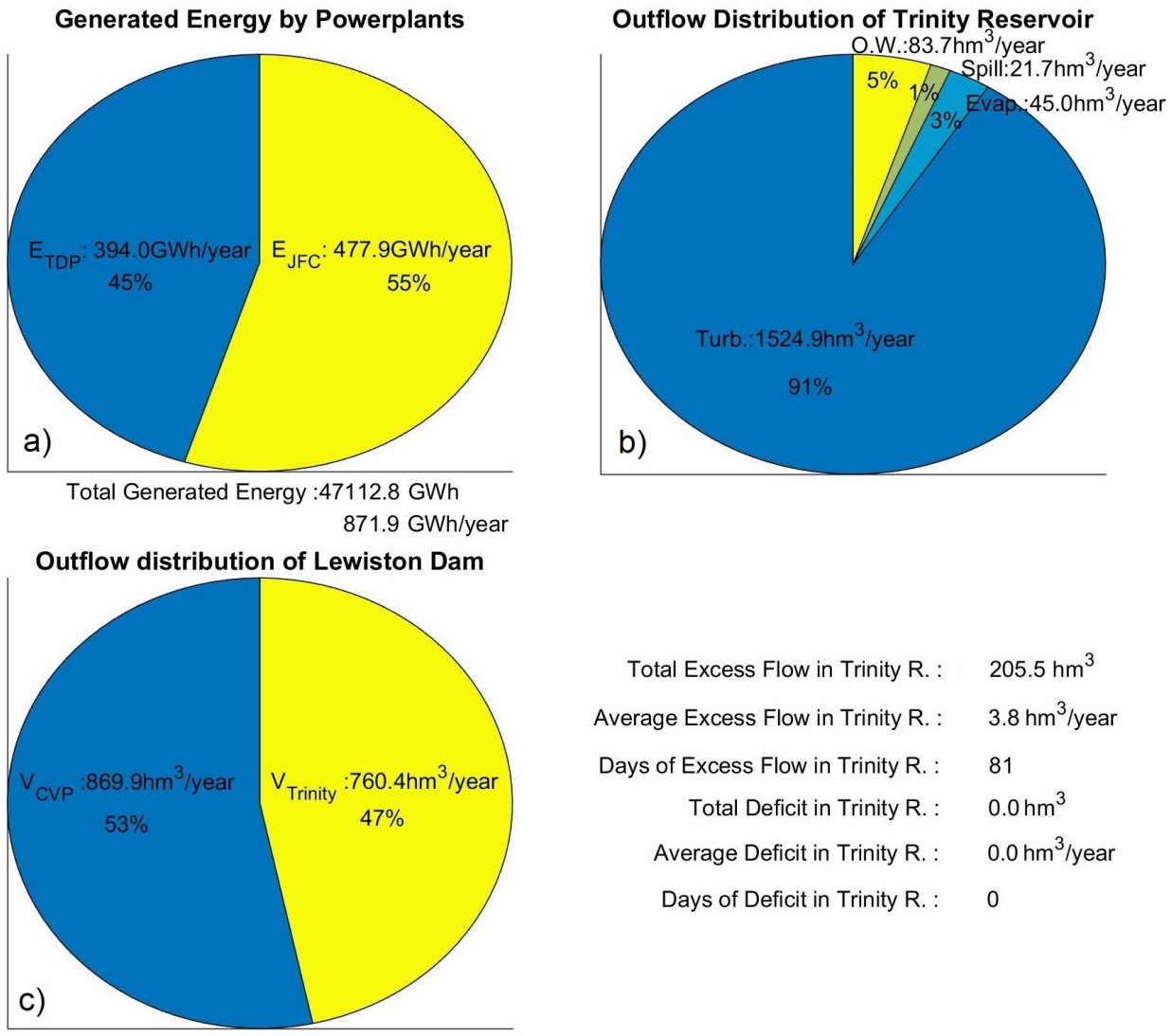

Figure 3.20: Pie chart simulation results of the run performed with the parameters of $F_{2,\text{opt}}$ solution a) allocation of energy generated by TDP (E_{TDP}) and JFC (E_{TDP}) b) Outflow distribution of Trinity Reservoir c) Outflow distribution of Lewiston Dam

After examining the Trinity Reservoir levels along with the boundary rule curves throughout the calculation period for both $F_{1,\text{opt}}$ and $F_{2,\text{opt}}$ in Figure 3.15 a and 3.18 a, we observe the reservoir is large enough that its storage does not drawdown and fill on a yearly basis and the resulting boundary rule curves follow almost a straight line despite they have a wide room for deviation between the elevations of their consecutive plateaus. Therefore, the release remains constant unless the current reservoir level switches its zone. However, it can be

noticed from both graphs that reservoir levels stay in the same zone for several years and as a result the release from the reservoir remains constant. From this observation we come to a conclusion that seeking an optimum reservoir operation policy specified with constant boundary curves but variable release fractions with time might achieve higher generated energy in the system with a minimum shortage index. Therefore, we investigate this policy in the next case study.

3.2.3 Case Study III: Optimization with RC 2

In the previous case study, we applied multi-objective optimization analysis to Trinity Reservoir operations by assuming 3 operational zones within its active storage with time variant boundaries but stable release fractions that define the releases to downstream for each zone. Now, we transfer the time variant parameterization attributions from boundary rule curves to the release fractions and here after we call the time variant release fraction functions as release rule curves that are denoted by $\kappa(t)$. 2 boundaries that differentiate one operational zone from the other two are still present but we assign them a constant storage value. The schematic representation of the adopted parameterization method in this case study is illustrated in Figure 3.21. Similar to the boundary curves of RC1 approach, by considering seasonal variabilities in inflow record and Trinity River flow demand we define the break point coordinates of one release rule curve with 6 parameters and they can be listed for the zone 1 fraction function $\kappa_1(t)$ as Δt_1, Δt_2, Δt_3, Δt_4, $\kappa_{1(1\text{-}3)}$ and $\kappa_{1(2)}$. Thus, only two parameters for the first and the second plateaus are required for each additional curve. Hence, in this reservoir operations policy setup that is named as RC2, the decision vector of total 12 parameters is $\mathbf{x} = \{\Delta t_1, \Delta t_2, \Delta t_3, \Delta t_4, S_{\text{L}}, \Delta_{\text{U-L}}, \kappa_{1(1\text{-}3)}, \kappa_{1(2)}, \kappa_{2(1\text{-}3)}, \kappa_{2(2)}, \kappa_{3(1\text{-}3)}, \kappa_{3(2)}\}$. The feasible ranges of these parameters are listed in Table 3.4. The flow diagram of the EROM model which illustrates the application of RC2 approach given in Figure 3.34 in Appendix section.

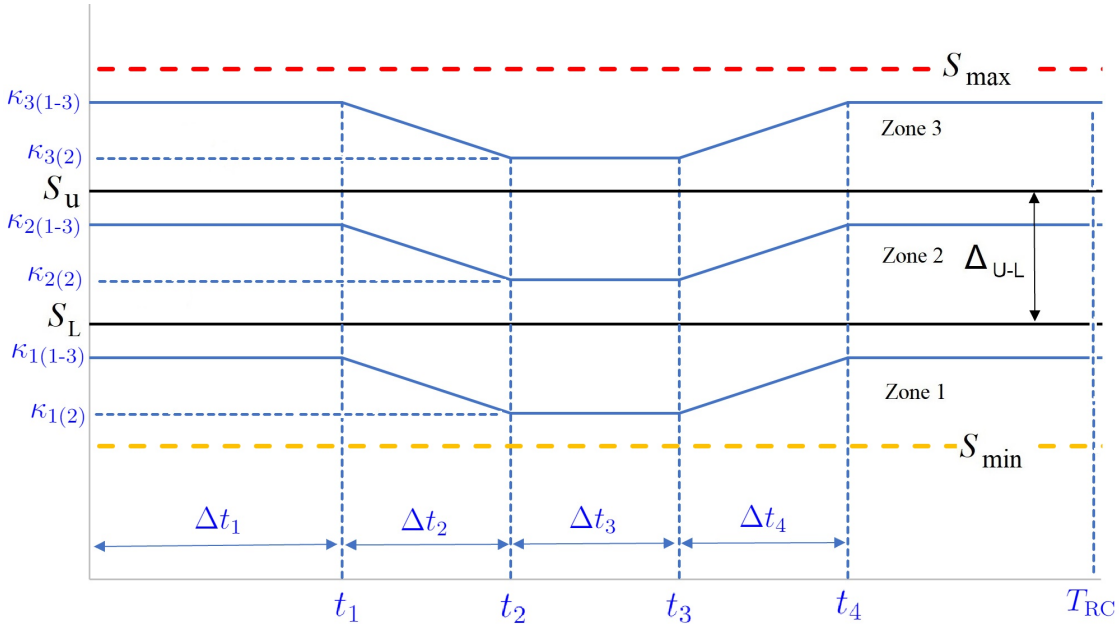

Figure 3.21: Schematic representation of RC2 approach: Upper and lower boundary rule curves (black solid lines) along with the release rule curves (blue solid lines) that belong to each storage zone.

Table 3.4: Model parameters in Case Study 2 and their ranges

Decision Variable	Minimum	Maximum	Units
Δt_1	0	365	Days
Δt_2	0	365	Days
Δt_3	0	365	Days
Δt_4	0	365	Days
S_L	S_{min}	S_{max}	hm^3
Δ_{U-L}	0	S_{min} - S_{max}	hm^3
$\kappa_{1(1-3)}$	0	1	-
$\kappa_{1(2)}$	0	1	-
$\kappa_{2(1-3)}$	0	1	-
$\kappa_{2(2)}$	0	1	-
$\kappa_{3(1-3)}$	0	1	-
$\kappa_{3(2)}$	0	1	-

The multi-objective optimization on the assumption of RC2 parameterization is performed by using 100 populations and 250 generations with AMALGAM. Figure 3.22 illustrates the objective function values of the final population that form the optimum Pareto front. The single-objective solutions ($F_{1,\text{opt}}$ and $F_{2,\text{opt}}$) are computed as follows. When the maximum average annual generated energy E_{av} is evaluated as 882.6 GWh, the shortage index (SI) becomes 13.06 % ($F_{1,\text{opt}}$). When the minimum value of SI reaches 0 %, E_{av} is calculated as 872.8 GWh ($F_{2,\text{opt}}$). The solutions out of $F_{1,\text{opt}}$ and $F_{2,\text{opt}}$ in Figure 3.22 illustrate the tradeoff between E_{av} and SI.

3.23 illustrates the Pareto uncertainty for each model parameter of the last population. The overall uncertainty of the parameter values is reduced in comparison with the same figure obtained from the optimization with RC1 approach (Figure 3.11). In addition, similar to the results of RC1 approach, for all samples that satisfy the rank 1 Pareto front, fraction function of zone 3 is stabilized with values 0.11 and 0.13 for $\kappa_{3(1\text{-}3)}$ and $\kappa_{3(2)}$, respectively. On the other hand, unlike the RC1 approach not only the storage and release related parameters of rank 1 Pareto samples are valued at certain points in their feasible ranges in clusters but also the values of time parameters are lumped around certain points (Figure 3.25). This is because relaxing the release fractions in the new parameterization strategy results in the distinct adaptation of release rule curve to the seasonality of the inflows and Trinity River demand. This inference is clearly supported by Figure 3.26 a. In this figure, most of the release rule curves of zone 1 and zone 2 that are plotted from the parameter values of rank 1 Pareto samples show a distinct deflection within the same period starting from early November ending in early July. This period also corresponds to the wet period of the Trinity River Basin as it is depicted in Figure 3.3. Figure 3.5 shows that Trinity River flow demand also increases within this period.

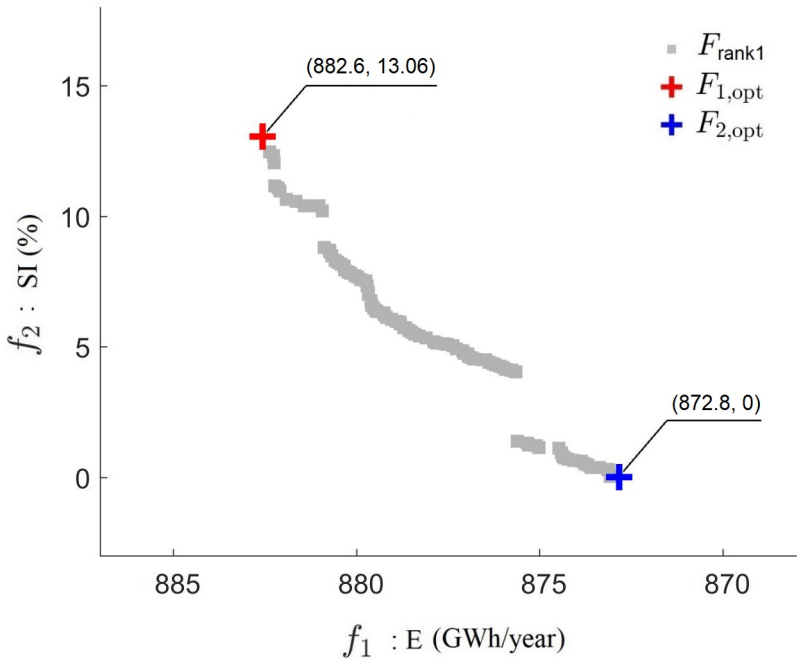

Figure 3.22: Illustration of objective function values of rank 1 Pareto samples that form Pareto front (RC2 assumption)

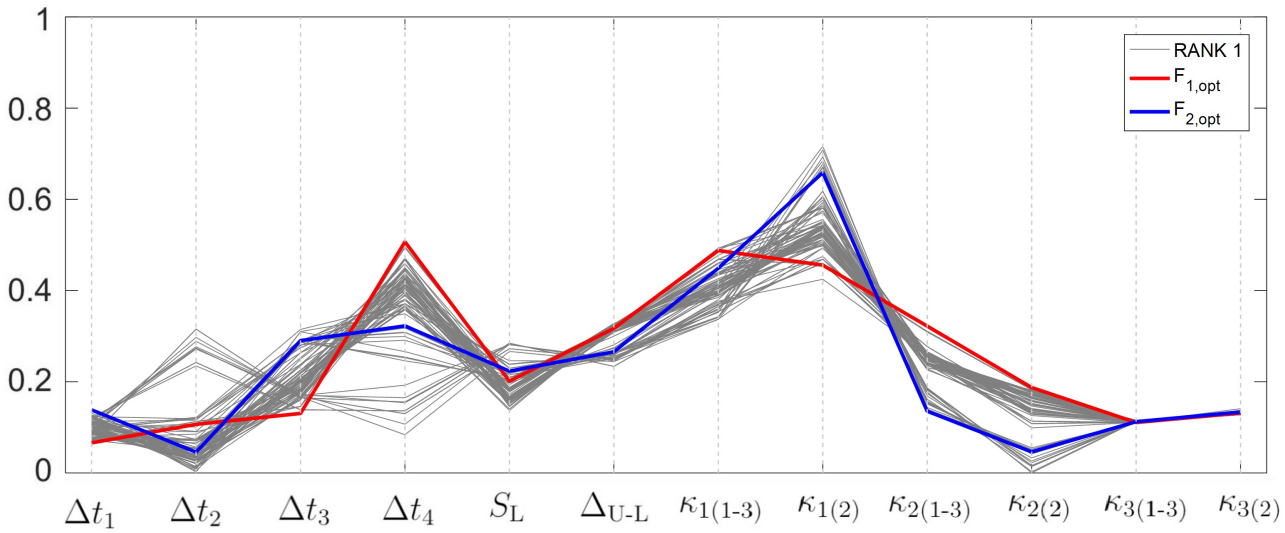

Figure 3.23: Normalized ranges of Pareto solution samples (RC2 assumption)

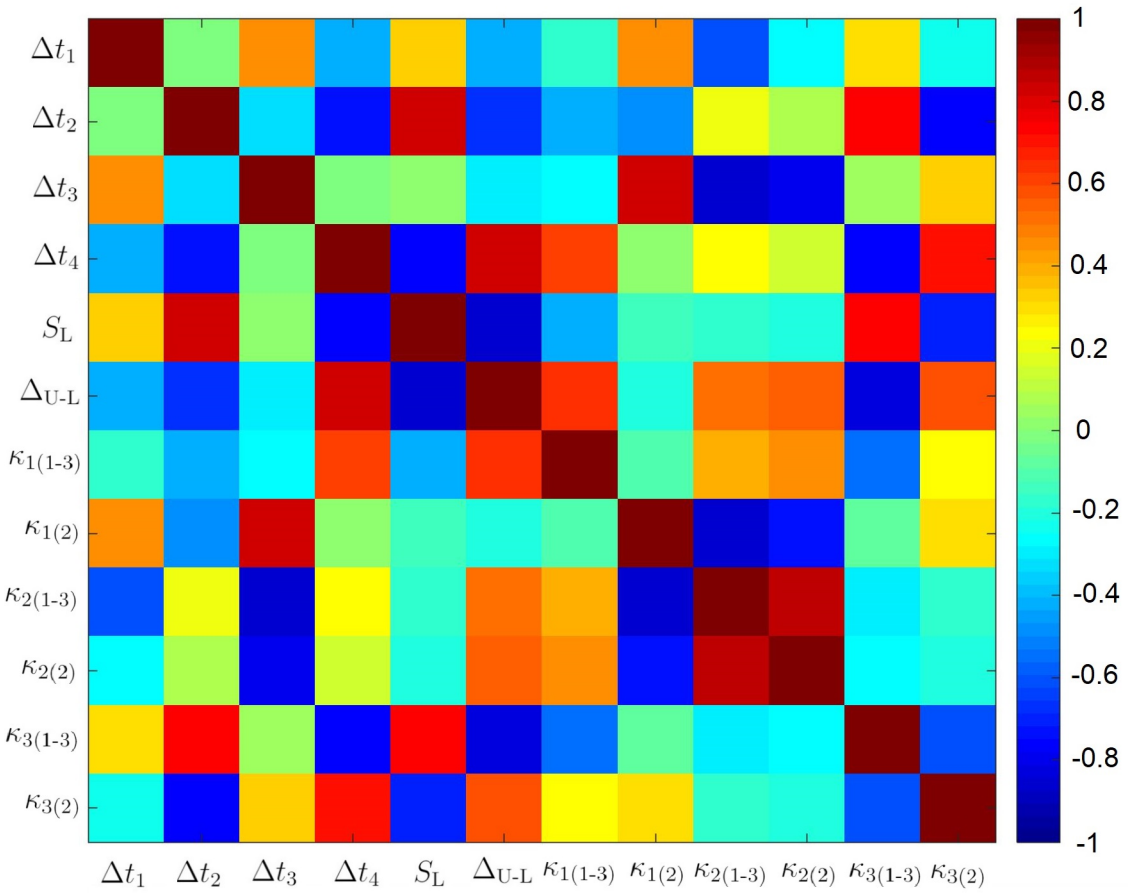

Figure 3.24: Map of correlation coefficients of Pareto parameter samples (RC2 assumption)

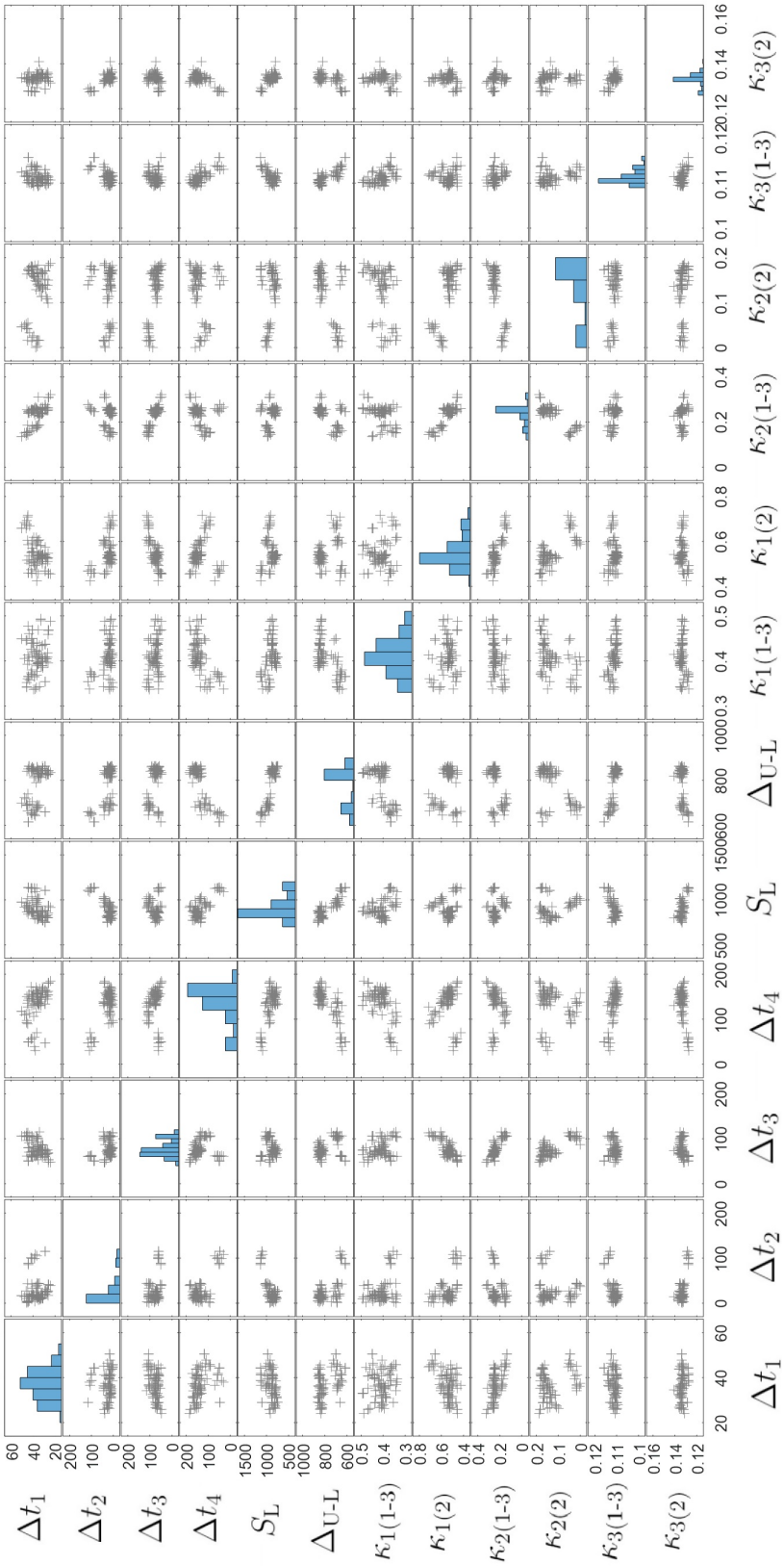

Figure 3.25: Marginal distributions and scatter plots of Pareto rank 1 solutions (RC2 assumption)

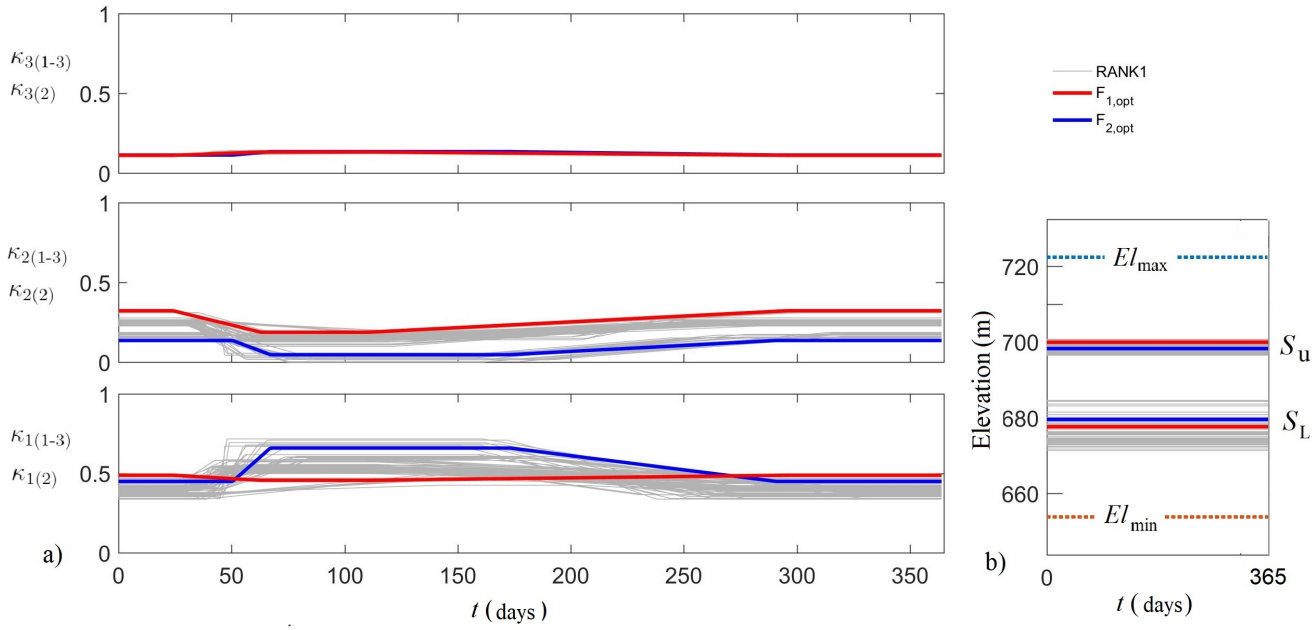

Figure 3.26: Release and boundary rule curves plotted from the values of associated rank 1 Pareto samples a) Release rule curves plotted from the values of Rank 1 Δt_1, Δt_2, Δt_3, Δt_4, $\kappa_{1(1-3)}$, $\kappa_{1(2)}$, $\kappa_{2(1-3)}$, $\kappa_{2(2)}$, $\kappa_{3(1-3)}$ and $\kappa_{3(2)}$. b) Depiction of lower and upper boundary rule curves (S_{U} and S_{L}, respectively) on the active storage range (Lower group of lines represent lower boundary rule curves that separate conservation zone into 2 zones, upper group of lines represent upper boundary rule curves that discern flood control zone from conservation storage)

Simulation Results of $F_{\mathbf{1,opt}}$ solution

After completing the optimization process, the resulting parameter values of $F_{1,\mathrm{opt}}$ and $F_{2,opt}$ solutions are run with EROM to acquire and examine the simulation results in details. Figure 3.27a shows that the water level traces almost the same alignment with the one results from the RC1 approach. The elevation of lower and upper boundary rule curves are assigned as 677.60 m and 699.90 m, respectively. These levels converge to the mean values of the boundary rule curves of the same Pareto solution of RC1 approach illustrated in Figure 3.15. The water level at Trinity Reservoir is mostly in the conservation zone and it drops below El_{min} plenty of times. However, it rises up and enters the flood protection zone, follows within that zone approximately 10 years in total and barely reaches the maximum operation level 6 times in those periods. The number of days of deficit in Trinity River release

is computed as 2576 with an average magnitude of 55.5 hm^3/year that resulted in a shortage index of 13.06. Excessive releases to Trinity River is minimized to 0.03 hm^3/year since the Trinity Reservoir spills only 0.6 hm^3/year which corresponds to 0.03 % of it is annual average outflow. Therefore, the designated flood protection zone allows almost no spillage from the reservoir. Thus, the average annual turbined flow from TDP becomes 1552.4 hm^3/year and constitutes the 92 % of its annual outflow. In summary, almost same values of $El(t)$, V_{CVP}, V_{Trinity}, E_{TDP} and E_{JFC} are obtained compared to the simulation results of the same Pareto solution of case study 2. However, the upgrade from constant to the time variant water release fractions helps decrease the excessive flows even more than it is succeeded by RC1 approach against the performance of firm yield analysis. In addition, the new approach also results in less serious shortages according to the results of the $F_{1,\mathrm{opt}}$ solution of case study 2.

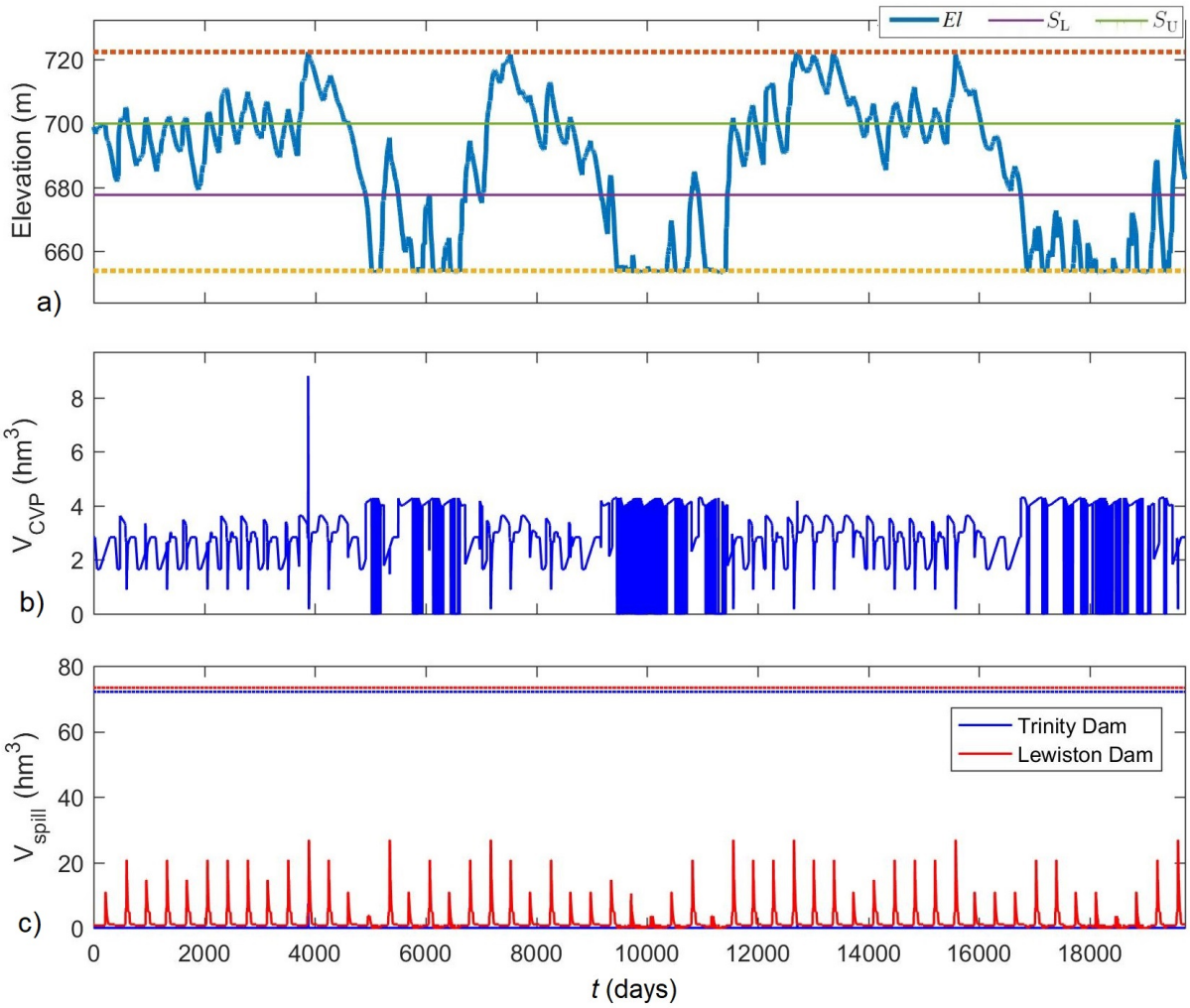

Figure 3.27: Simulation results of the run performed with the parameters of $F_{1,\text{opt}}$ solution of RC2 approach in daily basis. a) Reservoir water level along with boundary rule curves (S_U and S_L) and release fractions of the operational zones (κ_1, κ_2 and κ_3) b) Flow diverted to CVP (V_CVP) c) Spilled flows (V_spill) from Trinity Dam (blue) and Lewiston Dam (red) and their spillway capacities (dashed horizontal blue and red lines, respectively)

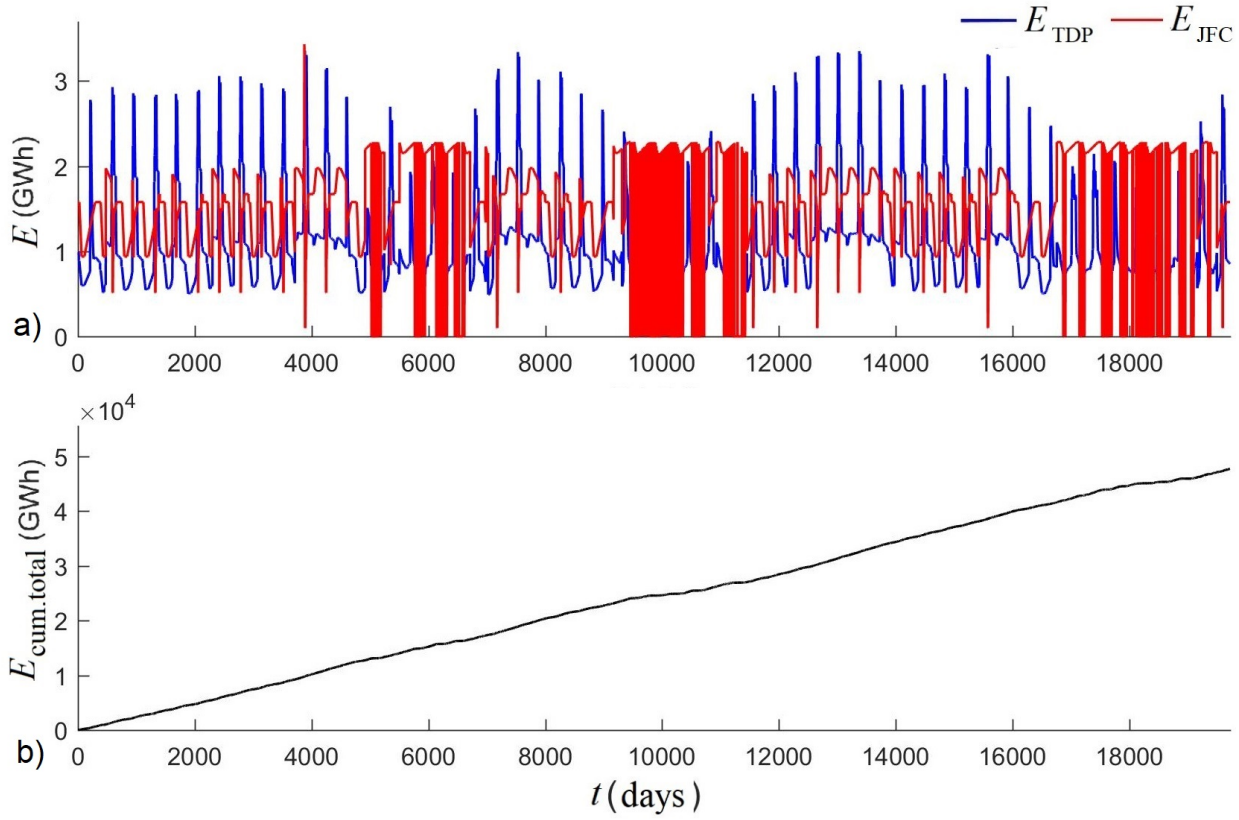

Figure 3.28: Energy related simulation results of the run performed with the parameters of $F_{1,\text{opt}}$ solution of RC2 approach in daily basis. Generated energy related results of AMALGAM analysis in daily basis a) Daily energy generation at TDP (blue) and JFC (red) b) Cumulative plot of total generated energy

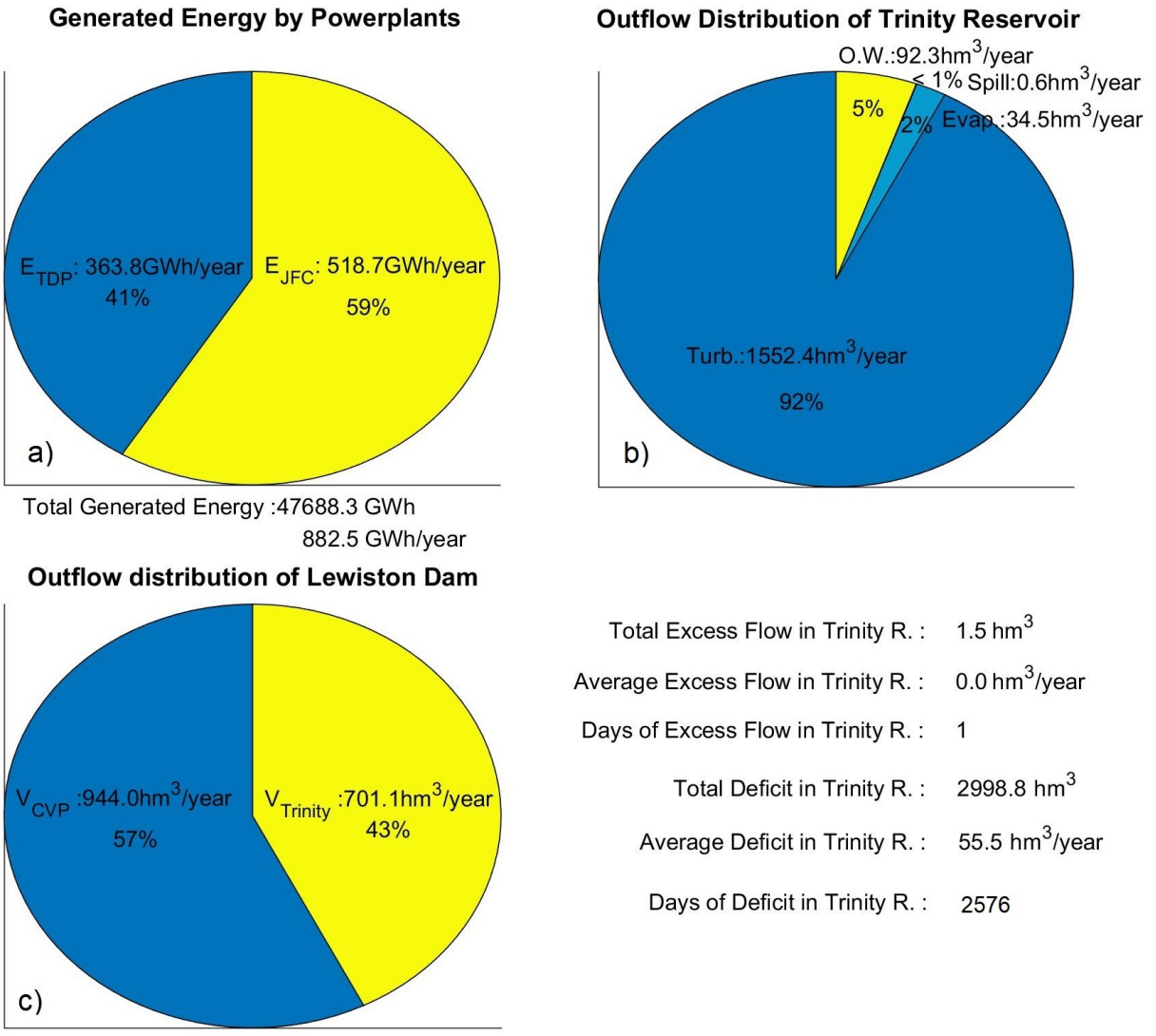

Figure 3.29: Pie chart simulation results of the run performed with the parameters of $F_{1,\text{opt}}$ solution of RC2 approach a) allocation of energy generated by TDP (E_{TDP}) and JFC (E_{JFC}) b) Outflow distribution of Trinity Reservoir c) Outflow distribution of Lewiston Dam

Simulation Results of $F_{\mathbf{2,opt}}$ solution

After running the simulation with the parameter values of $F_{2,\text{opt}}$ solution of RC2 approach, the resulting reservoir level versus time plot given in Figure 3.30 almost perfectly matches with the one belongs to the same Pareto solution of RC1 approach. The elevations of lower and upper boundary rule curve which correspond to S_{L} and S_{U} are 679.55 m and 698.25 m,

respectively. These values also overlap with the upper plateaus of boundary rule curves of RC1 approach. The time variant release fractions help the reservoir level recover from the extreme drawdowns slightly better than the RC1 approach. This results in a slight increase in annual energy generation at TDP since the mean reservoir level rises.

However, the rate of excessive flow to Trinity River from Lewiston Dam is increased from 3.8 hm^3/year to 4.2 hm^3/year. Apart from the small reduction in the plateaus of boundary rule curves the only parameter which attempts to maintain the reservoir level far from the minimum water level is the reduced value of $\kappa_2 = 0.12$ while κ_1 and κ_3 are selected same as the ones belong to $F_{1,\text{opt}}$ solution. This attempt leads to a 20.7 hm^3/year rise in spill and 11.4 hm^3/year evaporation and 26 hm^3/year drop in turbined outflows at Trinity Dam. The spilled flow from Trinity Dam constitutes a massive inflow volume in a small period that its majority can not be diverted to CVP because of limited CCT capacity and turns into excessive releases to Trinity River from Lewiston Dam for 83 days in 54 years of calculation period with an average annual flow of 4.2 hm^3/year whereas $F_{1,\text{opt}}$ solution fails to meet 57.6 hm^3/year portion of Trinity River demands. These two contradicting occurrences between $F_{1,\text{opt}}$ and $F_{2,\text{opt}}$ result in the majority of 75.7 hm^3/year of reduction in CVP water supply as well as the generated energy at JFC. Even though the average water level at Trinity Reservoir increases the energy generation at TDP in $F_{2,\text{opt}}$, it can only compensate 33.9 of 44.1 GWh/year energy loss in JFC compared to the one obtained from $F_{1,\text{opt}}$. The Figures 3.18, 3.19 and 3.20 summarizes the values discussed above by illustrating them in the related graphs and charts.

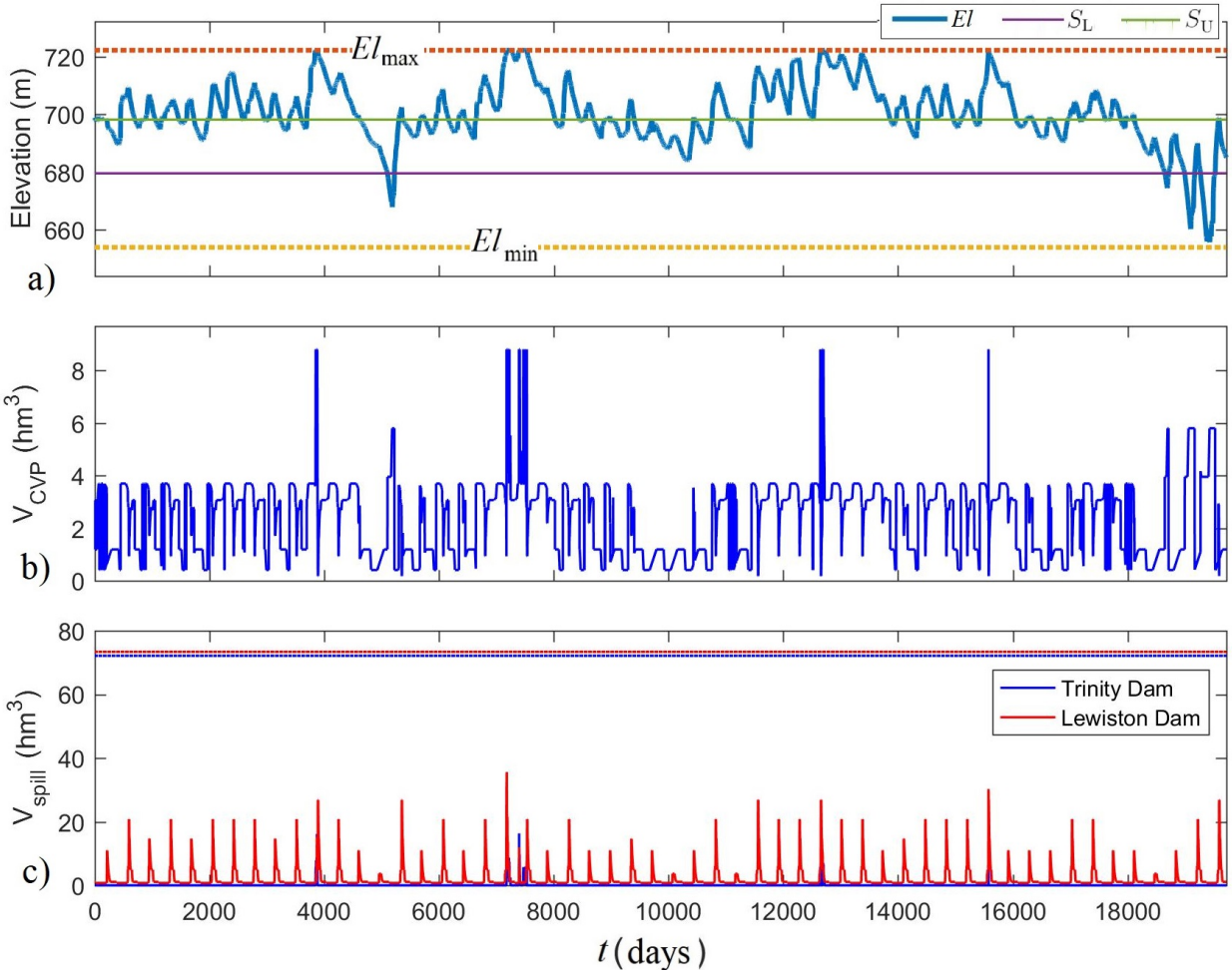

Figure 3.30: Simulation results of the run performed with the parameters of $F_{2,\text{opt}}$ solution in daily basis. a) Reservoir water level along with boundary rule curves (S_U and S_L) and release fractions of the operational zones (κ_1, κ_2 and κ_3) b) Flow diverted to CVP (V_CVP) c) Spilled flows (V_spill) from Trinity Dam (blue) and Lewiston Dam (red) and their spillway capacities (dashed horizontal blue and red lines, respectively)

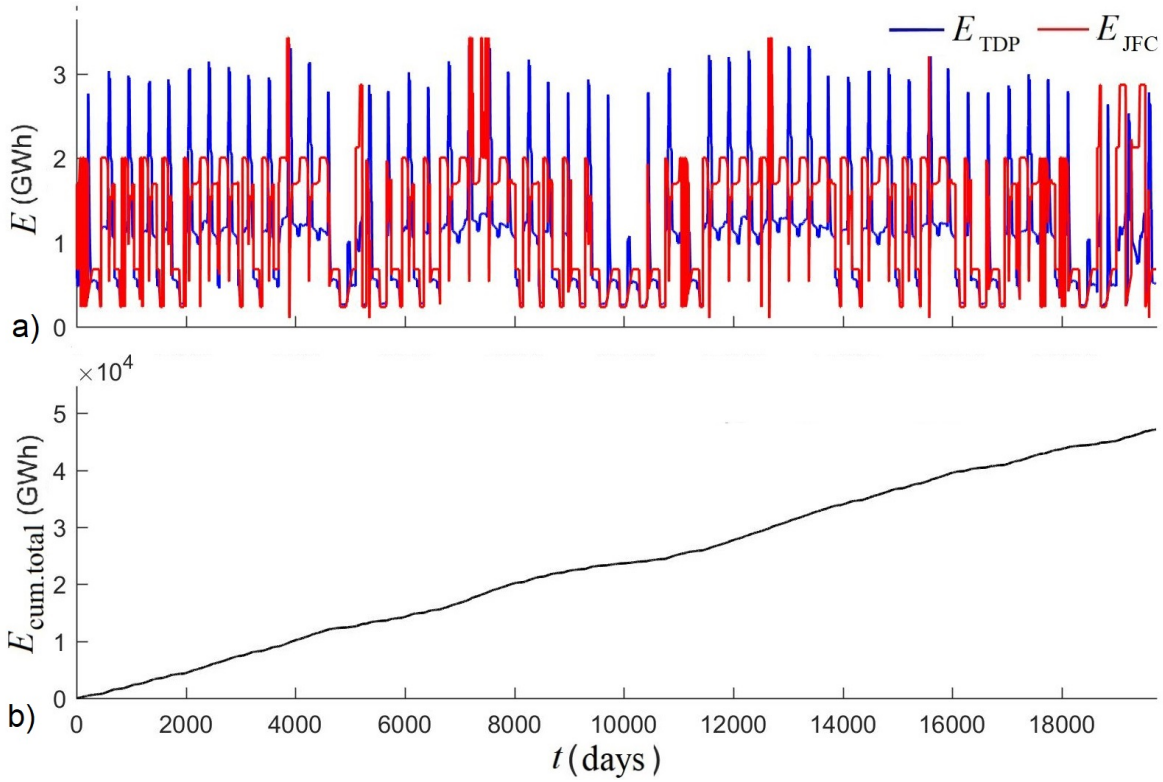

Figure 3.31: Energy related simulation results of the run performed with the parameters of $F_{2,\text{opt}}$ solution in daily basis. Generated energy related results of AMALGAM analysis in daily basis a) Daily energy generation at TDP (blue) and JFC (red) b) Cumulative plot of total generated energy

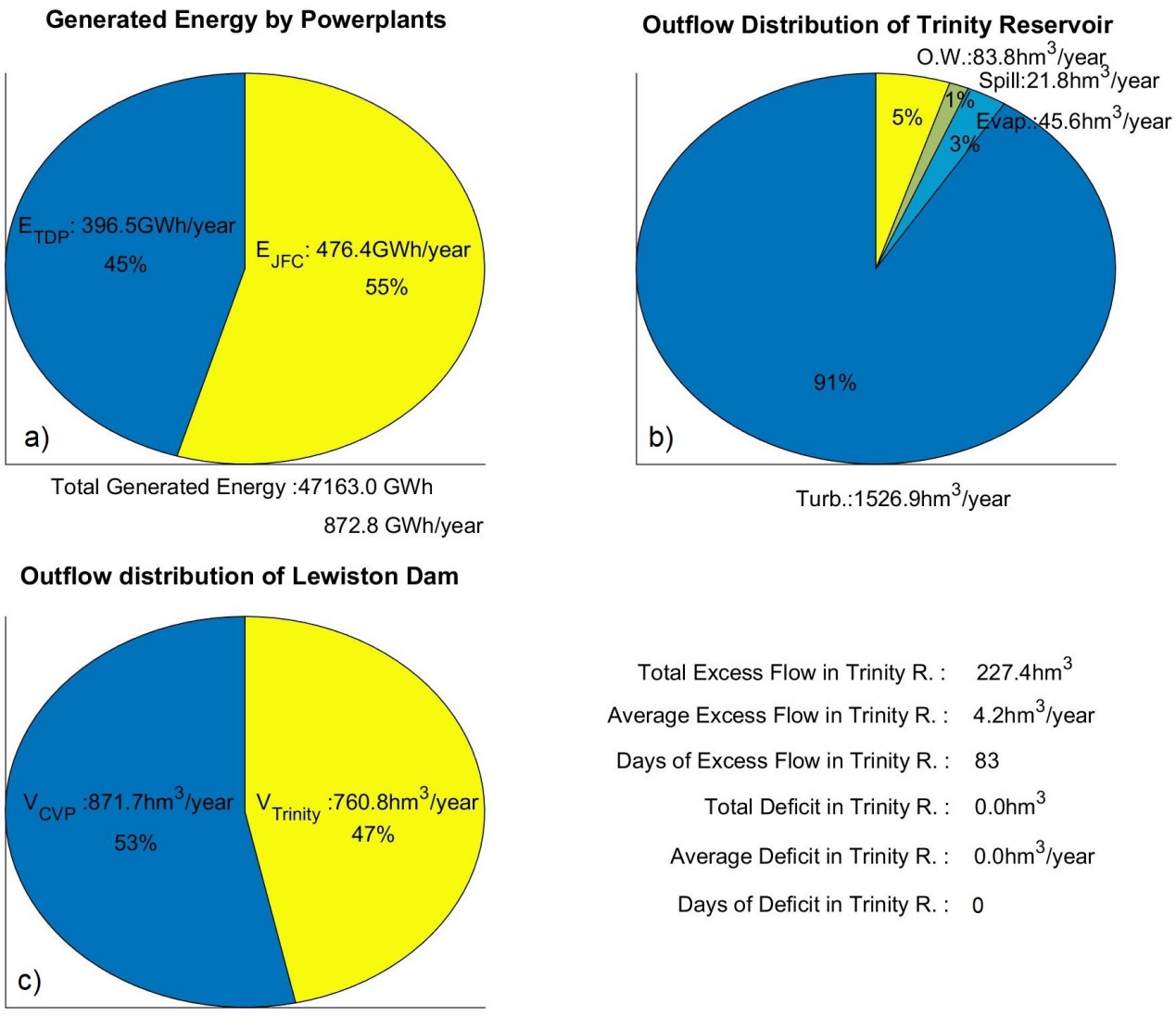

Figure 3.32: Pie chart simulation results of the run performed with the parameters of $F_{2,\text{opt}}$ solution a) allocation of energy generated by TDP (E_{TDP}) and JFC (E_{JFC}) b) Outflow distribution of Trinity Reservoir c) Outflow distribution of Lewiston Dam

3.3 Summary and Conclusions

In this thesis, we have introduced the Elaborate Reservoir Operation Management model, EROM, which simulates the storage and power generation of a single reservoir or the system of reservoirs that have one or multiple purposes in response to the record of inflow values and site characteristics under a predetermined operation strategy. As the name suggests, the model differs from the other long term reservoir operation analysis models with its sophisticated tools which provide more thorough representation of the real systems to be modeled. A system of reservoirs in any configuration can be easily introduced to the model to establish the flow traffic among the reservoirs. In addition, it provides a wide range of fixed time step size alternatives from one hour to one month to perform the simulations by selecting its explicit solver. As an alternative to the explicit solver, the simulations can be performed with its ODE solver in order to minimize the integration errors and help decide what time step size is more appropriate for the accuracy of prompt explicit solver. EROM is designed to analyze the operation of reservoir systems with hydropower purpose more in particular so that it can perform unit based energy calculations. Each power plant of the reservoir system to be applied to the model may consist of different number of energy generating units and each unit may have different technical characteristics such as turbine type, minimum and maximum operative flow rates and discharge - unit efficiency relationships. The unit dispatch optimizer module of the model allocates the inflow of a powerplant to its turbines in a way to maximize the overall plant efficiency. Moreover, it allows user to opt for dynamic tailwater consideration which is an important factor for the estimation of generated energy from the reaction type turbines. Furthermore, hydraulic losses in the penstock system that conveys reservoir water to the turbines of the powerplant can be calculated by two widely adopted equations that are integrated to the model. For this, the model is capable of analyzing the penstock networks in any configuration and the assembly of pipes that constitute the penstock network and their geometrical and hydraulic characteristics can be simply entered

to the model by the user. Finally, the simple call of the model function makes it easy to integrate with the optimization algorithms.

Three case studies are performed on the operation management analysis of two dams, Trinity Dam and Lewiston Dam that are located on the Trinity River in Northern California, so as to test the application of a real project into the model and calculate the numerical results. These dams are the main components of the Trinity River Division which accomplishes the inter-basin water transfer from Trinity River Basin to the Central Valley Project (CVP) of California. During this diversion process, apart from the diversion benefits, two hydropower plants utilize the potential energy of stored water in the system. However, as a result of the massive diversion more than 30 years from the river, riverine habitats and geomorphological conditions were degraded and the environmental studies recommend a specified release schedule to be followed by the managers for each year to the river for the recovery. The inflow record of 54 years, site characteristics and the properties of the energy generating units in the power plants as well as operational constraints are entered to the model so as to better mimic and measure the real performance of the system. All of the case studies are performed by using the explicit solver under the assumption of daily time step, stable unit efficiency and stable tailwater level. In the first case study, a firm yield analysis is performed to determine the maximum constant rate of flow that can be diverted to CVP after meeting the ecological flow demands of Trinity River and generated energy in this process. The result of the first case study provide a basis to compare and assess the performance of developed operation strategies in the following case studies. Discounting the fact that resulted in a failure to maintain the flow rates of the spillways of both dams below their capacity, average annual energy generated from the powerplants, E_{av}, in the firm yield operation strategy is calculated as 813 GWh/year without causing any shortage in the supply of Trinity River demands. In the second and third case studies, two different rule curve based operation optimization analysis of the system are successfully performed by integrating EROM model with the evolutionary multiobjective optimization algorithm, AMALGAM, and specifying 2

objective functions as the maximization of average annual generated energy, f_1:E_{av} and the minimization of shortage index, f_2:SI. In the second case study, 10 parameters are arranged to define a yearly operation policy named as RC1 approach that relates the releases to the storage deviations at the Trinity Reservoir. In the third case study, the yearly operation policy is set up with 12 parameters and named as RC2 approach with an aim to derive an even more efficient operation strategy than the one found from RC1 approach. Consequently, the multiobjective optimization successfully increased E_{av} from 813 GWh/year that is calculated from the firm yield operation strategy to a maximum of 872.8 GWh/year without causing any shortage in the ecological water supply to the Trinity River. This result is obtained from the RC2 approach as the single objective optimum solution of the f_2:SI. In addition, two Pareto fronts are obtained one per each of case study 2 and case study 3 which is a good indicator of managing to select conflicting objectives for the multiobjective optimization analysis. It is also concluded that the RC1 setup makes possible to reach the maximum, 883.1 GWh/year, energy generation with a permit of $SI = 13.55$. The intermediate solutions between these single objective optimum solutions of two different rule curve approach describe the significant tradeoff between the E_{av} and SI. Other findings from the results of the case studies are listed as follows

1. In both of the approaches in the second and third case studies and case study 3, the designation of a nearly 1260 hm^3 of empty space as a flood protection zone is found necessary not to violate the spillway capacity of the dams at any time. It is also found that the designation of flood protection zone at Trinity Reservoir improves the energy efficiency of the system considerably.

2. Trinity reservoir is large enough that its storage does not drawdown and fill on a yearly basis and the optimized boundary rule curves of RC1 approach follow almost a straight line despite they have a wide room for deviation within the active storage limits of the reservoir.

3. The mean elevation of boundary rule curves obtained from RC1 approach and the boundary lines that are derived from RC2 approach almost perfectly match while they both designate three operational zones in the active storage of the Trinity Reservoir.

4. Time parameters Δt_1, Δt_2, Δt_3 and Δt_4 of rank 1 Pareto solutions of RC1 approach are well-distributed over a wider span in their feasible ranges, other parameter values are clustered around one or more specific points. The release fraction parameter $\kappa 3$ which defines the release in zone 3 has the smallest Pareto uncertainty and all of the $\kappa 3$ values are sampled from a narrow range around 0.12.

5. Unlike as they were obtained from the RC1 approach, the values of time parameters of rank 1 Pareto samples are lumped around certain points within their feasible ranges. This is because relaxing the release fractions in the RC2 approach results in a significant adaptation of release rule curve to the seasonality of the inflows and Trinity River demand. Most of the release rule curves of zone 1 and zone 2 show a significant deflection within the same period starting from early November ending in early July. This period also corresponds to the wet period of the Trinity River Basin. Trinity River flow demand also increases within this period.

6. While the average annual volume of CVP diversion in the firm yield analysis is calculated as 806.9 hm^3/year, it is increased to 869.9 hm^3/year and 871.7 hm^3/year from the optimization analysis with RC1 and RC2 approaches, respectively. It is noticed that these values converge the average annual supply of Central Valley Project record of 868.37 hm^3/year.

7. The contributions of TDP to the average annual energy generation of the system are calculated as 46%, 45% and 45%, respectively to the order of key studies. However, the contribution of generation at TDP to the total generation of 769 GWh/year is specified from the records as 55%. This result show that even in firm yield analysis we calculate more energy at JFC and its corresponding percentage in total energy. Even though it is

known that the installed capacity of JFC is higher than that belongs to TDP and this information contradicts with the inference that we get from the record, we anticipate that the reason of the difference between the model results and the records might have been arised from the lack of publicly accessible detailed technical characteristics of TDP and JFC that can not be applied to the model. In addition, excessive releases to the Trinity River might have been necessitated because of other demands of the lower parts of Trinity River. It is also thought that the coordinated operation of the system that is investigated in this thesis with the downstream components of the CVP project might be also a reason to deem this difference as a reasonable occurrence.

Even though EROM is designed to simulate the performance of multiple reservoir systems in order to obtain the optimum operation policy of the systems with the integration of optimization algorithms, in this Master's thesis it has not been tested with the real-world data of multiple reservoirs. In our future work, we are willing to apply EROM integrated to AMALGAM to develop highly efficient policies for the operation of a system of multiple reservoirs via multiobjective optimization.

.

Nomenclature

S	(m^3)	Reservoir water storage	ρ	(kg/m^3)	Density of water
g	(m/s^2)	Gravitational acceleration	η_t	(-)	Turbine efficiency
η_g	(-)	Generator efficiency	q	(m^3/s)	Turbine flow rate
H_{net}	(m)	Net head	q_d	(m^3/s)	Turbine design flow rate
H_d	(m)	Design head	γ	(-)	minor hydraulic loss ratio
f	(-)	Friction factor	L	(m)	Penstock length
D	(m)	Penstock diameter	ν	(m^2/s)	Kinematic viscosity
H_g	(m)	Gross head	Z_{twl}	(m)	Tailwater level
t	(day)	Time	Z_{jet}	(m)	Nozzle elevation
H_f	(m)	Hydraulic losses	Z_{up}	(m)	Upstream water elevation
I	(m^3/s)	Inflow	Q_r	(m^3/s)	Total rate of release
O	(m^3/s)	Outflow	H_f^+	(m)	Major hydraulic loss
ΔT	(day)	Time interval	H_f^-	(m)	Minor hydraulic loss
Q_{evap}	(m^3/s)	Evaporation rate	n_{man}	($s/m^{1/3}$)	Manning's roughness coefficient
Q_{seep}	(m^3/s)	Seepage rate	ε	(m)	Pipe roughness
Q_{spill}	(m^3/s)	Spillway flow rate	η_u	(-)	Unit efficiency
E_{pan}	(m/month)	Evaporation pan measurement	q_{min}	(m^3/s)	Minimum operational turbine discharge
K_{pan}	(-)	Evaporation pan coefficient	q_{max}	(m^3/s)	Maximum operational turbine discharge
A	(m^2)	Reservoir surface area	Q_{Pmin}	(m^3/s)	Minimum operative flow rate of the power plant
S_{max}	(m^3)	Reservoir maximum capacity	Q_{Pmax}	(m^3/s)	Maximum operative flow rate of the power plant
d	(-)	Number of decision variables	m	(-)	Number of objective functions
S_{min}	(m^3)	Storage at minimum operation level	$\mathbf{x}$	(-)	Decision vector
V_{spill}	(m^3)	Volume of spilled water	$\mathbf{F}$	(-)	Objective space
n	(-)	Number of power generating units	$\mathbf{P}$	(-)	Set of pareto optimal solutions
K	(-)	Number of pipes along the penstock alignment	E_{av}	(GWh/year)	Average annual generated energy
E	(GWh)	Generated energy	SI	(-)	Shortage index
L	(m)	Pipe length	ν	(m^2/s)	Kinematic viscosity
T_{RC}	(days)	Period of operation strategy	w	(-)	Number of power plants in the system
V_{Demand}	(hm^3)	Volume of water demand	$V_{Shortage}$	(hm^3)	Volume of shortage in water supply
El_{max}	(m)	Maximum reservoir operation level	El_{min}	(m)	Minimum reservoir operation level

Q_{TDP}	(m^3/s)	Flow rate of Trinity Dam Powerplant	Q_{JFC}	(m^3/s)	Flow rate of Judge Francis Carr Powerplant
Q_{TDPmin}	(m^3/s)	Min. flow rate of TDP	Q_{JFCmax}	(m^3/s)	Min. flow rate of JFC
Q_{TDPmax}	(m^3/s)	Max. flow rate of TDP	Q_{JFCmax}	(m^3/s)	Max. flow rate of JFC
Q_{TOW}	(m^3/s)	Flow rate of Trinity Dam outlet works	Q_{TOWmax}	(m^3/s)	Max. flow rate of TD outlet works
$Q_{\mathrm{rel,TD}}$	(m^3/s)	Sum of flow rates of TDP and TD outlet works	$Q_{\mathrm{rel,TDmax}}$	(m^3/s)	Controlled release capacity of TD
$Q_{\mathrm{spill,TD}}$	(m^3/s)	Flow rate of TD spillway	$Q_{\mathrm{spill,TDmax}}$	(m^3/s)	Flow rate capacity of TD spillway
Q_{Tr}	(m^3/s)	Recommended rate of release from LEW to Trinity River	Q_{Trmax}	(m^3/s)	Max recommended rate of release from LEW to Trinity River
$Q_{\mathrm{tail,TD}}$	(m^3/s)	Total flow rate released to downstream from TD	Q_{CVP}	(m^3/s)	Flow rate diverted to CVP
$Q_{\mathrm{tail,LEW}}$	(m^3/s)	Total flow rate released to downstream from LEW	E_{TDP}	(GWh/year)	Average annual energy generation at TDP
E_{JFC}	(GWh/year)	Average annual energy generation at JFC	V_{Trinity}	(hm^3/year)	Average annual volume of water released to Trinity River
V_{CVP}	(hm^3/year)	Average annual volume of water diverted to CVP	$\Delta_{\mathrm{U-L}}$	(hm^3)	Shift parameter
Δt	(day)	Time interval parameter	S_{U}	(hm^3)	Upper rule curve in terms of storage
S_{L}	(hm^3)	Lower RC in terms of storage	$S_{\mathrm{L}(2)}$	(hm^3)	Storage value of 2nd plateau of lower RC
$S_{\mathrm{L}(1-3)}$	(hm^3)	Storage value of 1st and 3rd plateaus of lower RC	$\kappa_{1(1-3)}$	(-)	1st and 3rd plateaus of release fraction of zone 1
κ_1	(-)	Release fraction of zone 1	$\kappa_{2(1-3)}$	(-)	1st and 3rd plateaus of release fraction of zone 2
κ_2	(-)	Release fraction of zone 2	$\kappa_{3(1-3)}$	(-)	1st and 3rd plateaus of release fraction of zone 3
κ_3	(-)	Release fraction of zone 3	$F_{1,\mathrm{opt}}$	(-)	Single objective solution of 1st objective function
$\kappa_{1(2)}$	(-)	2nd plateau of release fraction of zone 1	$F_{2,\mathrm{opt}}$	(-)	Single objective solution of 2nd objective function
$\kappa_{2(2)}$	(-)	2nd plateau of release fraction of zone 2	$\kappa_{3(2)}$	(-)	2nd plateau of release fraction of zone 3

Bibliography

V. Martínez Alvarez, M.M. González-Real, A. Baille, J.F. Maestre Valero, and B. Gallego Elvira. Regional assessment of evaporation from agricultural irrigation reservoirs in a semi-arid climate. *Agricultural Water Management*, 95(9):1056 – 1066, 2008. ISSN 0378-3774. doi: https://doi.org/10.1016/j.agwat.2008.04.003. URL http://www.sciencedirect.com/science/article/pii/S0378377408000917.

BT Bower, MM HufSchumidt, and WW Reedy. Design of water resources systems: Chap. 11. *Operating procedures: Their role in the design of Water-reSources Systems by Simulation analysis*, 1962.

Jessica Brandt, Jay Doering, and P Eng. Towards an improved model for predicting hydraulic turbine efficiency. *University of Manitoba*.

E. Elba. *Strategies for Protection and Sustainable Environmental Management of the High Aswan Dam Reservoir in Egypt Considering Climate Change*. disserta Verlag, 2017. ISBN 9783959353540. URL https://books.google.com/books?id=yD7vDQAAQBAJ.

Jon Finch and Ann Calver. Methods for the quantification of evaporation from lakes. October 2008. URL http://nora.nerc.ac.uk/id/eprint/14359/.

US Fish, Wildlife Service, Hoopa Valley Tribe, et al. Trinity river flow evaluation final report. *USFWS and Hoopa Valley Tribe*, 1999.

JL Gordon. Hydraulic turbine efficiency. *Canadian Journal of Civil Engineering*, 28(2): 238–253, 2001.

David Jarry-Bolduc and Emmanuel Cote. Hydro energy generation and instrumentation & measurement: hydropower plant efficiency testing. *IEEE Instrumentation & Measurement Magazine*, 17(2):10–14, 2014.

Richard E Krueger, Carlos G Bates, and Richard N Walters. *Selecting hydraulic reaction turbines*. Number 20. Office of Design and Construction, Engineering and Research Center, 1976.

John W. Labadie. Optimal operation of multireservoir systems: State-of-the-art review. *Journal of Water Resources Planning and Management*, 130(2):93–111, 2004. doi: 10.1061/(ASCE)0733-9496(2004)130:2(93). URL https://ascelibrary.org/doi/abs/10.1061/%28ASCE%290733-9496%282004%29130%3A2%2893%29.

E. T. Linacre. Evaporation trends. *Theoretical and Applied Climatology*, 79(1):11–21, Oct 2004. ISSN 1434-4483. doi: 10.1007/s00704-004-0059-2. URL `https://doi.org/10.1007/s00704-004-0059-2`.

Daniel P Loucks, Eelco Van Beek, Jery R Stedinger, Jozef PM Dijkman, and Monique T Villars. *Water resources systems planning and management: an introduction to methods, models and applications*. Paris: Unesco, 2005.

Jay R Lund and Joel Guzman. Derived operating rules for reservoirs in series or in parallel. *Journal of Water Resources Planning and Management*, 125(3):143–153, 1999.

Miguel A Marino and Hugo A Loaiciga. Optimal operation of a multiple reservoir system. 1983.

I Nalbantis and D Koutsoyiannis. A parametric rule for planning and management of multiple-reservoir systems. *Water Resources Research*, 33(9):2165–2177, 1997.

T Ohishi, E Santos, A Arce, M Kadowaki, M Cicogna, and S Soares. Comparison of two heuristic approaches to hydro unit commitment. In *Power Tech, 2005 IEEE Russia*, pages 1–7. IEEE, 2005.

Rodrigo Oliveira and Daniel P Loucks. Operating rules for multireservoir systems. *Water resources research*, 33(4):839–852, 1997.

RA Ponrajah and FD Galiana. Systems to optimise conversion efficiencies at ontario hydro's hydroelectric plants. In *Power Industry Computer Applications., 1997. 20th International Conference on*, pages 245–251. IEEE, 1997.

Deepti Rani and Madalena Moreira. Simulation-optimization modeling: a survey and potential application in reservoir systems operation. water resour manag. 24:1107–1138, 04 2010.

T J Rhone. *Hydraulic Model Studies of the Trinity Dam Morning-glory Spillway-Trinity River Division-Central Valley Project, California*. Number Hyd-467. US Department of Interior, Bureau of Reclamation, 1960.

Erinaldo F Santos and Takaaki Ohishi. A hydro unit commitment model using genetic algorithm. In *Evolutionary Computation, 2004. CEC2004. Congress on*, volume 2, pages 1368–1374. IEEE, 2004.

Sara Séguin, Pascal Côté, and Charles Audet. Self-scheduling short-term unit commitment and loading problem. *IEEE Transactions on Power Systems*, 31(1):133–142, 2016.

T Sousa, JA Jardini, and RA De Lima. Hydroelectric power plant unit efficiencies evaluation and unit commitment. In *Power Tech, 2007 IEEE Lausanne*, pages 1368–1373. IEEE, 2007.

Ming-Yen Tu, Nien-Sheng Hsu, and William W.-G. Yeh. Optimization of reservoir management and operation with hedging rules. *Journal of Water Resources Planning and Management*, 129(2):86–97, 2003. doi: 10.1061/(ASCE)0733-9496(2003)129:2(86).

Ching-pin Tung, Shao-yiu Hsu, Chia-Ming Liu, and Jr-Shin Li. Application of the genetic algorithm for optimizing operation rules of the liyutan reservoir in taiwan 1. *JAWRA Journal of the American Water Resources Association*, 39(3):649–657, 2003.

Jasper A. Vrugt. U a l multi-criteria optimization using the amalgam software package : Theory , concepts , and matlab implementation. 2016.

Tony L Wahl and Elisabeth A Cohen. *Determination of Controlled-Release Capacity from Trinity Dam*. Number 830. USBR Technical Service Center, 1999.

R.A. Wurbs. *Modeling and Analysis of Reservoir System Operations*. Prentice Hall PTR, 1996. ISBN 9780136059240. URL https://books.google.com/books?id=HwkfAQAAIAAJ.

Ralph A. Wurbs. Reservoir‐system simulation and optimization models. *Journal of Water Resources Planning and Management*, 119(4):455–472, 1993. doi: 10.1061/(ASCE)0733-9496(1993)119:4(455). URL https://ascelibrary.org/doi/abs/10.1061/%28ASCE%290733-9496%281993%29119%3A4%28455%29.

William W-G Yeh. Reservoir management and operations models: A state-of-the-art review. *Water resources research*, 21(12):1797–1818, 1985.

Veysel Yildiz. *Numerical simulation model of run of river hydropower plants: Concepts, Numerical modeling, Turbine system and selection, and design optimization*. University of California, Irvine, 2015.

Appendix

Calculation of friction factor f (-) in Darcy-Weisbach equation

Value of f can be specified by Moody diagram with respect to mean velocity of water in a pipe V (m/s), pipe roughness ε and kinematic viscosity of water. The Moody diagram can be classified into three zones of data patterns corresponding to the flow regime in the pipe which is determined by Reynolds number Re (-). These zones are called as laminar flow $Re < 2000$, transitional flow $2000 < Re < 4000$ and turbulent flow $Re > 4000$. Equations which are used for the calculation of f is presented according to the pertaining flow regime in the following equations.

$$Re = \frac{VD}{\nu} \tag{3.8}$$

For laminar flow $Re < 2000$,

$$f = \frac{64}{Re} \tag{3.9}$$

For turbulent flow $Re > 4000$,

$$f = \frac{1.325}{\left[\ln\left(\frac{\varepsilon}{3.7D} + \frac{5.74}{Re^{0.9}}\right)\right]^2} \tag{3.10}$$

For transitional flow $2000 < Re < 4000$ (Cubical interpolation of Moody diagram),

$$f = X_1 + R\Big(X_2 + R(X_3 + X_4)\Big) \tag{3.11}$$

$$R = \frac{Re}{2000} \tag{3.12}$$

$$X1 = 7F_A - F_B \tag{3.13}$$

$$X2 = 0.128 - 17F_A + 2.5F_B \tag{3.14}$$

$$X3 = -0.128 + 13F_A - 2F_B \tag{3.15}$$

$$X4 = R(0.032 - 3F_A + 0.5FB) \tag{3.16}$$

$$F_A = {Y_3}^{-2} \tag{3.17}$$

$$F_B = F_A(2 - \frac{0.00514215}{Y_2Y_3}) \tag{3.18}$$

$$Y_2 = \frac{\varepsilon}{3.7D} + \frac{5.74}{Re^{0.9}} \tag{3.19}$$

$$Y_3 = -0.86859 \ln\left(\frac{\varepsilon}{3.7D} + \frac{5.74}{4000^{0.9}}\right) \tag{3.20}$$

Detailed Information about the Monte Carlo Optimization used in Unit Dispatch Optimizer (UDO) module of EROM

It is certain that the powerplant has to be operated within a discharge range from minimum to maximum operation limit of the powerplant since each of the units has one minimum and one maximum operational limit due to the frequency of the power grid which the generated power to be transmitted to and the capacity of the unit, respectively. The minimum and maximum operation limits of the powerplant Q_{Pmin} (m^3/s) and Q_{Pmax} (m^3/s) having N number of units can be expressed with the equations below.

$$Q_{\mathrm{Pmin}} = \min\{q_{\mathrm{min},1}, q_{\mathrm{min},2}, ..., q_{\mathrm{min},N}\} \tag{3.21}$$

$$Q_{\mathrm{Pmax}} = \sum_{j=1}^{N} q_{\mathrm{max},j} \tag{3.22}$$

Assuming that the efficiency of the turbines are only function of turbine discharge, optimum dispatch of any powerplant discharge between Q_{Pmin} and Q_{Pmax} over its turbines are calculated by the process given below.

1. The powerplant operative flow range between Q_{Pmin} and Q_{Pmax} is discretized into a user specified number of equally spaced flow rate values or by default 50 values.

2. Each of these flow rate values is distributed over the combinations of turbines which make the meeting of that flow rate mathematically possible. This process is repeated

1000 times by Monte Carlo sampling for every flow rate. Completion of 1000 samples can take longer for some of the flow rates since the probability of hitting turbine operative discharge limits might be very low while sampling for these flow rates. Therefore, a threshold is used to specify the minimum allowed probability of a successful hit in order to terminate and give user a warning in case of endless sampling.

3. After the completion of 1000 different distributions of every flow rate values over the turbines, the overall efficiency of the plant is calculated for every sample and the distribution that gives the maximum overall efficiency is assigned to that flow rate.

4. The flow rates, their optimum distributions over the turbines and the corresponding efficiency values are recorded in a table named as plant discharge-efficiency table which is the output of UDO.

   This procedure is performed at the initialization section of EROM as it is mentioned in Figure 2.5. During the simulations at every time step the weights of the optimum distribution correspond to the nearest flow rate in the plant discharge- efficiency table to the given plant discharge is used for the distribution over the turbines.

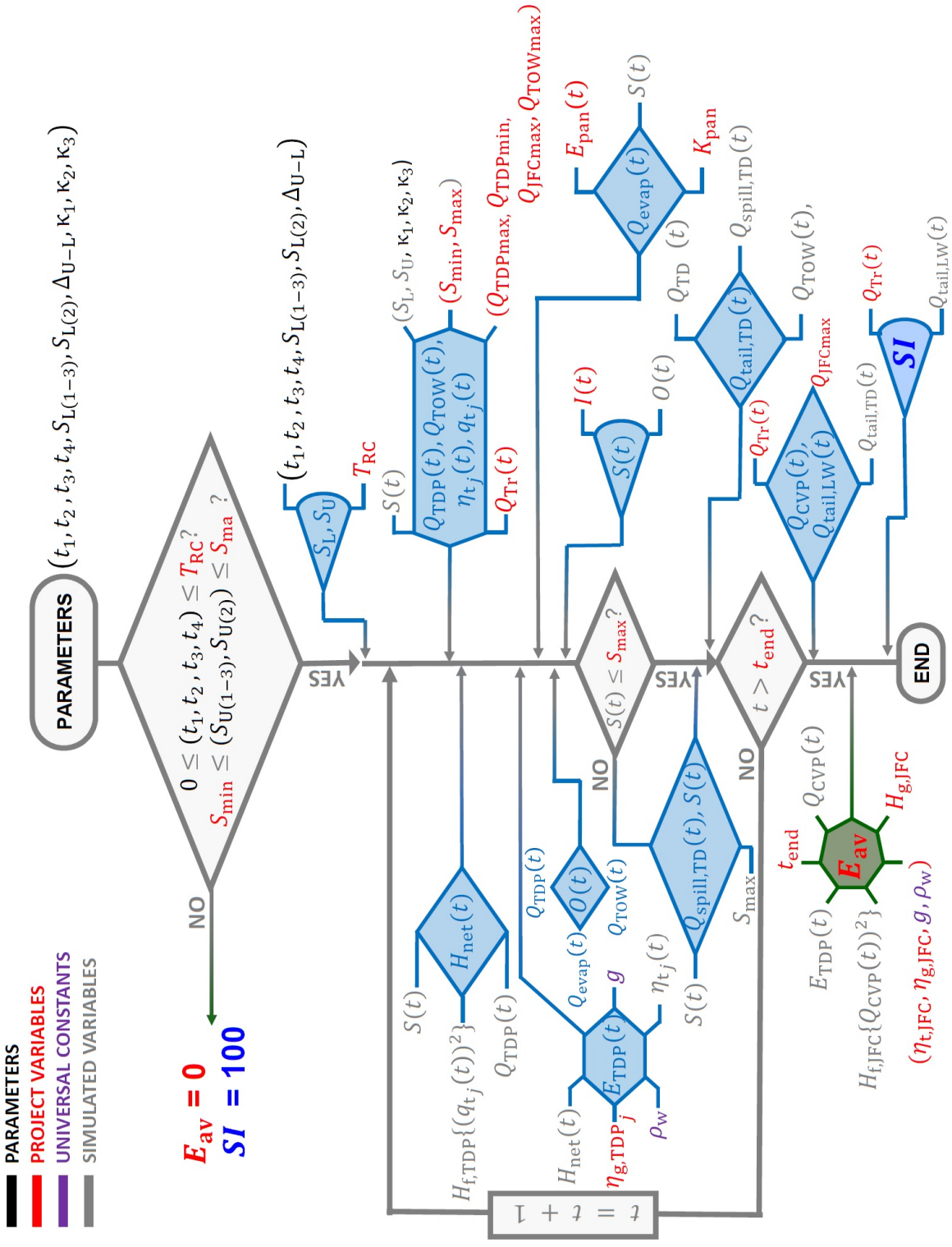

Figure 3.33: Flow diagram of EROM arranged with the parameters of RC1 approach

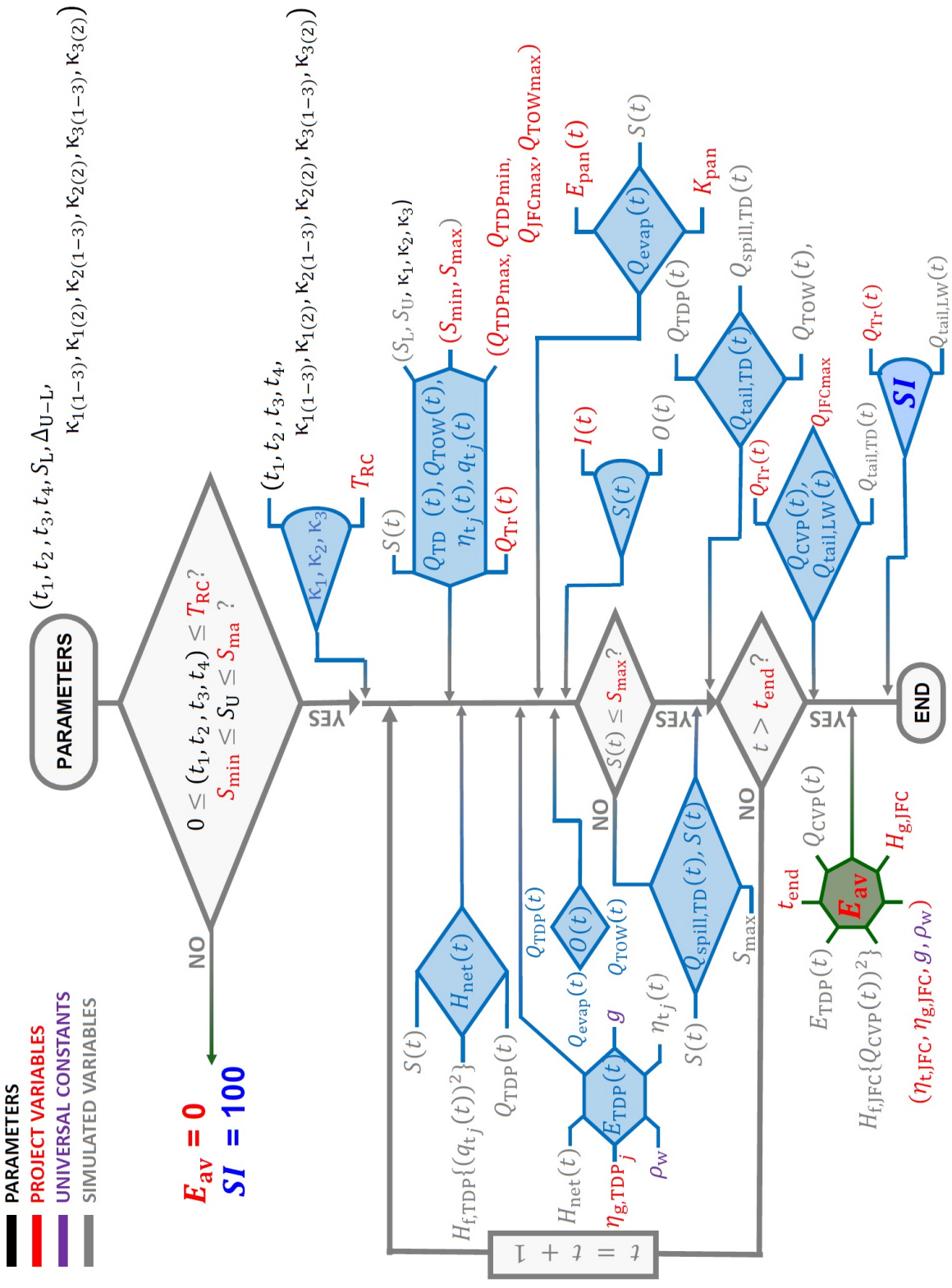

Figure 3.34: Flow diagram of EROM arranged with the parameters of RC2 approach